LBNL-41912

ERNEST ORLANDO LAWRENCE
BERKELEY NATIONAL LABORATORY

Time Resolved Infrared Studies of C-H Bond Activation by Organometallics

Matthew Charles Asplund

Chemical Sciences Division

June 1998

Ph.D. Thesis

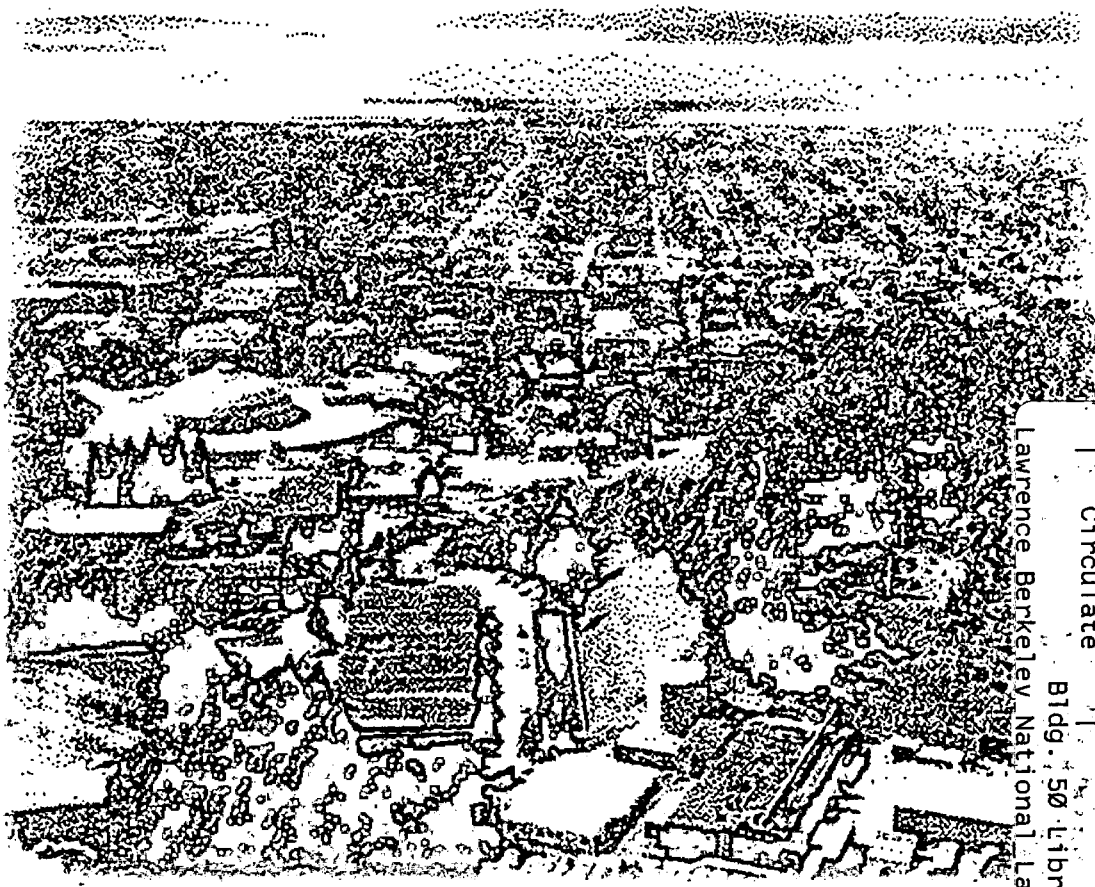

DISCLAIMER

LBNL–41912

Time Resolved Infrared Studies of C–H Bond Activation by Organometallics

by

Matthew Charles Asplund
Ph.D. Thesis

Department of Chemistry
University of California, Berkeley

and

Chemical Sciences Division
Lawrence Berkeley National Laboratory
University of California
Berkeley, California 94720

June 1998

This work was supported by the Director, Office of Energy Research, Office of Basic Energy Sciences, Chemical Sciences Division, of the U.S. Department of Energy under Contract No. DE-AC03-76SF00098.

Time Resolved Infrared Studies of C–H Bond Activation by Organometallics

by

Matthew Charles Asplund

Abstract

Time Resolved Infrared Studies of C–H Bond Activation by Organometallics

by

Matthew Charles Asplund

Doctor of Philosophy in Chemistry

University of California at Berkeley

Professor Charles B. Harris, Chair

One of the central focuses of chemistry is to understand the manner in which molecules interact and the reactions that occur as a result of these interactions. With the recent development of powerful tools for time resolved infrared absorption spectroscopy, we have an unprecedented opportunity to examine chemical reactions. The first of these developments is visible and near infrared ultrafast lasers, which have pulses 100 fs in duration, and can generate infrared light through difference frequency generation. The other major development is step-scan Fourier Transform Infrared (FTIR) spectroscopy, which allows us to collect infrared spectra in the nanosecond and microsecond time regime. The combination of these two techniques has allowed us to

probe the dynamics continuously through time from the femtosecond time domain, where the primary photophysical events occur, to nanoseconds and microseconds, where the final bond activation steps occur.

This work describes how these spectroscopy tools have been applied to the study of the photochemical activation of C–H bonds in organometallic systems, whichallow for the selective breaking of C–H bonds in alkanes. We have establish the photochemical mechanism of C–H activation by $Tp^*Rh(CO)_2$(Tp^*=HB-Pz^*_3, Pz = 3,5-dimethylpyrazolyl) in alkane solution. The initially formed monocarbonyl forms a weak solvent complex, which undergoes a change in Tp^* ligand connectivity. The final C–H bond breaking step occurs at different time scales depending on the structure of the alkane. In linear solvents, the time scale is <50 ns and cyclic alkanes is $\sim$ 200 ps. The reactivity of the $Tp^*Rh(CO)_2$ system has also been studied in aromatic solvents. Here the reaction proceeds through two different pathways, with very different time scales. The first proceeds in a manner analogous to alkanes and takes < 50 ns. The second proceeds through a Rh–C–C complex, and takes place on a time scale of 1.8 μs.

Much of the study of these C–H activation reactions has focussed on the spectroscopy of the CO ligands. We have shown the spectroscopy of several non-CO modes in the system. Spectroscopy of the Rh–H stretch at 2080 cm^{-1}has allowed for the unambiguous assignment of the time scale of final C–H bond breaking step. Spectroscopy of the pryazole stretches in the Tp^* ligand itself has confirmed that an

important step in the reaction pathway for this C–H activation system is the changing of the connectivity of the Tp* ligand.

To my wife,

Suzette,

and my wonderful children who have supported me so much.

Contents

List of Figures

List of Tables

Acknowledgements

I have so many people to whom I owe so much that I find it impossible to thank them all. I have enjoyed my work at Berkeley because of the wonderful science which I have done, but even more, I have enjoyed my work because of the wonderful people that I have known.

First I must thank my adviser Dr. Charles Harris, who has provided me with the facilities and the freedom to search out interesting problems in chemistry, and to pursue these problems until we found answers. I am also grateful to Vijaya Narasimhan who has always been willing to go to bat for the members of the group. Much less would be done were it not for her.

I would like to acknowledge the National Science Foundation for the funding which supported this work, and the Department of Energy for specialized equipment used in many of the experiments presented in this dissertation.

I owe much of my success as a graduate student to the people in my research group. I do not have space to mention everyone in the group, but there are some which I must make special mention of. Jason King was my first mentor here at Berkeley, and his influence is still strong. From him I learned that "Any night is a good night to take data" and to "Only take publication quality data". I also learned a lot about balancing science, family and life from his example. Steven Bromberg was a close friend and scientific collaborator. We spent many happy hours doing "Friday afternoon work", and talking about subjects both scientific and non-scientific. I am

grateful to Haw Yang for providing support to me during crucial times in my graduate career, and for many interesting and informative discussions. I am also grateful to Jason McNeill, with whom I have spent many hours fixing computers and talking. I am grateful for my interaction with Matt Wilkens who joined our group last year, and worked with me collecting much of the data presented in this dissertation. I have enjoyed his help and his company.

Along with my interaction with the Harris research group, I have also had the opportunity to collaborate with the Bergman and Moore groups at Berkeley. I have learned much from my interactions with Dr. Bergman about inorganic chemistry, and about the inorganic chemist's view of the world. Jake Yeston, a student in the Bergman and Moore groups, has been a terrific collaborator. I have on a number of occasions made difficult demands on him, and he was not just willing to help, but happy to help.

Much of the work presented in this dissertation was done in collaboration with Dr. Heinz Frei, a scientist in the Structural Biology Divion of Lawrence Berkeley Labs. Dr. Frei was a wonderful collaborator, and provided very helpful input on both the running of experiments, and the interpretation of data.

My love for research was developed as an undergraduate. As a sophomore, I began working with Dr. Nolan Mangelson at B. Y. U. performing experiments in X-ray spectroscopy, and learned to love solving problems, both large and small. I owe a great debt to Dr. Mangelson who gave me a great start in research, and continues

to be a good friend.

Next, I must thank my family. My parents have always encouraged me in all that I did. My mother was a constant support to me, and showed it as she tried to learn about liquid xenon, and laser spectroscopy. I regret that my father died too soon to see my graduation, but his memory is with me often in my work.

Lastly, I must thank my wife and children. Without them, I would not be doing what I am doing today. Suzette has put up with 6 years of being married to a graduate student, with its lack of money and long hours, and has never complained. I have often made it through difficult days because of the knowledge that I would get to go home to her and my children, and know that life was happy and good.

Chapter 1

Introduction

In the understanding of physical chemistry, one can identify two natural groupings of experiment and theory. These can be described by structure and dynamics, or similarly equilibrium and non-equilibrium. Recent progress on understanding equilibrium structure in both structure and dynamics has allowed us unprecedented insight into the structure of matter, and into the nature of the interaction of matter, which we call chemistry. Experimental techniques such as X-ray diffraction, NMR, IR, microwave and other spectroscopies have allowed us to measure very detailed properties of molecules. Computational techniques such as semi-empirical quantum calculations, *ab initio* quantum calculations and density functional theory have reached chemical accuracy for small systems, and allow further insight into equilibrium properties.

Understanding dynamic processes has proven more difficult, because it involves all of the complexity of understanding equilibrium structure but with the added

dimension of time evolution. Important steps have been made in this field both in computation and in experiment. On the computational side, advances in computer performance have led to an increase in the size and complexity of systems which can be studied by molecular dynamics studies. Increases in computational techniques as well as in computer power have also led to increases in the size and complexity of quantum structure calculations, and have allowed the calculation of semi-classical systems which promise much more realistic simulations than those available in pure classical simulations.

On the experimental side, the development of femtosecond laser systems has allowed for experimental probing of very early events in chemical reactions. Early work on small systems, including I_2, HCN, I_2^-, $M(CO)_6$ (where M=Cr, W, Mo), stilbene and N_3^- all provided insight into the early bond breaking and energy transfer dynamics in chemical reactions. Studies of photosynthetic systems, myoglobin and other biochemical systems have also provided important insight into chemical reactivity.

Recent advances in ultrafast lasers, including the development of Ti:Sapphire oscillators, regenerative amplifiers and optical parametric amplifiers, have made the generation of 100 fs infrared pulses possible. The move from visible spectroscopy to infrared spectroscopy is extremely important in chemistry, since the infrared region of the spectrum allows much better deduction of structural information. Understanding the data derived from probing electronic states in the visible region of the spectrum is difficult because interpretation requires knowledge of information about the elec-

tronic states. In simple systems this is possible, but in complex systems, especially systems in which there are intermediates with unknown structures, it can be difficult to interpret electronic spectra. Another advantage of infrared spectroscopy is that the width of the peaks is small compared to the spectral width available in the infrared. In visible experiments peaks associated with parent compounds, products and intermediates often overlap because their bandwidth is >3000 cm^{-1}compared to the 17 000 $cm^{-1}$of visible bandwidth. In comparison, for measurements in the studies described in this work, the peaks are 5 - 10 cm^{-1}wide and the measurements cover at least 350 cm^{-1}. This means that the absorption of the parent, intermediates and products are well isolated and thus easy to identify.

Infrared is also preferable to visible in this work because it is a direct probe of structure. For an isolated band, the frequency of a given absorption is based only on the reduced mass and the force constant of the bond. Even in cases of extended local modes, the frequency can still be associated with forces and masses in the molecule, and thus is directly related to structural details in the molecule. Electronic states also depend on structure, but in a much more complex way, and so understanding them requires calculations of the electronic states, including excited states, to correlate these structures with electronic absorptions.

The work in this dissertation shows the capabilities which transient infrared spectroscopy can bring to bear on a reasonably complex chemical system. It builds on work which was done using traditional spectroscopy techniques which use model ki-

netic schemes, and adds direct measurements of chemical reactions under realistic reaction conditions. Most importantly, it allows us to observe all of the intermediates which are formed during the course of the reaction, and to unambiguously describe their structure and thus begin to understand the processes which are involved in these chemical transformations. These experiments, coupled with theoretical calculations will help us to understand these important and interesting chemical reactions in much greater detail.

Chapter 2

Experimental

2.1 Ultrafast IR

In order to probe the dynamics of chemical systems in the first steps of the reaction, it is necessary to have an instrument capable of measuring events which occur on the timescale of ~100 fs. Measurements which depend on electronics for their time resolution are generally not capable of measuring signals shorter than 1 ns, the response time of the fastest infrared detectors. It is thus necessary to use pulses of IR light which are short, and use them to measure the dynamics during short periods of time following photoexcitation.

In our experiments, we have used a laser which is capable of producing infrared pulses which are ~80 fs in length, and tunable through the I.R. region. An important consideration in building our laser system was to allow flexibility in wavelength for

both pump and probe. Previous studies in chemical dynamics were often limited to the study of molecules which absorbed where a particular laser could produce light. We felt that it would be more important to create a laser which could produce broadly tunable pulses at several wavelengths simultaneously, allowing us to pick the interesting chemical systems, and then tune our laser to meet the needs of that particular system.

A schematic representation of the laser system is shown in 2.1 on page 8, and it has been described previously [2,3]. A summary of the laser is also provided in appendix B on page 135, which contains important parameters. The initial pulses in our system are produced by a Titanium Sapphire laser, operating at 80 MHz. The oscillator design is a standard design [4, 5] in a Z configuration. This oscillator provides a very stable source of 100 fs pulses at 800 nm. The output of the oscillator is amplified by two transversely pumped Bethune dye cells, using LDS-798 dye pumped by the output of a seeded 30 Hz Spectra Physics YAG laser in a configuration similar to that used by Murnane [6]. This laser is time synchronized by an electronic synchronization circuit which consists of a discriminator circuit and a D-flip flop. The light which leaks through the high reflector end of the oscillator cavity is focused on a photodiode, and the output of this photodiode is fed into the discriminator. When the lamps on the YAG fire, this sets the D-flip flop to be ready. When the next pulse comes from the oscillator, it triggers the flip flop which outputs a 5V electrical pulse. This pulse is then used to start a delay generator which controls the rest of the timing of the

laser and data collection system.

The 800 nm light is then split into into three beams by two beam splitters. One beam is amplified in another Bethune dye cell with LDS 798 dye to give 8 μJ of 800 nm light. The other two beams are focused in thin sapphire flat windows to generate continuum. The power and focusing of the 800 nm light is set to generate continuum just below the threshold at which the beam profile starts to degrade. These continuum beams are then filtered to give a 10 nm section of the spectrum, and amplified in a chain of Bethune cells. This allows two beams of independently tunable light, which for most of our experiments are set for 590 nm and 700nm.

The beam of 590 nm light is doubled in a BBO crystal to form a 295 nm pump beam, which is focused to a diameter of 200 μm in the sample and starts the reaction. The other two colors, 800 nm and 700 nm, are combined in a $LiIO_3$ crystal. This crystal acts as a difference frequency medium, producing a beam of IR light whose energy is the difference between 700 nm and 800 nm, which is 2000 cm^{-1}. This light is split into a signal and reference beam, passed through a monochromator and into two detectors. This allows us to correct for shot to shot laser noise in the system.

Infrared signals are collected by two matched InSb detectors from Electro-Optical Systems. These detectors were chosen to be matched well in their operating characteristics to minimize noise due to non-linearities between the two detectors. The output from the detectors is a pulse which is approximately 10 μs in width, and negative in voltage, with the integral of the peak being proportional to the photon flux

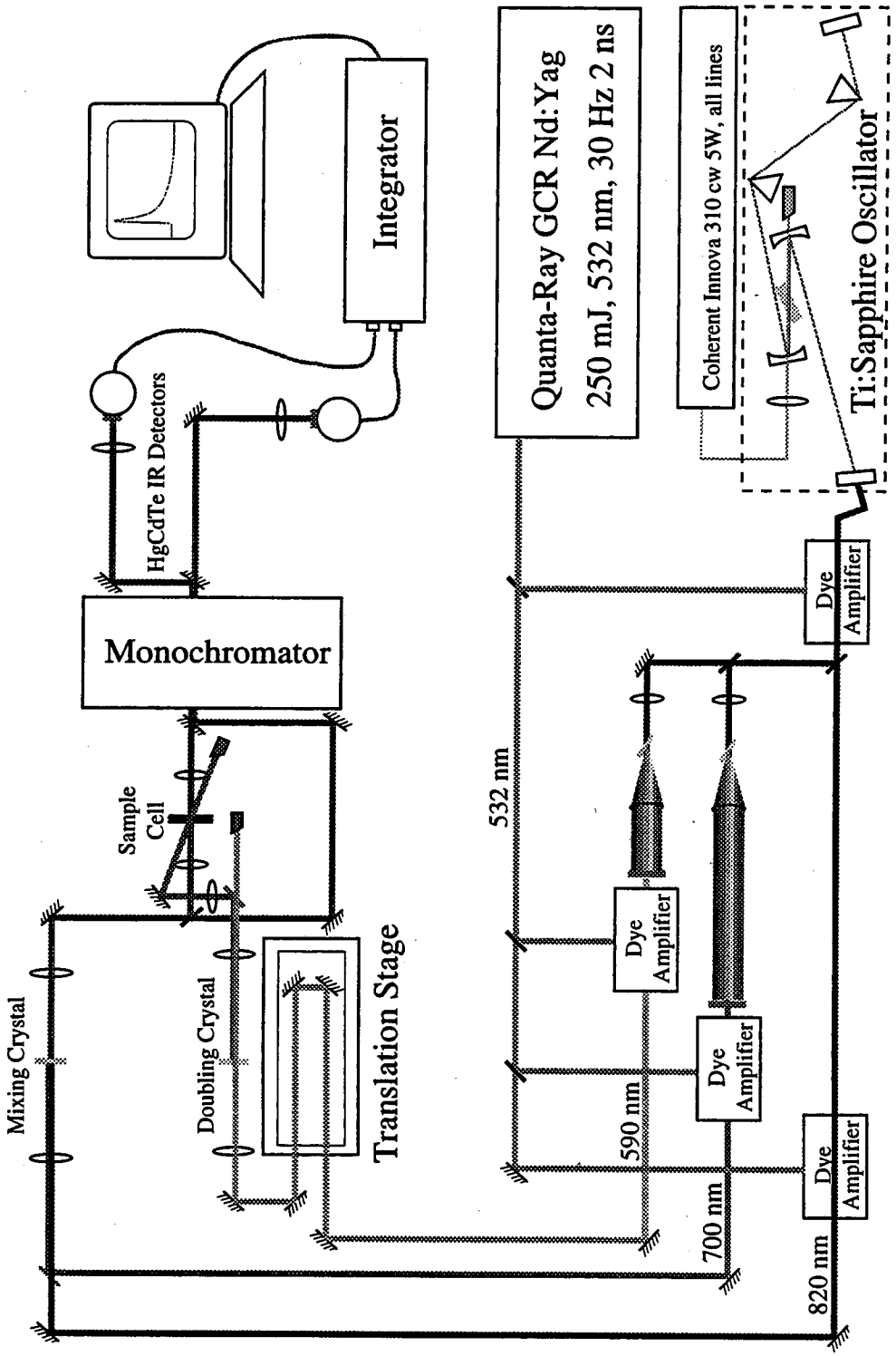

Figure 2.1: Schematic of our Femtosecond IR laser system

on the detector. In order to get maximum stability in the signal from the detector, we pass the pulse through integrators (Stanford Research model 250) and then the output of the integrators is digitized by a LeCroy model 4300B digitizer.

Signals are collected in two different modes depending on the type of experiment. In kinetics mode the monochromator is set to a specific wavelength, and the time delay between pump and probe is swept from before t_0 to some time after t_0. This measurement is repeated a number of times at a given wavelength until the signal to noise is sufficient for reliable fitting of the transient. This mode of operation is controlled by computer code initially written by Dan Russell [7] in our research group, though some modification of his code was necessary. A modified program `femto.exe` contains code for logarithmic scanning, viewing of averaged data, and several bug fixes.

In spectrum mode the monochromator is set at a given wavelength, and measurements are made at a small number of time delays, first with the pump beam blocked, and then with it unblocked. These measurements are repeated a number of times, and these repetitions are averaged. The monochromator is then changed to a new wavelength and the measurement is repeated. The computer code which implements this is `spectrum.exe`.

2.2 Step-scan FTIR

Traditional wavelength dispersive transient IR measurements have depended on a single frequency source, such as an IR diode laser or a glow-bar dispersed through a monochromator, and a time resolved IR detector. [8,9] Measurements are made one frequency at a time, though all times could be measured if the time response of the detector were fast enough. One of the big problems with this technique is that if the sample degrades over time, this degradation is reflected in the spectrum. This often makes absolute determination of time resolved spectra difficult.

Step-scan spectroscopy is different in that it collects information about all frequencies *and* all times at each laser pulse. This means that any sample degradation over the time of the experiment is reflected in the whole spectrum, rather that in just a subset of frequencies. Specifically, the time resolved interferograms are collected in such a way that the center spike of the interferogram is collected first and the long tail later. This means that even if the sample quality degrades over the time scale of the experiment, the peak positions are correct, and only the spectral resolution is degraded. The one difficulty with step-scan spectroscopy is that it requires many more laser shots to collect a time trace at a given frequency than traditional wavelength resolved spectroscopy. For instance a typical scan in the CO region of the spectrum (1700 - 2100 $cm^{-}1$) would require 30 laser shots averaged at each of 420 mirror positions. This means $420*30 = 12600$ shots are required to get kinetics at one frequency. We attempted to measure the nanosecond SS-FTIR signal of $Tp^{*}Rh(CO)_2$ in liquid

Xe, but found that the sample rapidly degraded after only 50-100 laser shots. Thus we were unable to get information on *any* frequencies without getting information about *all* frequencies.

The basic principles of Step-Scan FTIR are based on conventional FTIR, and were first described by Uhmann *et al.*. [10] In a standard FTIR, light from a broadband IR source is split by a beam splitter and one part of the beam is reflected off of a mirror mounted on a translation stage, while the other is reflected off of a fixed mirror. The two beams are then re-combined and passed through the sample and into the detector. The IR signal is then collected as the translation stage is scanned, giving an interferogram of the IR source modified by the sample absorption.

In Step-scan FTIR, rather than continuously scanning the translation stage and collecting a time domain signal on a millisecond time scale, the stage is moved in n discreet steps, stopping at each position to take m time traces, each representing a photexcitation event. These m time traces are averaged to decrease noise. The time resolution of the traces is limited by the detector response and the electronic amplification and digitization, and can be from 5 ns to 5 ms depending on the experimental setup. Each time trace provides p time slices spaced linearly. We can then form an $n \times p$ matrix of signal values for each $step \times time$ point, where each point A_{np} is a signal value. If we now consider looking along the n axis of mirror positions in the matrix (ie all A_{ip} for a given p) then we have interferograms at a given time p. We can then Fourier transform this interferogram to get a spectrum at

a given time p. This process is graphically demonstrated in figure 2.2 on page 14.

A very important aspect of step-scan spectroscopy involves the measuring of small time dependent changes in the spectrum. For a normal spectrum (see figure 2.3(a) you can see that there are static absorbances in the spectrum that are >0.25 O.D, and are often even larger. The transient spectrum in figure 2.3(b) on page 15 is the spectrum that we actually want to see, and it has features that are on the order of .5 mOD, or 0.05% of the static spectrum. If we assume an 8 bit digitizer, which has 2^8=256, the difference between two digitized values is $\frac{1}{256}$ = .00390, or .4%. This is almost 10 times less than the size of the signal which we want to observe, and so we are only effectively using 3 bits of the digitizer. This problem was elegantly solved by Palmer by using a high pass, or A. C. coupling filter on the output of the detector. [11,12] This filters out the constant offset, which is the static spectrum, and leaves only the part of the signal which changes in time faster than the time constant for the detector (generally 1 ms). Using this technique, we are able to use all of the dynamic range of the digitizer to digitize only the transient signal.

The Fourier transformed spectra are in raw signal form and need to be converted to absorbance units. In general we know that we calculate absorbance as:

$$A = -\log(\frac{I}{I_0}) \tag{2.1}$$

For step-scan measurements, we have I, the collected spectrum at each time slice,

which is actually the sum of the DC and AC portions of the signal. In order to get I_0 we collect an identical data set, but collecting the DC output of the IR detector, rather than the AC output. Thus the calculation in terms of DC and AC signals is:

$$A = -\log(\frac{AC + DC}{DC}) \tag{2.2}$$

Because the DC component of the signal is so much smaller than the AC component, we attenuate the DC signal, and amplifying the AC signal. For a typical experiment, we attenuate the DC signal by a factor of 2, and amplify the AC signal by a factor of 200. This means that we need to include a factor β of 400 in the calculation of the absorbance. This gives us a final equation:

$$A = -\log(\frac{AC + (\beta \times DC)}{(\beta \times DC)}) \tag{2.3}$$

This calculation is performed as part of the scripts used in the data analysis, which is summarized in appendix A on page 125.

Another problem with performing time resolved IR measurements is changes in the refractive index (η) caused by changes in temperature from the absorption of the U. V. light. These changes cause an overall decrease in the amount of light hitting the detector, and therefore look like an absorption. In step-scan, however, we take advantage of the fact that this change in η is relatively frequency independent, and therefore causes a constant offset in the interferogram. When we do the Fourier

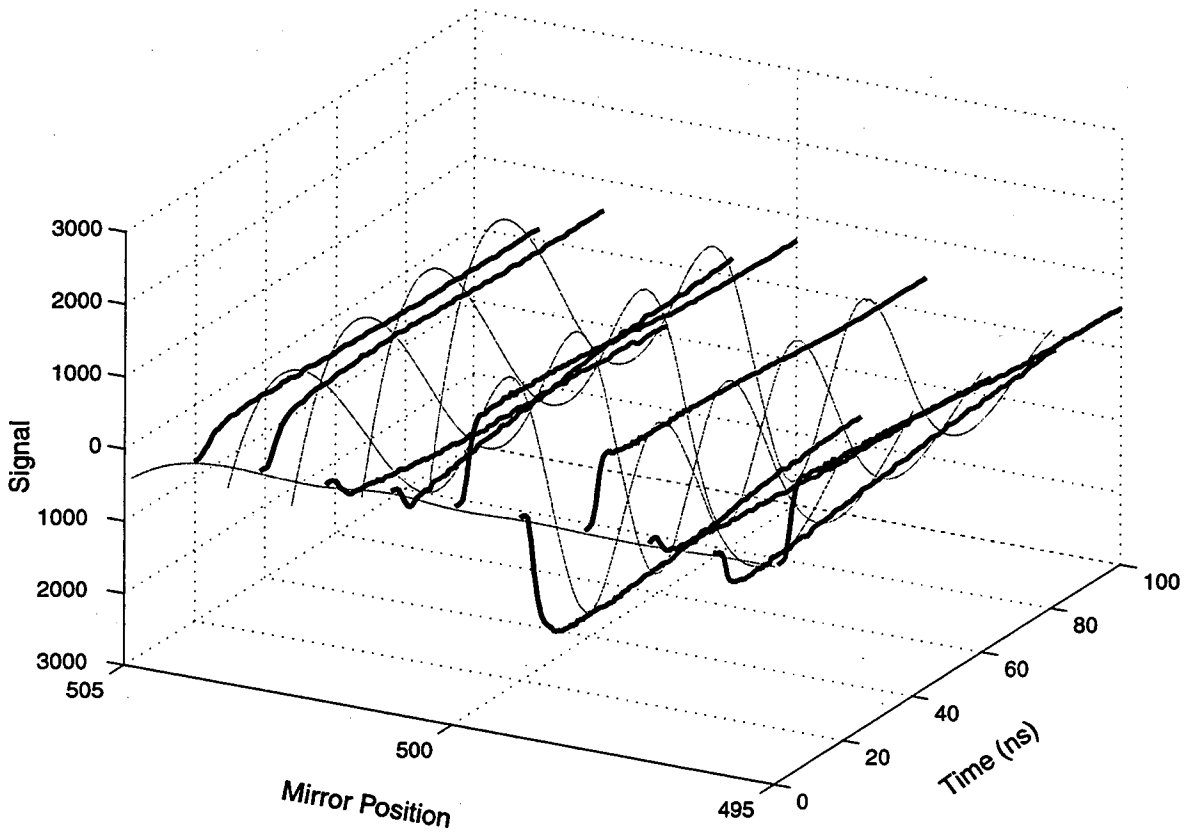

Figure 2.2: Schematic representation of data collection in stepscan experiments. Heavy lines represent the measured time traces, and light lines represent reconstructed interferograms.

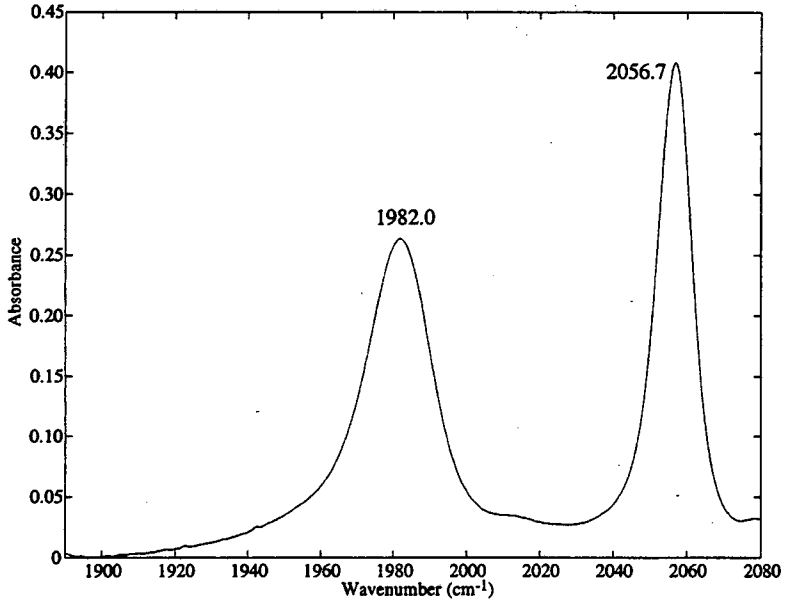

(a) Static Absorbance FTIR spectrum

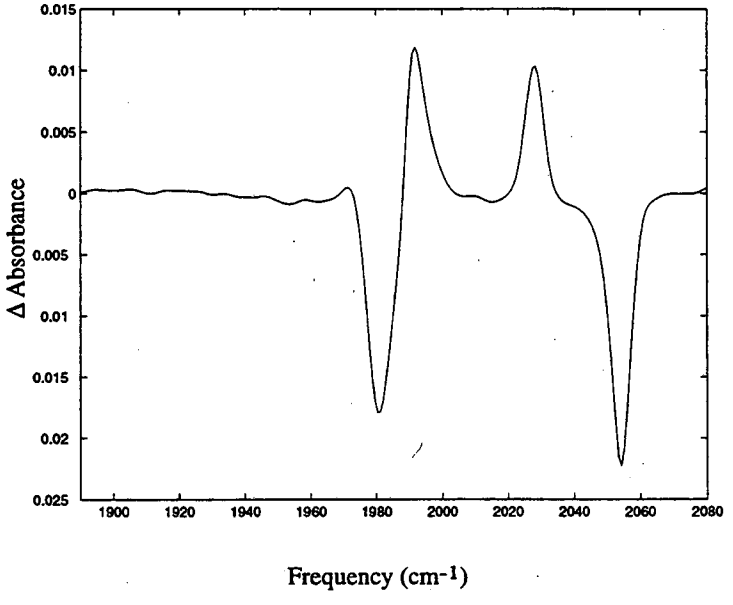

(b) Transient Absorbance FTIR spectrum

Figure 2.3: Typical FTIR static and time-resolved spectra

transform of the interferogram, this constant offset goes to zero, and the spectrum shows no offset.

Using the A. C. coupled step-scan technique as described, we have been able to measure signals as small as .1 mOD with signal to noise sufficient for fitting rise times, in under an hour. This represents a significant step forward in the field of time resolved infrared measurements.

Our spectrometer is a modified IFS88 described by Frei and co-workers [13–16], and shown in 2.4 on the facing page. We have made several important changes in the optics and detectors which are important to mention. Solvents such as cyclohexane have significant absorption in the spectral region in which we are probing. This means that in we need lots of IR photons to get sufficient signal from the detector. Specifically in this system, the IR comes from a globar source which is passed through an aperture to select some portion of the IR coming from the source. The light is then expanded onto a concave turning mirror, which focuses it in the sample. Another concave mirror collects and recollimates the light at the other side of the optical cavity, and further optics focus the IR on the detector. The size of the IR beam at the focus in the sample is controlled by the size of the aperture. In the configuration as described the size of the focus is significantly larger than the aperture because the concave mirrors do not act as perfect lenses when placed at 45° angle to the light.

In order to get the focusing of the IR beam close to the size of the aperture, we have changed the optical configuration of the spectrometer to use focussing lenses

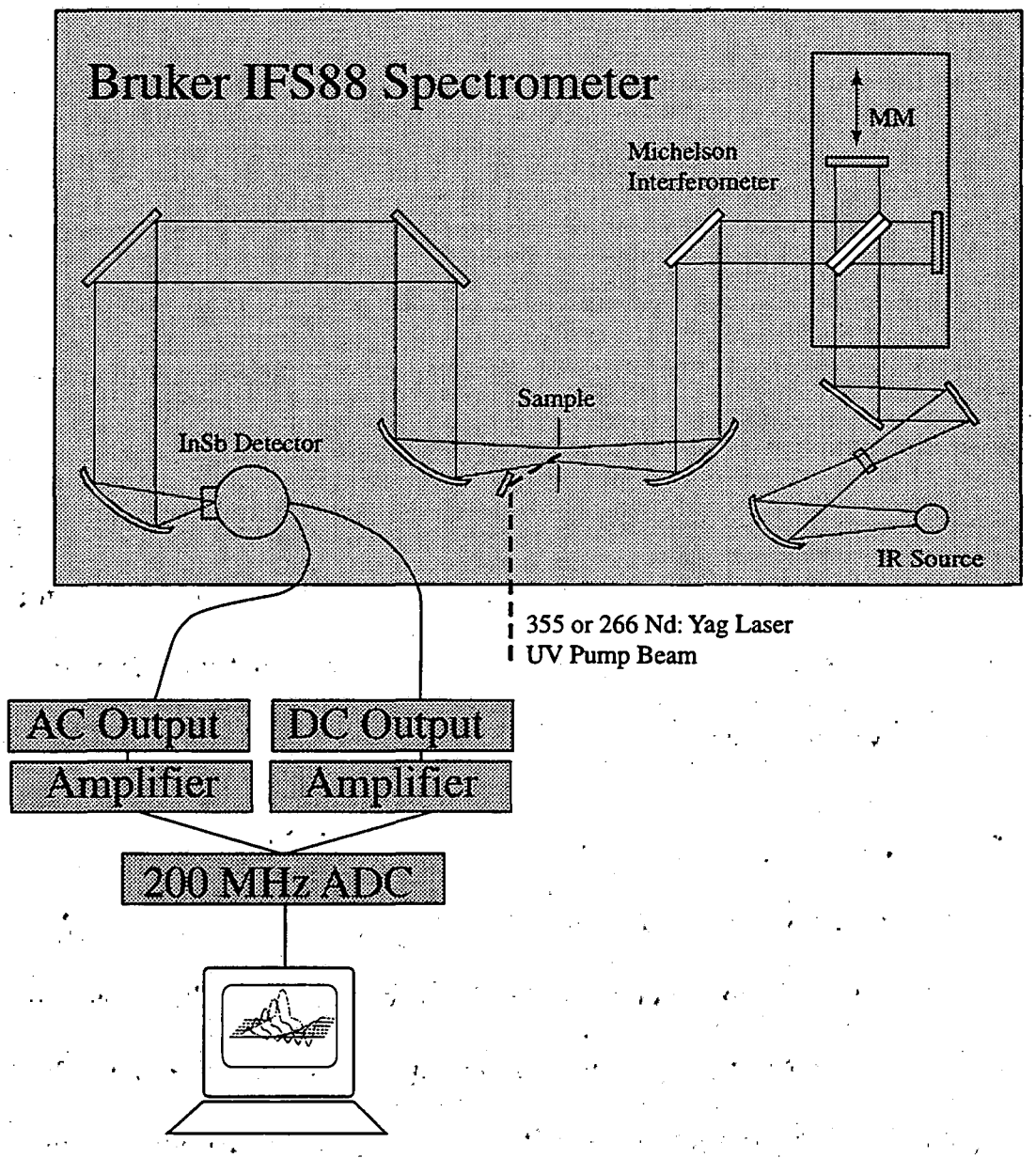

Figure 2.4: Schematic of Step-scan nanosecond spectrometer

rather than focussing mirrors. We have added a new set of planar turning mirrors which send the beam through the sample cavity without focussing, and added a set of 10 mm BaF focusing lenses which focus the IR beam. These were aligned by replacing the standard beam splitter in the scanner with a BaF beam splitter which transmits some visible. The first lens was installed, and the beam was centered on the opening on the other side of the cavity to insure that the first lens was not steering the beam. The second lens was then mounted, and the light was centered on the optics in front of the detector. The distance between the two lenses was then adjusted to give maximum signal on the detector. Finally germanium plates with a special IR anti-reflective coating were placed over the ports between the sample chamber and the scanner and detector sections to assure that UV did not damage either of those sensitive components. A diagram showing the optics configuration is shown in figure 2.5 on the next page.

The pump beam is either the second or third harmonic of Spectra Physics DCR-10 YAG laser output, at 355 nm of 266 nm, or the second harmonic of the output of a Spectra Physics PDL nanosecond tunable pulsed dye laser, usually at 300-320 nm. This is steered into the cavity by quartz right angle prisms from the laser. The laser is placed in another room to minimize RF noise in the detector from the lamps and Q-switch. The laser light is focused by a 500 mm quartz lens so that the size of the pump beam in the sample is the same as the diameter of the IR beam in the cell. Any UV light which passes through the cell is blocked by a card to avoid damaging

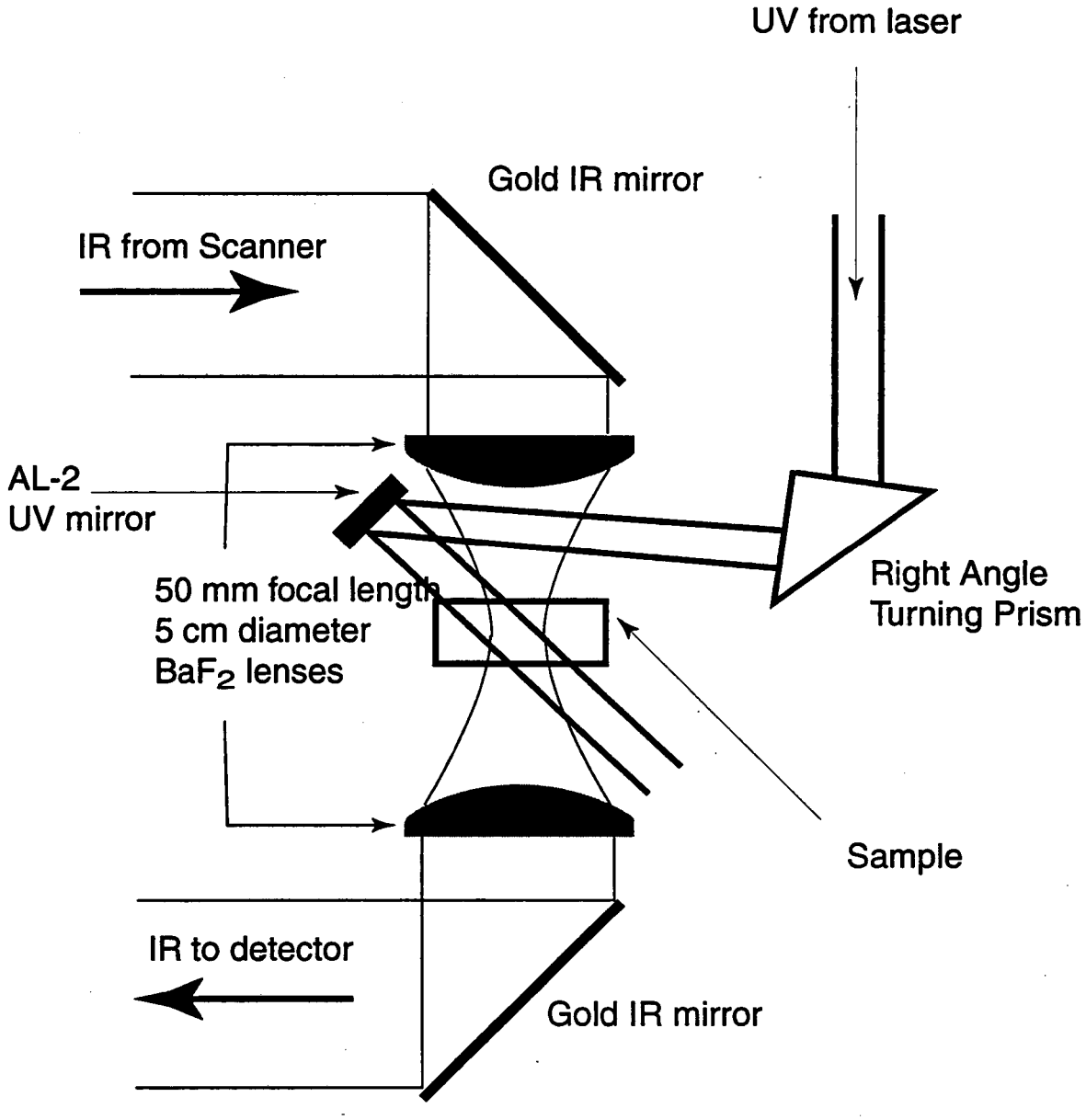

Figure 2.5: Modified FTIR optics used in these measurements. UV and IR beams are focussed to 5 mm diameter inside of sample cell.

the germanium plate. It was found that with careful alignment, the overlap of the pump and probe beams was stable over the 7 - 10 days during which we performed our experiments.

Time resolution for step-scan measurements is given by the detector response time and the response times of the amplifiers and digitizer. For these experiments, an InSb detector was used with a nominal 42 ns FWHM. In order to measure this response, we used the 1064 nm output of the YAG laser. Diffuse reflections of these pulses were detected by a near-IR Si photodiode with a 1 ns response time, and by the InSb detector. Sample traces of the outputs of these two detectors are shown in figure 2.6 on page 22. The solid line is the measure of the laser output with a fast detector, and represents the real pulse width of 14 ns. The dashed line is the output of the InSb detector. The signal from the InSb is wider, and has a long tail. This suggests that even though the output has a 42 ns FWHM, the actual instrument response function will be longer than this.

In order to measure the true response of the system, we need a system in which we can measure an instantaneous growth of a product. The system which we chose as a model system is $Cr(CO)_6$. It is well known [2,17,18] that within tens of picoseconds after photoexcitation, $Cr(CO)_6$ looses a CO ligand, forms a solvent complex, and vibrationally cools. The solvent complex is then stable on the nanosecond time scale, and can be measured by step-scan spectroscopy. Measurements were made using the 42 ns InSb detector, 4 mJ of 355 nm UV light from a frequency tripled YAG laser,

and a 0.5 mm thick sample. The spectrum of the reaction is shown in figure 2.7. This shows the a bleach of the parent absorbance at 1985 cm^{-1}, and the formation of two new pentacarbonyl peaks at 1958 $cm^{-1}$and 1932 cm^{-1}. Kinetics of the growth of the peak at 1958 $cm^{-1}$are shown in figure 2.8 on page 24. The signal is fit to a Gaussian with a FWHM of 42 ns convolved with an exponential growth which a time constant of 62 ns. This gives a quantitative measure of the minimum time constant which we can reliably measure.

2.3 *Ab Initio* Calculations

An important part of the process of understanding chemical process, is trying to use mathematical models to model the physical system. For these measurements we are using infrared absorbance due to molecular vibrations to identify structures. While it is possible to use chemical intuition and comparison with other molecules to do spectral assignments (which we have done with much success) it is also useful to perform structure calculations to aid in assignments. Recent calculations by Jonas and Thiel [19] have shown that density functional based calculations are capable of reproducing experimental vibrational frequencies to less than 30 $cm^{-1}$of accuracy.

Calculations for this paper we done on a 600 MHz DEC Alpha computer, running Digital UNIX 4.0b with 128 MB of memory. The package used for the computations is Jaguar version 3.0 by Schrödinger Inc, Portland OR. This package was chosen because it allows fast calculation of organometallics using density functional theory

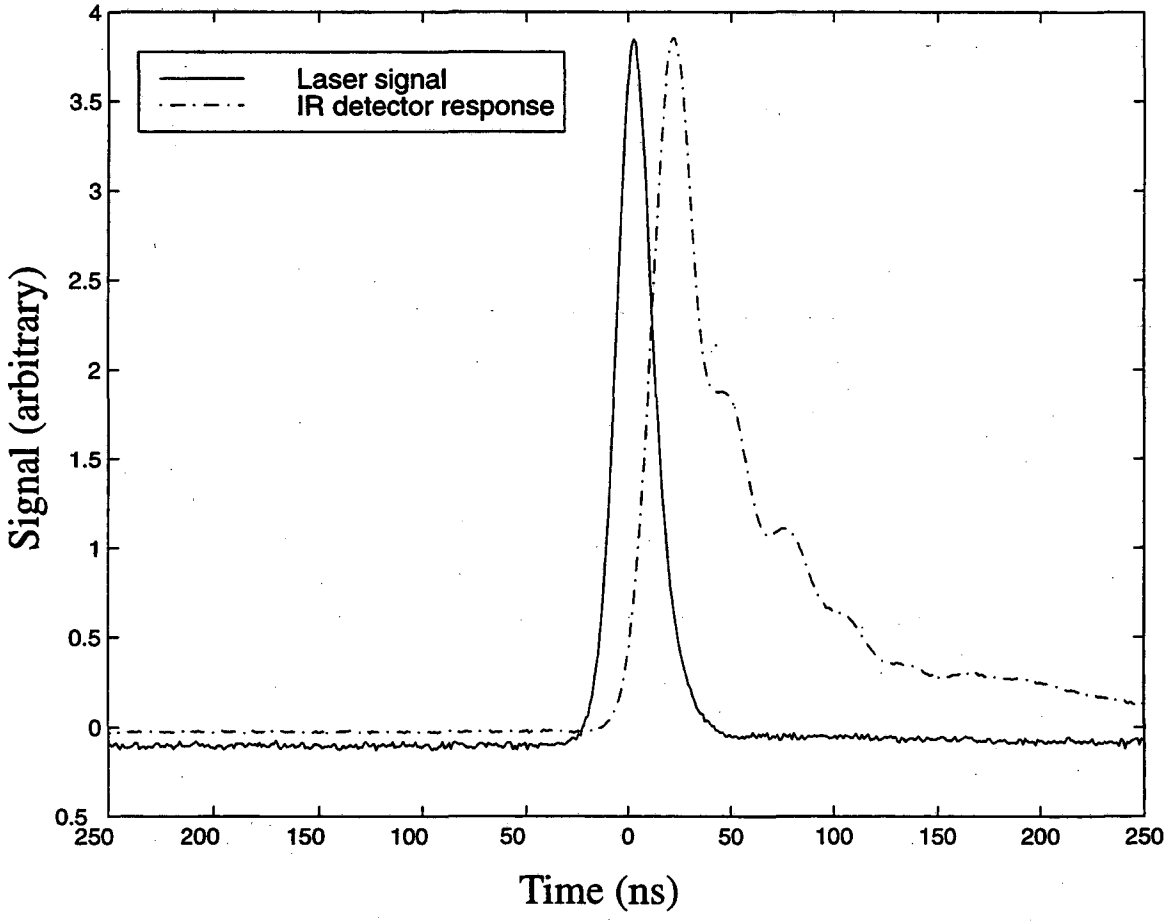

Figure 2.6: Detector response of the InSb IR detector to a 12 ns YAG pulse at 1064 nm

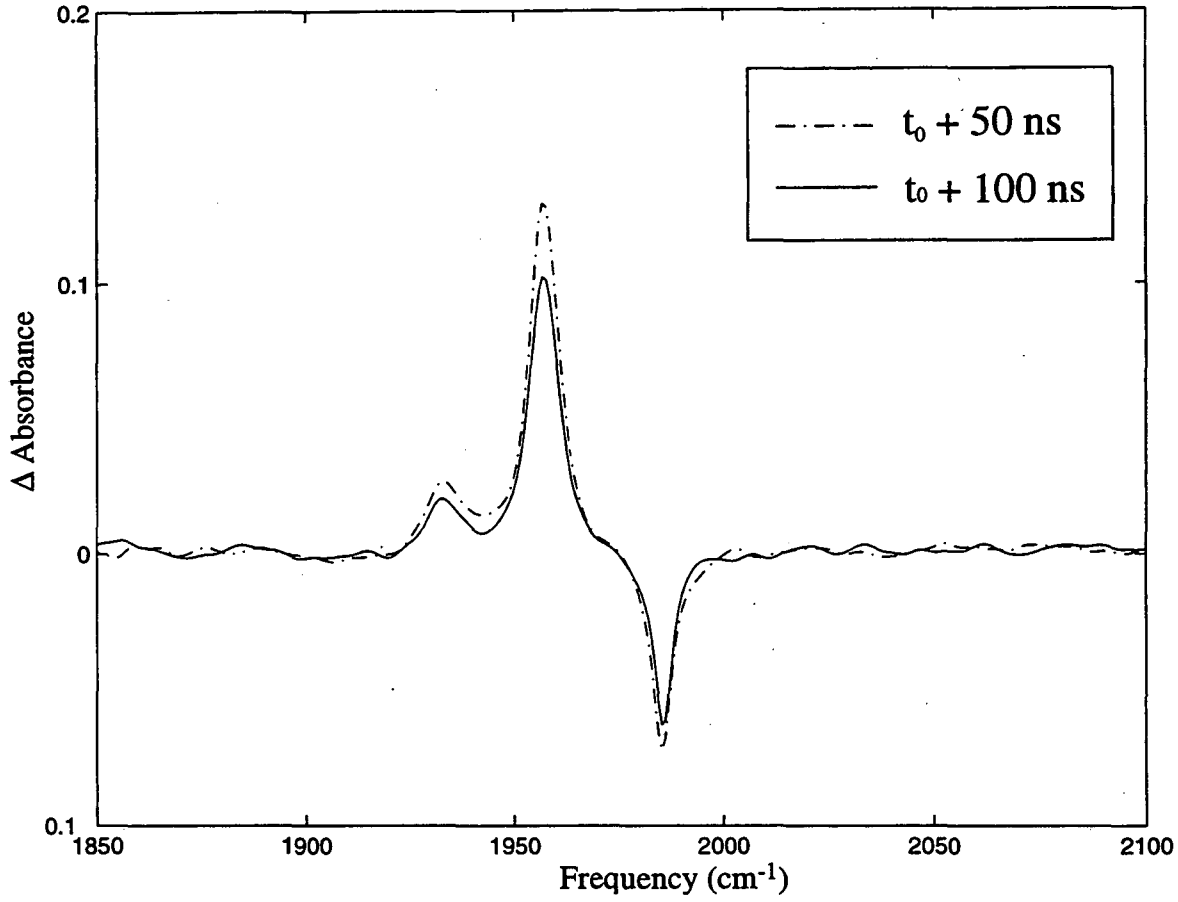

Figure 2.7: Photolysis of $Cr(CO)_6$ in cyclohexane after photoexcitation at 355 nm

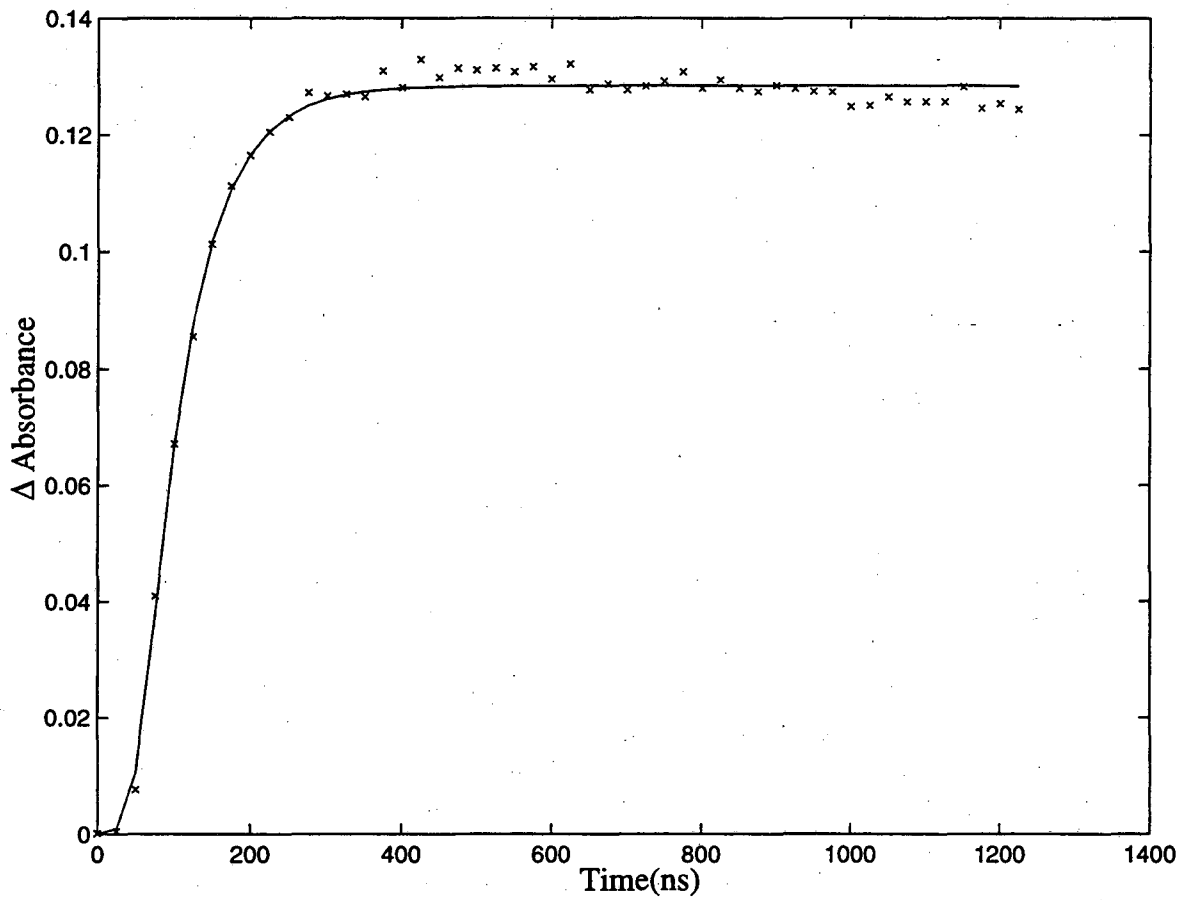

Figure 2.8: Kinetics of the growth of $Cr(CO)_5$ after photoexcitation of $Cr(CO)_6$ in cyclohexane. The solid line is a fit to the data with a 42 ns Gaussian convolved with a 70 ns exponential rise.

and effective core potentials. This allowed us to calculate equilibrium geometries and vibrational frequencies for large molecules (including Tp*Rh(CO)(H)(R) and Cp*M(CO)(H)(R), M=Rh and Ir, as discussed in chapter 4. For a molecule such as Tp*Rh$(CO)_2$, the geometry calculations took approximately 48 hours to converge with a moderate sized basis set.

For the calculations presented here, the LACVP basis set was used. This puts a 6-31G basis set on all elements lighter than K, and for all heavier elements an Effective Core Potential (ECP) was used derived from the work at Los Alamos National Laboratories. The ECP basis set contains an effective core and the outermost core orbital for the atom. For the larger systems, the calculations were performed without diffuse or polarization functions to cut down on the time required for computation.

Calculations of the vibrational frequencies were performed in the optimized geometry using a fully numerical calculation of the Hessian matrix. While it would have been much quicker to perform an analytical calculation of the Hessian, Jaguar is unable to perform analytical derivative calculations for ECP basis sets, and using the Hessian from the optimization gives incorrect results. Unfortunately, the calculation of the Hessian became the limiting factor in modeling different compounds.

2.4 Picosecond visible absorption

All of the vibrational cooling studies were performed on a picosecond dye laser system in our lab. It has been described previously in the literature [20–22]. Basically,

it consists of a 25 ps actively modelocked Argon ion laser, which pumps a dye laser with Rhodamine 6G dye. This produces 1 ps pulses at 85 MHz repetition rate, which are then amplified by a chain of longitudinally pumped dye cells. The amplifiers are pumped by a 10 Hz Molectron Nd:YAG, which produces 220 mJ of light at 532 nm. The lasers are synchronized by a system similar to that used for the femtosecond IR system (see section 2.1 on page 5). The total output of the amplifiers is 1 mJ at 590 nm, with 1.2 ps pulses. Later measurements were made with a slightly different system. Our argon ion laser failed, and we changed to an Antares Nd:YLF laser pumping a dual dye jet dye laser. Using this configuration, we were able to get 800 fs pulses at 590 nm with 1 mJ pulse energy.

After amplification, the light is telescoped into a KTP* crystal to form 295 nm UV light. The visible and UV light are separated by dichroic mirrors, and the UV delayed on a translation stage with respect to the visible to give us time resolution. The visible light is focussed into a water cell to form white light continuum, and a small wavelength range is selected by a 10 nm bandpass filter and the light is filtered through a spatial filter. Two 5 mm thick quartz uncoated windows select 4% portions of the visible light. One is passed through the sample and into a photodiode for measurement. The other is passed to another photodiode as a reference. The photodiode signals are collected, integrated, and digitized to give a signal at a given wavelength, and at a given time. This system is able to observe absorbance changes of .1 mOD after 20 - 40 scans, allowing us to observe small concentration changes.

2.5 Nanosecond UV/visible absorption

An important part of this work has been following chemical reactions through all applicable time scales. In the infrared, we were able to use a combination of ultrafast IR measurements and step-scan FTIR. In looking at the course of these reactions, it became apparent that we needed information about the nanosecond UV and visible absorption changes. These measurements were made in collaboration with Dr. Jim Lewis in the Kliger group at U. C. Santa Cruz. They have developed a system for measuring UV/vis full spectrum absorption measurements in the tens of nanoseconds range. Their system is described in the literature [23, 24]. Basically it consists of a mercury flashlamp, a monochromator, and an intensified diode array from EG&G instruments. The lamp produces a microsecond pulse of white light, which is focussed in a cell, and then focussed into the monochromator, and imaged onto the diode array. The nanosecond time resolution is given by pulsing the bias on the diode array intensifier; when the intensifier is off, no signal gets to the array, and so data is only collected when it is turned on. Gating and timing is controlled by a Stanford Research digital delay generator. Photolysis is performed by the third or fourth harmonic of a Nd:YAG laser, which is also synchronized by the delay generator.

Data is collected as full spectra at a given time delay, and integrated over a short time window, ten nanoseconds for the data shown here. Measurements made with this system are very sensitive, allowing us to see signals of a few mOD after collection of a few laser pulses.

2.6 Sample Preparation

In the study of organometallic compounds, the synthesis and careful handling of samples is of tremendous importance. For these studies, compounds were supplied by several collaborating groups here at U. C. Berkeley. $Tp^*Rh(CO)_2$was synthesised by Dr. Bruce McNamara and Mr. Jake Yeston, and $Bp^*Rh(CO)_2$by Mr. Yeston, who work with Dr. Robert Bergman and Dr. Brad Moore. The compounds were made according to the standard published method [25, 26] and characterized using NMR analysis, and IR spectroscopy. Because the $Tp^*Rh(CO)_2$and $Bp^*Rh(CO)_2$are air and water sensitive, samples were made in a nitrogen filled dry box, and were kept sealed from outside air during the experiment. Solutions were prepared to have an optical density (OD) between 0.6 and 1.0 at the pump wavelength, giving a concentration of $\sim$ 1 mM for $Tp^*Rh(CO)_2$in or aromatic solvents. Samples of $Bp^*Rh(CO)_2$were approximately 2 mM because of their increased solubility in alkane solvents. Solvents used in sample preparation were purchased from Aldrich Chemical, and dried over molecular sieves, degassed and purged with N_2 prior to sample use. Deuterated solvents were purchased from Cambridge Isotope Laboratories and were dried, degassed and purged with N_2. Samples of the $Os(bpy)_3$ were synthesised by Mr. Niels Damrauer, a student working with Dr. James McCusker, and were dissolved in spectral grade solvents, and purged with N_2 for 15 minutes prior to use.

In both femtosecond and nanosecond systems, the samples were circulated continuously through a Harrick infrared sample cell with 3 mm CaF_2 windows to allow both

UV and IR light through the sample. Sample thickness was set by Teflon spacers, which were 1 cm thick. The sample was flowed by a peristaltic pump through Viton tubing. For the nanosecond spectra, it was especially important that there be no vibrations in the sample, and so for these experiments, the peristaltic pump was used to pump sample to a reservoir above the level of the sample holder. The sample was then gravity fed through the cell, giving a vibrationless flow. The temperature of the samples was not actively controlled, but the volume was sufficiently large to avoid heating due to laser irradiation.

Chapter 3

Fundamental Photophysical Events

3.1 Vibrational Cooling

The field of ultrafast chemical dynamics is fundamentally tied to a class of reactions which are initiated by absorption of a photon (or several photons). This is necessary because accurate probing of the course of a process requires accurate knowledge of when that process began. Thus if we wish to know time scales of events to less than 100 fs, we need to know the time when evolution started to less than 100 fs. This leads to the requirement that all reactions which we study are initiated by absorption of a photon.

In the case of chemical reactions this can often be a problem. The Frank-Condon principle states that absorption of a photon must lead to a vertical transition in the molecular potential plot. For bond dissociation this means that we have to excite

the molecule into the dissociative potential at a point very close to the equilibrium geometry, and that we will therefore add extra energy over the bond dissociation energy (which is the difference between the minimum energy of the ground state and the minimum energy of the excited state). This extra energy can be very important in understanding the course of reactions. If we study slow reactions (reactions with time scales >1ns) this energy is certain to have been equilibrated between the modes of the molecule and the modes of the surrounding solvent before reaction occurs. However, if we study fast reactions (reactions with time scales <10ps) then we have to understand the interaction of the transfer of this excess energy with these reactions.

A comprehensive review of the I_2 system has been written by Harris *et al.* [27], but I will give a brief overview here. After the I_2 molecule absorbs light at $\sim$ 500 nm, the molecule dissociates, and some number recombine in less than 1 ps. These molecules have significant excess energy, and this energy is transfered to the solvent. This can be monitored through observation of the electronic energy of the electronic excitation in the visible. This is possible because of the shape of the electronic states in I_2 (see 3.1 on page 33). For a harmonic oscillator, the majority of the wavefunction is at the turning points in the potential, and so we expect most of the absorption to be at the turning points also. If an I_2 molecule is in a vibrationally excited state, this means that the absorption is split and shifted to the red and to the blue with respect to the ground state absorption. As the molecule "cools" to lower vibrational states, the wavefunctions shifts more towards the center of the well, and the absorptions

therefore shift towards the blue and red. This shift depends on the specific structure of the ground and excited state potential energy surfaces.

Early studies on I_2 showed a slow recovery of the parent molecule after photodissociation [28, 29]. These studies used only a single wavelength probe, and so were unable to see the vibrational cooling. Work by Harris *et al.* [20] probed the I_2 dynamics over a broad range of the visible and near infrared spectrum and showed that the long parent recovery was due to vibrational cooling. Further work by Xu *et al.* [30] used transient Raman to confirm the role of vibrational cooling in the evolution of the chemical system. Basically it was shown that for I_2, the timescale for vibrational cooling was 70 to 140 ps in alkane solvents and in halomethanes. Experiments in liquid Xe gas show that the cooling time is much longer, 1 ns, which was expected because of the lack of available solvent modes to absorb the vibrational energy.

More recent work on I_2^-, the anionic form, shows significantly different behavior. Barbara and co-workers [31–33] and Ruhman and co-workers [34–37] show that the vibrational cooling time for I_2^- in alcohol solvents and water is 2 to 4 ps. Studies in CO_2 clusters by Lineberger and co-workers [38, 39] support this time scale. This is a very significant difference in the cooling time when compared to I_2 and suggests that there are significant differences in the interactions between the solvent and the solute. A first obvious difference is the addition of a long range coulombic charge/dipole interaction between the I_2^- and the alcohol solvent. In the case of I_2, the interactions are modeled as primarily repulsive interactions on the Lennard-Jones potential, and

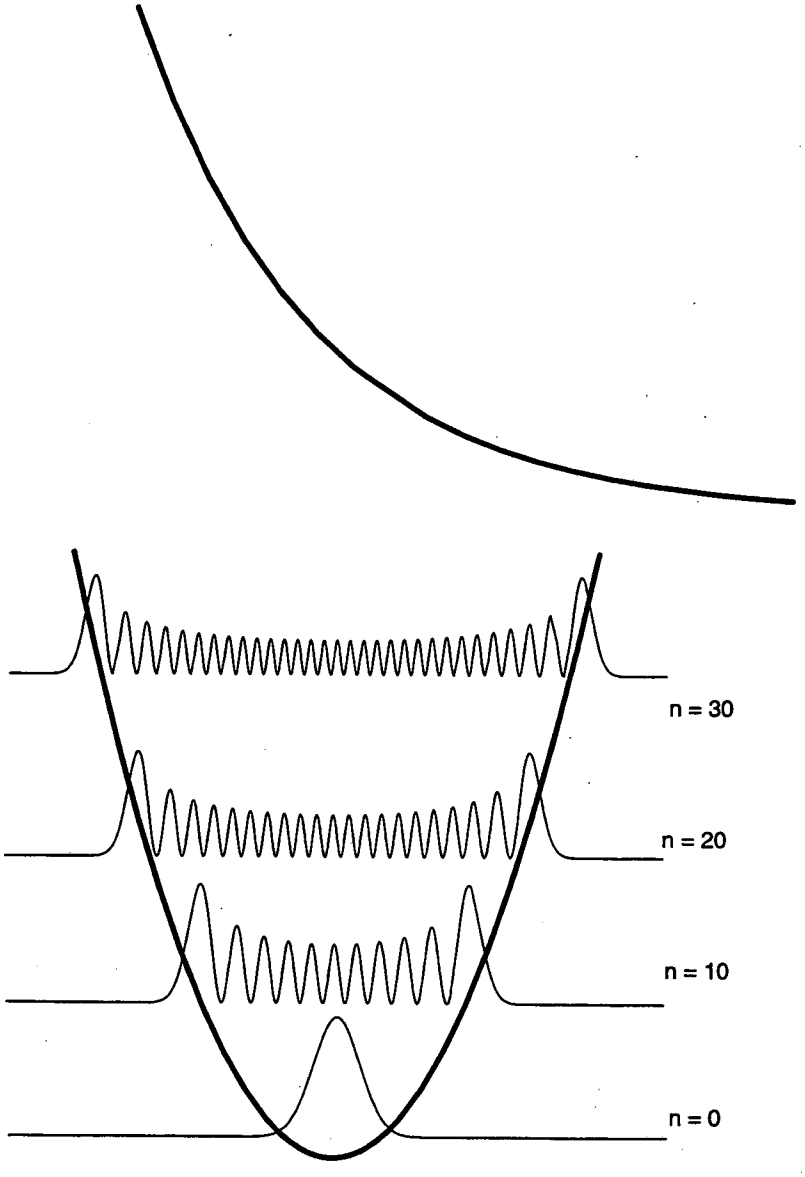

Figure 3.1: Electronic states involved in the vibrational cooling in I_2

so are very short range collisional interactions. In the case of I_2^- the coulombic interaction couples the solute with many more solvent molecules through this attractive interaction. Another important difference is the oscillator frequency of the two different molecules. I_2^- has an additional electron which weakens the I-I bond, leading to a vibrational frequency of 115 cm^{-1}, almost a factor of two lower in frequency than the 215 cm^{-1}frequency of I_2. Benjamin *et al.* [40, 41] studied the relative importance of these effects using molecular dynamics simulations and found that both the change in frequency and the addition of the coulomb interaction contributed to the increase in the vibrational cooling rate.

Experiments performed by our group [1,22] sought to address issues related to this. This was done by measuring the rate of vibrational cooling of various diatomic halides in different polar and non-polar solvents. Measuring the vibrational cooling times for charged and dipolar solutes in a series of solvents with varying polarities has allowed us to examine different aspect of this phenomena. Data for the cooling of I_2^- in the non-polar solvent CCl_4 are shown in 3.2 on page 36. The difference between the two scans is that the solvent CCl_4 has no permanent dipole, and therefore no charge/dipole interaction with the solvent, while the $CHCl_3$ has a small permanent dipole which can interact with the charge. If the long range coulomb interaction were important in the cooling dynamics, one would expect to see different cooling behavior in the two solvents. The data in figure 3.2, however does not show significantly different cooling behavior between the two solvents. Note that the difference in apparent time

scales is due to differences in the sample and not in the dynamics. Because of the low solubility of the I_3^- ion in the non-polar CCl_4 solvent, it was necessary to use a 1 cm cell rather than the 1 mm cell used for the rest of the experiment. This means that as the pump and probe beams propagate through the sample, the probe beam travels faster than the pump beam (because the probe beam is significantly to the red of the pump beam). This means that, rather than a single time delay between pump and probe for the sample, there is a distribution of delay times depending on how far the beams have traveled through the sample. For our experiments, we measured that the instrument response function for our system changed from 1.5 ps to 5.5 ps when going from 1 mm to 1 cm. If we fit the data to a single exponential decay, we get a decay time of $\sim$5 ps for both solvents. Thus the interaction of the charged solute and the dipole of the solvent appears to make no difference to the decay time.

One possibility for the similarity of the cooling times comes from the fact that we are trying to dissolve an ion in a non-polar fluid. This means that there must be some coulombic interaction between the solute and the solvent to screen the ions, or that the ions are not screened from each other, and are thus in close proximity to each other. This problem is, unfortunately, unavoidable and we need to find a way to generate charged ions from neutral molecules if we are to more properly address this problem.

A similar system which can also address this problem is the photodissociation of HgI_2. This has recently been studied by Pugliano *et al.* [42]. This system forms a

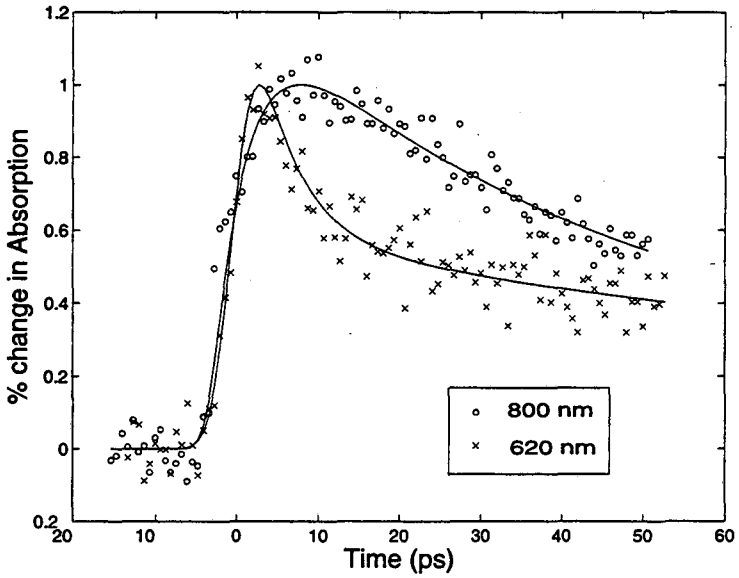

(a) CCl_4, $\mu = 0.0$

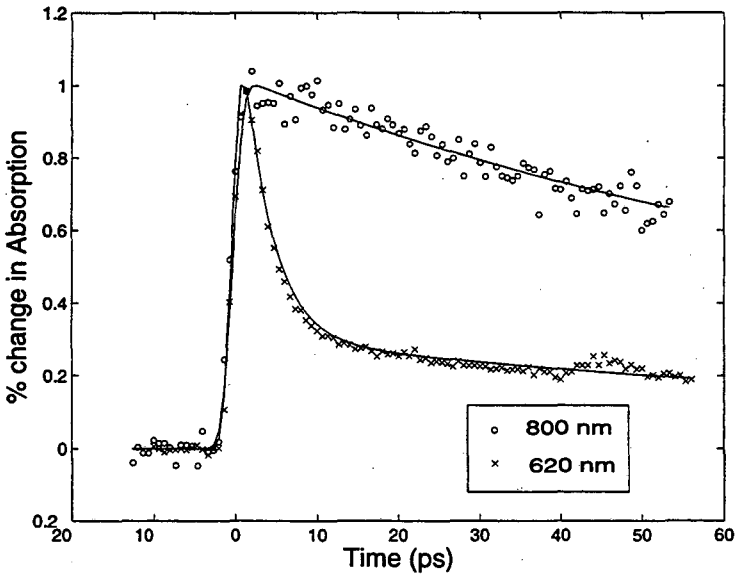

(b) $CHCl_3$,$\mu = 1.0D$

Figure 3.2: Vibrational relaxation of I_2^- in chloroalkanes. See reference [1] for experimental details

strong dipole, HgI, from a non-dipolar HgI_2 after absorption of a photon, and their data show that for HgI_2 in ethanol the vibrational cooling is <2 ps. This seems a perfect system to look at the effect of coulomb interactions. In the equilibrium state, HgI has a dipole of $\sim$ 2D, though at large internuclear separations, it converges to 0D, since it dissociates to Hg + I. HgI_2 also has reasonable solubility in non-polar solvents, and the HgI and I fragments formed from photodissociation are not charged and therefore the fragments are expected to separate well.

Data from HgI are shown in 3.3 on page 40. These transients have a growth of a new absorption in the visible which corresponds to the formation and cooling of the HgI fragment. Fitting results for the transients are shown in table 3.1 on page 39. A first trend which we see is that the cyclohexane and carbon tetrachloride do not have significantly different cooling times. More importantly, the data show that the long time offset is significantly larger for the non-polar solvents, and the short time cooling dynamics are much smaller. This suggests that there is some spectral shift in the absorbance of the HgI fragment between polar and non-polar solvents. Thus for the non-polar solvents we are seeing only formation of the HgI fragment in its vibrationally cooled state at 500 nm, whereas for the polar solvents we are looking at a vibrationally hot state at 500 nm.

To help clarify this matter, we performed experiments with Dr. Kliger at U. C. Santa Cruz. Using his nanosecond transient visible spectrometer, we were able to measure the spectrum of the HgI fragment at longer times after excitation. Repre-

sentative data in 3.4 on page 41 show the HgI absorption at 100 ns after excitation, and show an important difference between the methylene chloride and cyclohexane solvents: the HgI absorption in methylene chloride is significantly blue shifted with respect to HgI in cyclohexane, from 525 nm to 500 nm. This means that the energy in the HgI excited state is higher in methylene chloride than in cyclohexane, probably because of a change in the dipole between the ground and excited state. When the molecules is excited, the solvent is oriented to solvate the ground state, and thus is not equilibrated for the excited state. This increases the energy of the ground state with respect to the equilibrated state. (This effect is similar to the Stokes shift discussed in chapter 3.2.) Because of this spectral shift, the absorption at 500 nm is probing a different portion of the vibrational manifold in the non-polar solvents than in the polar solvents. This provides a good explanation for the picosecond data.

The next logical step would be to probe over a range of wavelengths in the visible region, especially further to the red. This work was planned, but before we were able to complete it, technical complications related to the picosecond laser system forced us to stop the work. It seems probable that in polar solvents we are seeing a transient decay which represents the vibrational cooling. In non-polar solvents, we see no decay, and know that the absorption is shifted to the red, and that we would thus be looking at the bottom of the vibrational manifold. Given this, the rise time at 500 nm should be related to the vibrational cooling, and in both cyclohexane and carbon tetrachloride the rise time is 2 - 3 ps, similar in time scale to the polar solvent.

Solvent	τ_1(ps)	%	τ_2(ps)	%	Offset %
CCl_4	3.5	22	11.7	5	73
C_6H_{12}	5.8	4	99	15	81
CH_2Cl_2	3.0	71	50	16	14
CH_3CN	2.1	40	110	28	32
C_2H_5OH	2.5	36	140	23	41

Table 3.1: Fitting parameters for HgI vibrational relaxation. The percentages (%) are the relative amplitudes of the fast and slow decays, and the long-time absorbance change.

It can be thus concluded that the interaction of a permanent dipole with the dipole of a solvent does not considerably alter the vibrational cooling in this system. This is in agreement with data for IBr and IBr^- studied earlier by King [22]. There are still many questions which remain to be answered, and much work which can be done in this field.

3.2 Solvation

An important part of understanding the reactions of molecules in condensed phase is understanding how the intermediates interact with the surrounding solvent. In many reactions there are large changes in the charge distribution after after excitation, and the way the new charge distribution interacts with the solvent can be very important. As an example, if one looks at an S_N2 reaction, (see 3.5 on page 43) one can see the importance of this effect. At early times before the reaction, the I^- ion is on the right, and the solvent is equilibrated for that charge distribution. At the transition state, however, the two halide atoms are equally charged, and the overall

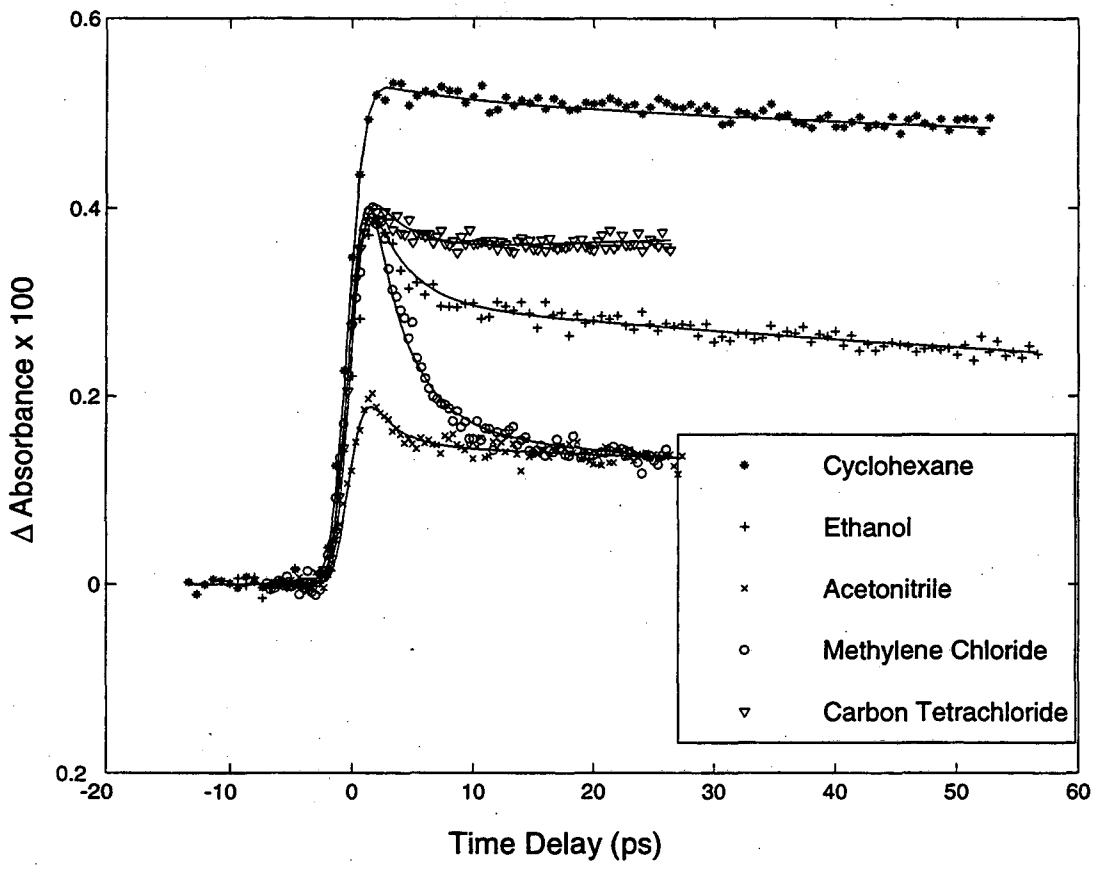

Figure 3.3: HgI absorption at 500 nm in a variety of solvents.

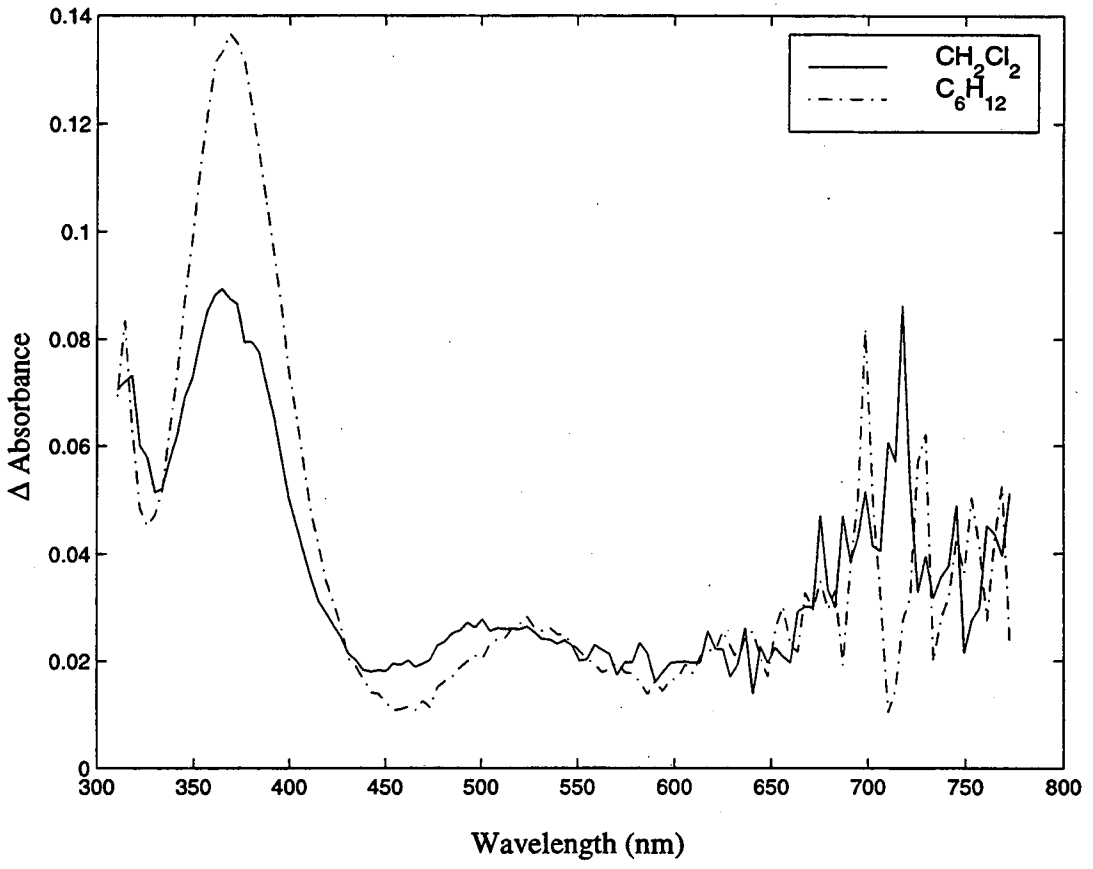

Figure 3.4: Spectrum of HgI fragment 100 ns after photexcitation by 266 nm pulse

dipole is zero. In the final product, the iodine is not charged, but the chlorine atom is, and so that solvent must change to solvate this new charge distribution. The most important time to understand is when the complex is near the transition point, because that is when the charge is changing the most. When it is in this state, the solvent is oriented toward solvating the iodine atom as a negatively charged ion. In order to proceed to product, it must overcome the unfavorable solvation and push the negative charge over to the chlorine. To understand the effect of this solvation on the course of the reaction, we can imagine two extremes. In the first, the solvation is very slow with respect to the movement along the reaction coordinate. As it moves toward the transition point, the solvent is still solvating the initial charge distribution, and so in order to cross through the transition state, it must move up in energy into a non-favorable solvation state. Thus it will be more energetically favorable to return to the original reactants, rather than to form products. At the other extreme, where the solvent fluctuates on a very short time scale, one can imagine that in the time when the molecule is near the transition state, the solvent responds very quickly to the change in charge distribution, so there is no energy cost to moving into the product form, and therefore the reaction is more likely to proceed to products. Thus, in order to understand these reactive conditions, we need to understand solvation on a short time scale.

Many measurements have been made on solvation dynamics. The most common experimental method is to measurement the time dependent Stokes shift of a dye

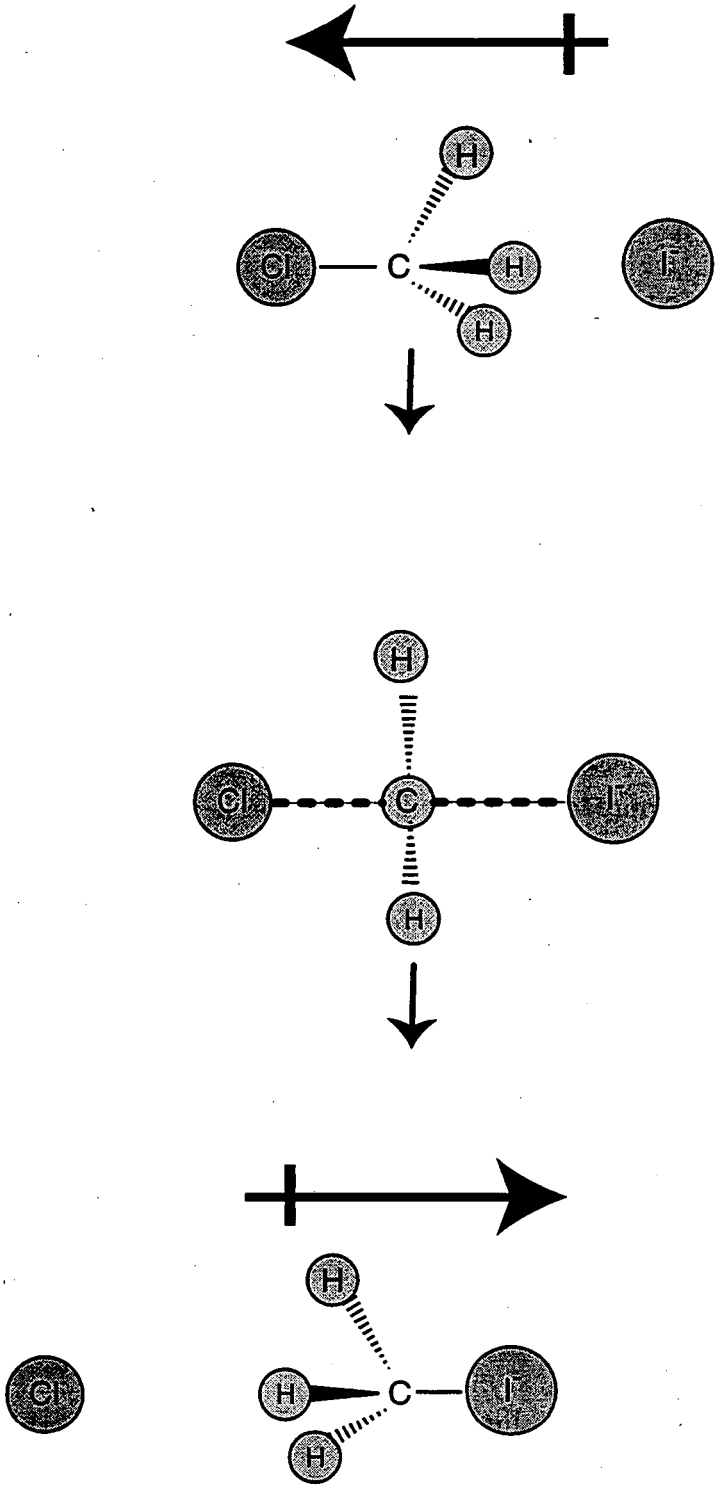

Figure 3.5: Evolution of the dipole moment of a molecule during an S_N2 reaction

dissolved in some solvent. A dye is chosen which has a large dipole change between ground and excited states, and this dye is excited by an ultrashort laser pulse. As it is initially formed in the excited state, it is in a non-equilibrium solvation state, and this increases the energy of the excited state with respect to the ground state. This means that fluorescence to the ground state is blue shifted from the equilibrium fluorescence. As the solvent reorganizes to solvate the new charge distribution, the fluorescence red shifts and the time scale of this shift can be used to measure the solvation time. This method of measuring time dependent Stokes shift has been extensively reviewed by Jarzeba and Barbara [43], and a series of recent studies, including a good theoretical development has been published by Rosenthal *et al.* [44].

An interesting approach to studying solvation is shown by Lian *et al.* [45]. This approach involves probing the change in solvent infrared bands following excitation of a solute for shifts in their frequency due to the change in the charge environment. In this approach, one uses a solvent such as acetonitrile, which has a narrow intense infrared absorption. After excitation, the changes in the electrical environment due to the excitation of the solute will cause changes in the frequency of this band. By tracking this band through time, it is possible to measure the solvation time. This has the advantage of measuring solvent properties directly, rather than indirectly through the electronic states of the solute. Measurements using this methodology have been made by Lian et al [45] using LDS750 dye. These show that the signal size is small, but that it is possible to measure solvent responses in this way. They were able to

make measurements which were in rough agreement with previous data from Stokes shift measurements.

One of the difficulties of understanding the results of these measurements, and also the earlier Stokes shift measurements, is that while the charge distribution of the ground state is well known, the charge distribution of the excited state is not. This means that it can be difficult to build good models for the relaxation process. Another difficulty is that the molecules are large and complex, and dynamics in the molecule, including new vibrational modes and low lying excited states, can contaminate the solvation signal. An important advance would thus be the use of a smaller, better understood system, where we know all of the vibrational modes in the ground and excited state, and where we know the charge distributions in both the ground and excited state.

A system which fits these criteria is the $Os(bpy)_3$ system. It is well known that the photoexcitation is a metal to ligand charge transfer (MLCT) state onto one of the bipyradyl rings. In the ground state it has no dipole, but the excited state has a dipole pointing from the Os metal center to the bipyradine to which the electron has been transferred. A tremendous advantage of using this chemical system is that it is very well understood. It is possible to use electrochemical methods to produce an analog of the excited state, and to measure its spectrum and other properties. It is also much easier to perform calculations on this class of molecules because of the symmetry of the ligands. Calculations by Daul *et al.* [46] show that it is possible to

perform *ab initio* calculations on the similar $Ru(bpy)_3$ system, and they were able to calculate very specific properties of the excited states of this molecules.

Initial experiments were carried out in CH_3CN in hopes of seeing the shift in the CN stretch frequency at 2237 cm^{-1}. Results are shown in figure 3.6 on page 48, and fitting data is shown in table 3.2 on the facing page. We note first that there is a signal which is *very* broad, more than 300 cm^{-1}. This is similar to the signal which we saw in LDS750 in CH_3CN [47], and far too broad to be a simple stark shift of the CN stretching band. We also studied $Os(bpy)_3$ in various solvents, and the results are shown in figure 3.7 on page 49. Note that the signal in methylene chloride is almost identical to the signal in acetonitrile and benzonitrile, even though it has no absorptions in this region of the spectrum. Note also that the time behavior is similar in all three solvents even though previous work [43] suggests that they should show very different solvation times.

A potential identity for this IR absorption is an inter-ligand electron transfer state (ILET). In this picture, the $\sim$2000 cm^{-1}represents the energy difference for moving the excited electron from one bipyradyl ligand to another, and thus the time scale for the decay represents the localization of the charge onto one bipyridine ligand. This ILET state has been studied by Kelley and co-workers [48, 49] using picosecond visible anisotropy measurements. However they found that the times for decay for these ILET states are on the 10's of picosecond time scales, and so are much longer than we have observed.

λ (nm)	ν (cm^{-1})	τ_1 (ps)	amp.	τ_2 (ps)	amp.	offset
4348	2300	–	–	2.0	.60	.49
4545	2200	.30	.82	1.8	.20	.79
4651	2150	.40	.45	9.0	.33	.41
4762	2100	.40	1.07	5.0	.76	1.1
5000	2000	.10	3.24	1.1	1.4	1.7

Table 3.2: Fitting parameters for solvation of $Os(bpy)_3$ in CH_3CN

Another possible explanation for the signal is that there is solvent or window signal at that wavelengths which we are probing. If we look at the anisotropy data in figure 3.8 on page 50, we see that the signal has a definite non-zero anisotropy after t_0, and so there must be some correlation between the orientation of the excited $Os(dpb)_3$ molecule and the mode which is absorbing the IR light. More likely we are seeing the absorbance from an excited state, or from the ILET state, both of which would be correlated. This is an interesting system, which definitely warrants further study.

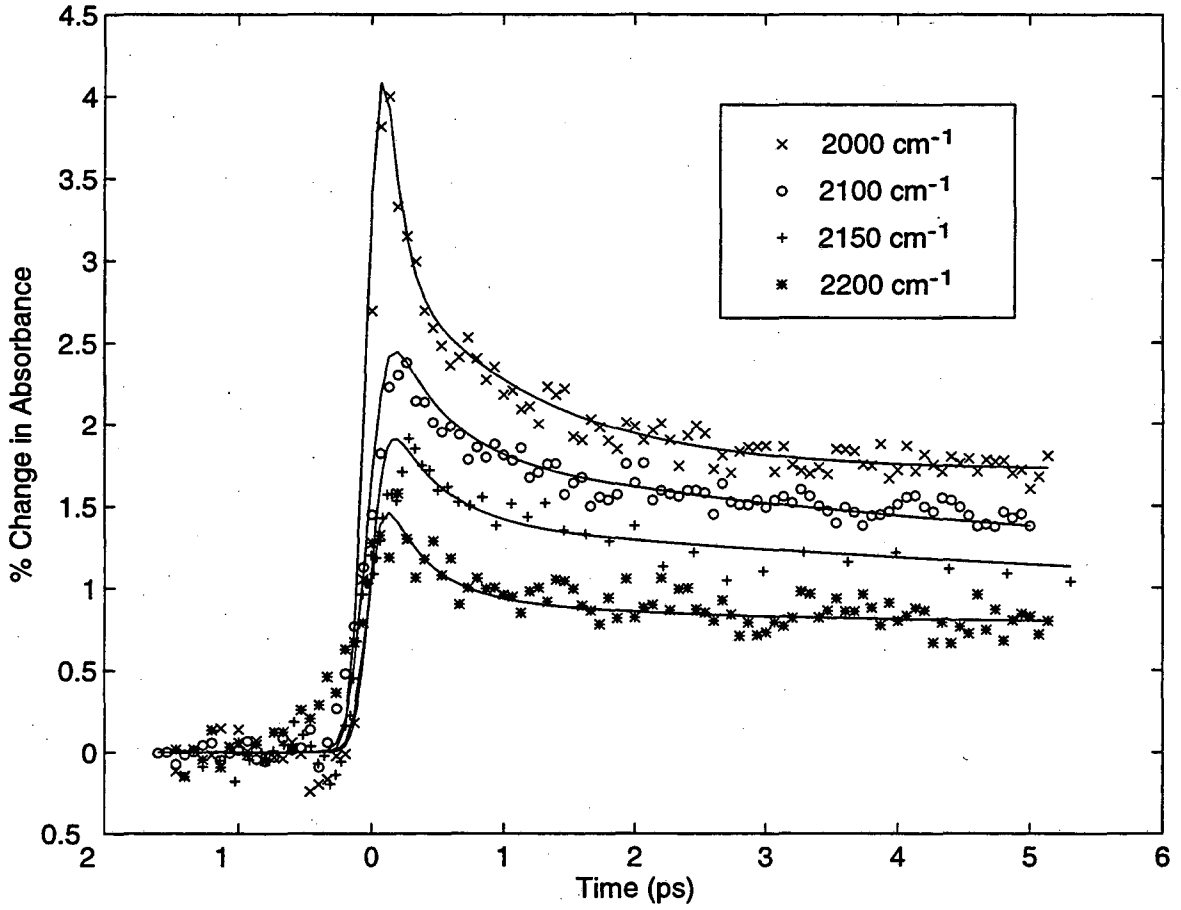

Figure 3.6: Transient absorption of $Os(bpy)_3$ after photoexcitation in CH_3CN

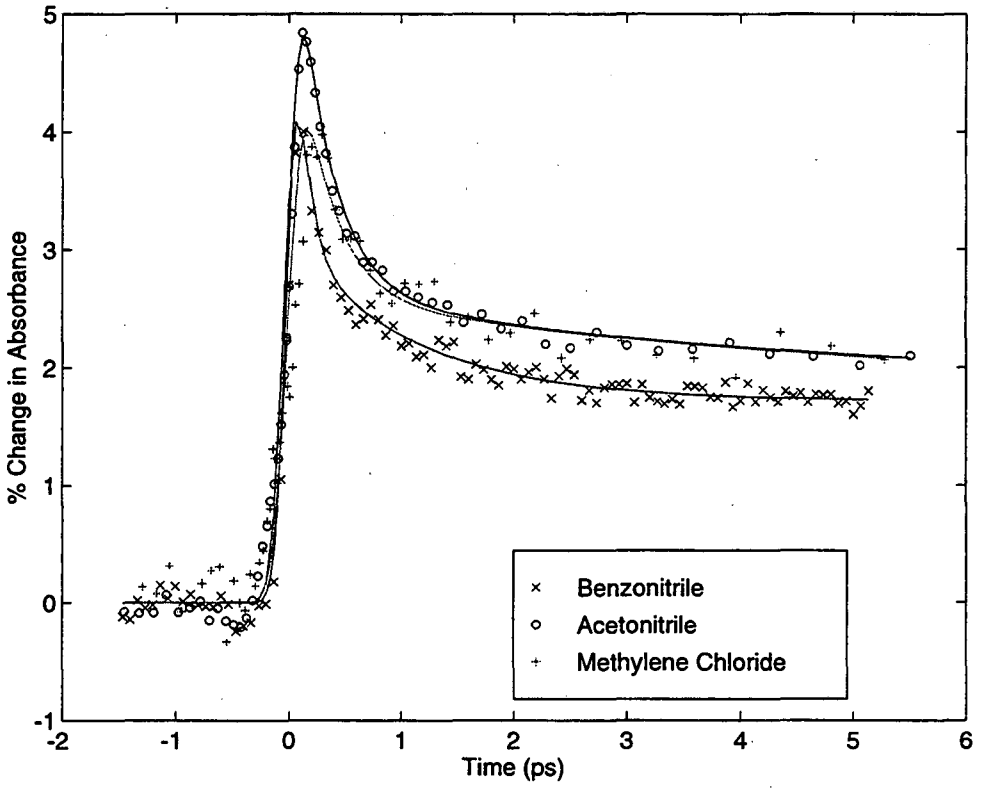

Figure 3.7: Transient absorption of $Os(bpy)_3$ in various solvents at 2000 cm^{-1}

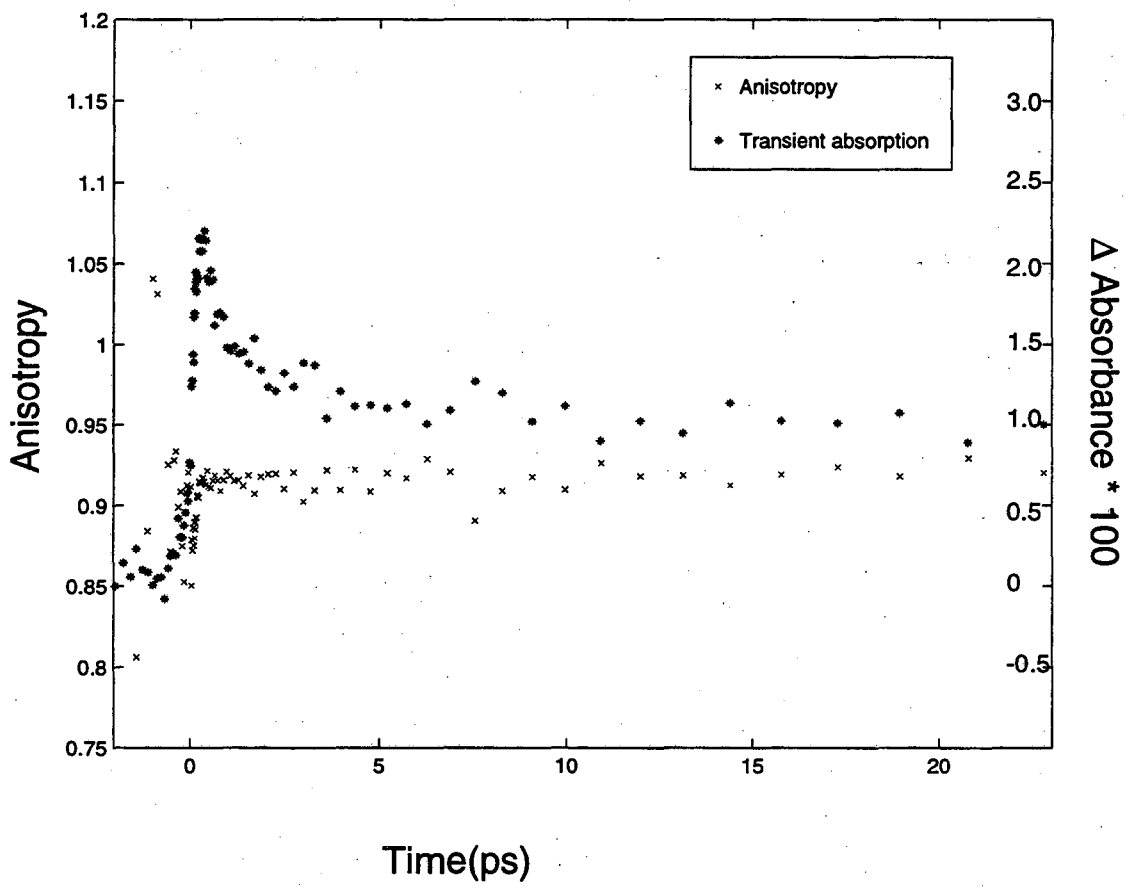

Figure 3.8: Anisotropy of $Os(dpb)_3$ after photoexcitation in CH_3CN at 5000 cm^{-1}

Chapter 4

Mechanisms of C-H Activation Reactions

4.1 Introduction to C–H Activation Chemistry

One of the richest chemistries known is that of Carbon and its compounds. The earth is filled with reserves of carbon, much of it in the form of alkanes. This form is common because it is very unreactive, as evidenced by its traditional name *paraffin*, coming from the Latin *parum affinis* meaning without affinity. We have over time developed a way to break C–H bonds, but unfortunately it has mostly involved the making of C–O bonds as part of combustion. While very useful, it is not a particularly good chemical use of these substances.

The development of room temperature, catalytic methods for functionalizing C–

H bonds in alkanes has been an area of active research. The ability to perform this chemical transformation is important for several reasons. Firstly, the standard methodology for functionalizing alkanes involves high temperature, high pressure, free radical reactions with halogen gas leading to alkyl halides. The free radicals are reactive enough to break the ~100 kcal/mol C–H bonds in the alkane, and the resulting alkyl chloride has a C–Cl bond which is 84 kcal/mol. This means that we are crossing a barrier which is very large in comparison to the energy difference between reactant and product. Thus, we are expending much more energy than necessary to break the C–H bond. Secondly, the free radical reaction breaks all types of C–H bonds, but with the reactivity:

$$C_6H_6 > 3°C > 2°C > 1°C > CH_4 \tag{4.1}$$

Thus in a $HC(CH_3)_3$, one would expect that the primary product would be $ClC(CH_3)_3$, but with $HC(CH_3)_2(CClH_2)$ and $ClC(CH_3)2(CClH_2)$ as minor products. While this is useful, one is often interested in functionalizing bonds in other orders, especially favoring primary carbons on longer chains. This functionalization is not easy to do with free radical mechanisms. Finally, one is often interested in breaking a C–H bond in a compound which is too unstable to survive the high temperatures in free radical reactors. A method which could break specific bonds in a molecule at room temperature would allow more selective reactions as part of a larger synthetic

framework.

It has been long known that homogeneous activation of H_2 is possible using organometallic compounds. This has been established by the study of H–D exchange [50, 51]. It is also well known that heterogeneous catalysis systems are able to break C–H bonds, and that it should be possible to mimic the reactivity of these systems with single molecules. The important part of the reaction is to develop an organometallic complex which is sufficiently electrophilic, that it is thermodynamically favorable to form the alkyl hydride metal complex from the alkane complex. Further, in 1971 Jetz and Graham found that the Si–H bonds in silanes could be activated with a photochemically initiated homogeneous catalyst, using the general reaction scheme:

$$M(CO)_n + R_3SiH \rightarrow R_3SiMH(CO)_{(n-1)} + CO \qquad (4.2)$$

where M = Cr, Mn, Co or Fe and R=C_6H_5 or Cl [52]. This suggested that activation of C–H bonds using similar methods should be possible.

A pair of important breakthroughs came almost simultaneously in 1982. First Janowicz and Bergman [53] reported that photolysis of $CpIrP(R_3)H_2$ (R = Ph or Me) in benzene formed as a product $CpIrP(R_3)(H)(Ph)$. The irradiation is important because it provides a means to make very reactive intermediates, since the energy in a UV photon is large in chemical terms. It was also shown that the complex was

reactive with alkanes as well as arenes. The second discovery came later that year by Hoyano and Graham [54] who showed that the similarly structured $Cp^*Ir(CO)_2$, when photolysed in alkane or arene solution, yielded a C–H activated product.

While these reactions were known to work, little was known of the mechanisms involved in the reactions. Early measurements showed that the reactions proceeded quickly enough that simple measurements of the mechanism were not possible. The initial approaches to understanding the reactions involved attempts to slow down the reactions to allow intermediates to be observed.

The simplest way to slow down the reaction is to remove the solvent. The reaction proceeds by interaction of the metal complex with the surrounding solvent, so if the solvent is removed it should be possible to isolate the initial photoproduct. This was done by Wasserman *et al*, who studied the $CpRh(CO)_2$ system in the gas phase. [55,56]. Their measurements showed an instantaneous bleach at 2003 and 2060 cm^{-1}, and the appearance of a new peak at 1985 cm^{-1}. The bleaches coincide with the ground state absorbance of the symmetric and anti-symmetric CO stretches in the parent compound, and so the disappearance of these peaks must result from the breaking up of the parent compound. The appearance of a single CO stretching band in the product suggests that the photon is exciting the complex such that one CO ligand dissociates, leaving a CpRh(CO) monocarbonyl fragment. Addition of a small amount of alkane caused the creation of another peak at 2037 cm^{-1}250 ns after photoexcitation. This was assigned to be the activated alkyl hydride product.

It is well known that mechanisms can differ in liquid phase from the gas phase, and so it was important to look as liquid phase reactivity. In order to slow down the reaction, it is necessary to add a diffusion controlled step in the reaction scheme. Unfortunately, the metal monocarbonyls formed after photoexcitation are extremely reactive. This reactivity is necessary to enable them to break the C–H bonds, but it also means that they are reactive to almost all liquids, including fluorinated solvents, so studies were difficult. Bengali *et al.* [57, 58] studied the reaction of the closely related $Cp^*Rh(CO)_2$ (where Cp^* is the methylated form of the Cp ligand) in liquid Kr and Xe, the only solvents which were known to be completely unreactive. In these solvents the reaction follows the following scheme:

$$Cp^*Rh(CO)_2 \xrightarrow{h\nu} Cp^*Rh(CO)(S) \rightleftharpoons Cp^*Rh(CO)(HR) \rightarrow Cp^*Rh(CO)(H)(R) \quad (4.3)$$

where S is either Kr or Xe, and R is and alkyl group. Assuming that the concentration of alkane is small, the monocarbonyl will form a complex with a Xe or Kr solvent atom immediately after formation, and this solvent will exchange with an alkane at a diffusion controlled rate to form an alkane complex, and finally a C–H activated product. Thus they were able to measure the rate of the C–H bond activation process by looking at the concentration dependence of the rate in rare gas solution. They measured a rate of $\sim 20\mu s$ for activation of neopentane at 163 - 193 K. Further work by Schultz *et al.* [59] which studied cyclohexane shows that the k of the reaction is

$7.6 \times 10^{-4} s^{-1}$.

While this provides important insight into the reaction mechanism, it would be preferable to measure the reaction dynamics directly. The first direct, ultrafast infrared measurements on C–H activating compounds were made by Heilweil and coworkers [60,61] who studied $Cp^*Rh(CO)_2$ and $Cp^*Ir(CO)_2$ using ultrafast IR absorption spectroscopy. They found that there were no new monocarbonyl peaks observable in the spectrum. This supports the assertion that the initial species formed in C–H activation reactions is a monocarbonyl, and that the non-reacting excited molecules remain as dicarbonyls. More recently, Bromberg *et al.* [62] studied C–H activation by $Cp^*Ir(CO)_2$ using ultrafast visible spectroscopy. They observed a new electronic absorption after photoexcitation, which decayed away after 30 - 40 ps. They concluded that the low quantum yield is due to the partitioning between a CO dissociative state and their observed non-dissociative electronic excited state.

In order to understand the mechanism of theses reactions, it is necessary to study a system in which a larger percentage of excited molecules are in the CO dissociative state. The molecule $Tp^*Rh(CO)_2$as studied by several different groups [63–67] has a quantum yield of 30%, providing a sufficient concentration of intermediates to measure their structural changes. The Tp^* generally shows similar chemistry (a good review comparing C–H activation in Cp, Cp^* and Tp^* systems has recently been published by Lees [68]) to the Cp and Cp^* ligands and so is a good molecule for comparison to previous work.

Ultrafast studies of the C–H activation by the $Tp^*Rh(CO)_2$compound [69–71] have established the mechanism of this reaction. Figure 4.1 on page 59 shows the spectrum of the $Tp^*Rh(CO)_2$chemical system at several times after photoexcitation. At the earliest times, we see a bleach at 1980 and 2050 cm^{-1}corresponding to the depletion of the parent CO absorptions. At early times we also see a new peak, due to an intermediate A1 at 1972 cm^{-1}. It is known that this species is a monocarbonyl since there are no other peaks in the spectra. The small peaks on the low energy end are higher vibrational states which are initially populated due to the excess energy from the photon. Kinetic scans, shown in figure 4.2 on page 60 allow us to measure the time constant for peaks in the spectrum. After 23 ps, the molecule is cooled and the peaks have coalesced into a single peak at 1972 cm^{-1}. This vibrational cooling time is comparable to those found in work on other metal carbonyls such as $CpCo(CO)_2$ [60, 72], $(acac)Rh(CO)_2$ (acac=acetyl acetonate) [73] and $M(CO)_6$ (M=Cr, Mo or W) [30, 69, 74, 75]. Intermediate A1 then decays away with a time constant of 200 ps.

On the same time scale, a new intermediate A2 grows in with a CO absorption at 1992 cm^{-1}. This species also contains only one CO stretch, and so is also a monocarbonyl. From the spectral shift of the stretching frequency (20 cm^{-1}higher in energy) it can be inferred that the electron density on the metal center has decreased. This means that there is less back-bonding into the CO stretch and a correspondingly higher vibrational frequency. Ultrafast measurements show that A2 persists to >1 ns,

but nanosecond step-scan measurements show that in cyclohexane it has a lifetime of 230 ns, and that it quantitatively converts to the final C–H activated product which has a CO absorption at 2032 cm^{-1}.

4.2 Changes in Coordination of the Rh Metal Center

One of the most interesting features of the reaction of $Tp^*Rh(CO)_2$is the change in connectivity between the Tp^* ligand and the Rh metal center during the course of the reaction. There has been much speculation in previous work about the possibility of "ring slip" in Cp-metal systems, and the importance of that in the reactivity of those compounds. [63,76–84] This previous work highlights the fact that it is possible for molecules to undergo changes in ligand connectivity in order to stabilize reaction intermediates. Most of the evidence which has been shown has focussed on showing that a reaction is associative in nature, and thus there must be a change in the ligand to avoid an extremely unstable 20-electron intermediate.

The $Tp^*Rh(CO)_2$C–H activation system is extremely interesting in this regard for two reasons. First, it has been well established by previous work on this system [69,70] that this system proceeds through a dissociative mechanism. [1] What makes it most

[1]The difference between an associative mechanism and a dissociative mechanism involves the order of the bond breakage and formation steps. In an associative mechanism, the entering ligand complexes first, and then the leaving ligand detaches. In a dissociative mechanism, the leaving ligand detaches, leaving an coordinatively unsaturated metal center, and then the entering ligand

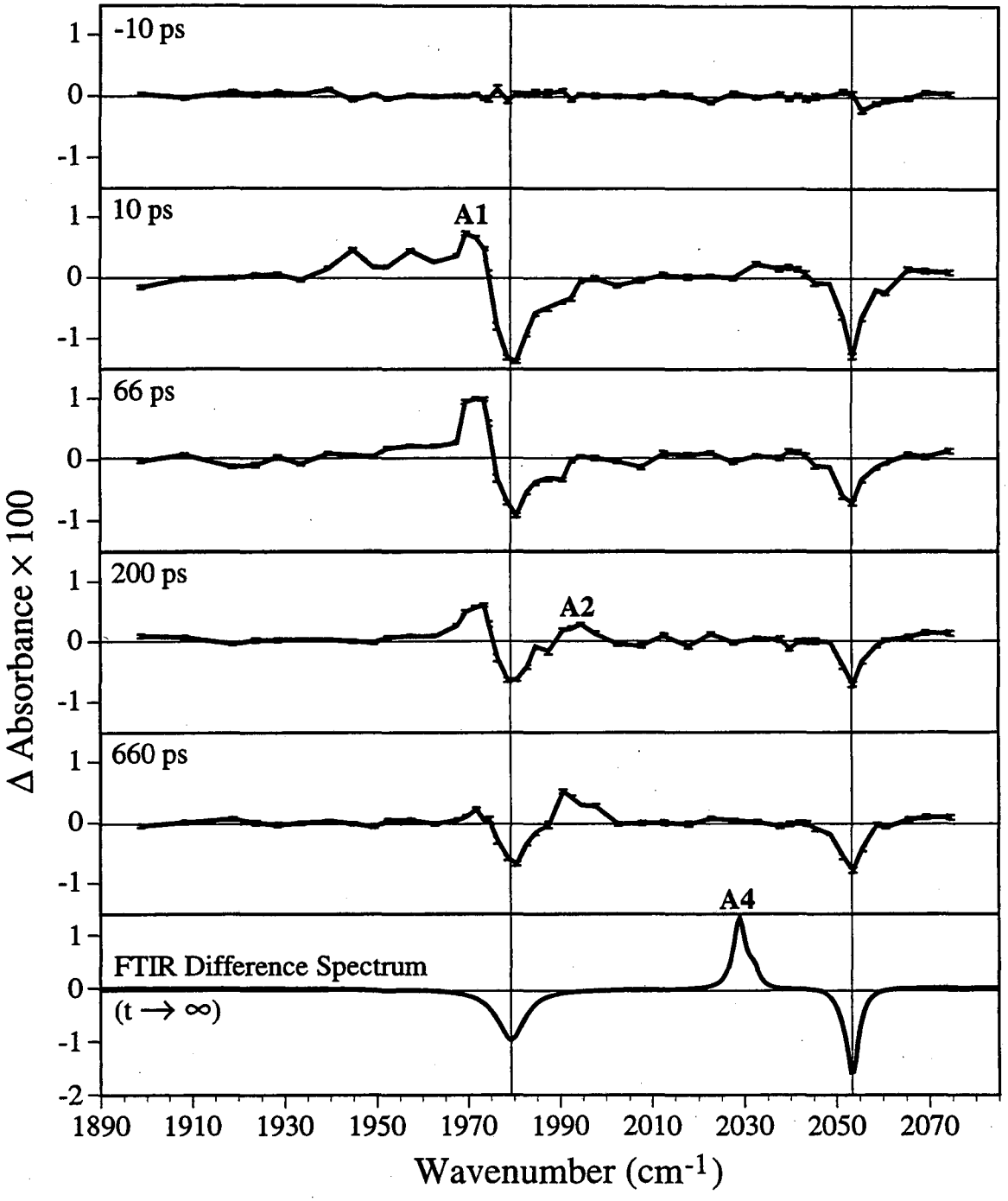

Figure 4.1: Femtosecond spectra of C–H activation by $Tp^*Rh(CO)_2$in cyclohexane, showing intermediates **A1**, **A2** and the final product **A4**

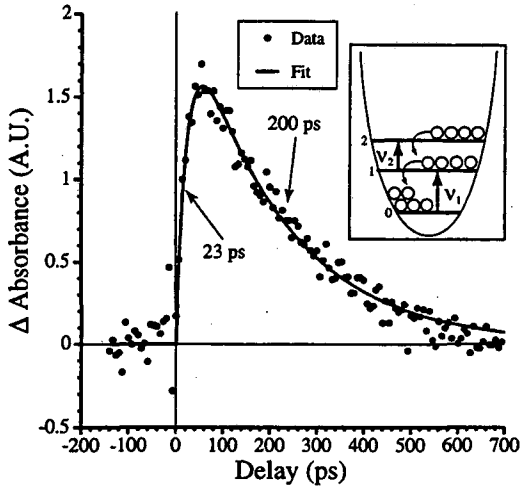

(a) Initial solvent complex at 1972 cm^{-1}. Rise time is due to vibrational cooling of the complex, and decay is due to conversion to η^2 complex

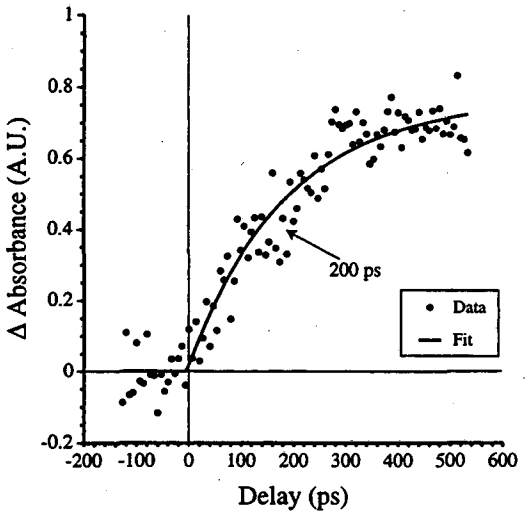

(b) η^2 solvent complex at 1990 cm^{-1}. Rise time shows formation time of the complex

Figure 4.2: Femtosecond dynamics of intermediates A1 and A2. Inset shows a schematic of vibrational cooling. ν_1 is the frequency of the 0-1 transition (1972 cm^{-1}), and ν_2 is the frequency of the 1-2 transition (1955 cm^{-1})

interesting is that even though it is known to be dissociative, there is still a ring-slip like step in the reaction scheme.

In the $Tp^*Rh(CO)_2$system a question of considerable interest is the order of the final reaction. Previous work has shown [69,70] that after 200 ps, the monocarbonyl solvent complex changes from η^3 to η^2. In cyclohexane, 230 ns after initial photoexcitation the C–H bond is broken, and the final product is in an η^3 state. When we exposed the similar bis-pyrazole Rhodium analog, $Bp^*Rh(CO)_2$, to light when dissolved in cyclochexane, we observed that no matter how much light is absorbed or how much time is allowed, the $Bp^*Rh(CO)_2$ never shows any C–H activated product formation. [63,67,85] This suggests that the η^2 rhodium complex is not capable of breaking the C–H bond and that therefore the transition state must involve the η^3 complex rather than the η^2. This further suggests that the $Tp^*Rh(CO)(S)$ complex must break the C–H bond when the Tp^* ligand is in the η^3 state.

Looking at the dynamics of the processes involved in the reaction, (see figure 4.5 on page 66) we know that the de-chelation of the Tp^* ligand happens 200 ps after photoexcitation. Since the third pyrazole ring is still attached to the Tp^* ligand, we would expect that the re-chelation would also happen on a time scale comparable to or shorter than the 200 ps of the De-chelation. Density functional theory results by Hall et al [86] show that there is only a small energy difference between the η^3 and η^2 monocarbonyl solvent complexes. He found that an η^2 intermediate was stabilized by

---

attaches.

9 kcal/mol, and that the shift in the CO stretch due to forming the η^2 intermediate matched the experimental results. We can thus assume that there is only a small barrier to changes in chelation state, and so this should be a fast process.

Breaking the C–H bond, on the other hand, should have a large barrier of activation. If we assume that the rate limiting step in the reaction is the breaking of the C–H bond, then we need to understand the importance of the Tp* ligand in the reaction. Given the time constant of the final reaction, we know that if the final part of the reaction is stepwise, then it must be < 50 ns since see a single exponential rise for the product and decay for the intermediate. One possibility is that the rate limiting step is the re-chelation and then the C–H bond breakage takes place quickly. This makes little sense since the barrier for re-chelation is so much less than the barrier for C–H bond breakage. A second possibility is that the C–H bond breakage is the rate limiting step, and that the re-chelation occurs quickly. This would imply that the C–H bond would be broken by an η^2Tp*Rh(CO)(RH) complex, however we know that the very similar Bp*Rh(CO)$_2$ does not activate C–H bonds. [63, 67, 85] This suggests that the η^2Tp*Rh(CO)(RH) complex, which is very similar to the Bp*Rh(CO)(RH) complex, cannot activate the R–H bond, and thus the activation does not occur from the η^2 state.

A final possibility is that the Tp*Rh(CO)(RH) exists in an equilibrium between η^2 and η^3 states, with the C–H activation occurring in the η^3 state. IF this is true, we would expect to see a small peak at 1972 cm^{-1}, with time behavior similar to

the behavior of the peak at 1990 cm^{-1}. If we look at the time resolved spectra in figure 4.3 on the following page, there is a small peak at 1972 cm^{-1}. The peak is on the low energy side of the parent bleach, which makes it hard to be sure if this is a peak, or a spectral artifact. If we look at the kinetics of this peak (shown in figure 4.4 on page 65, we can see that this peak changes through time. If we fit the dynamics of this peak in cyclopentane or cyclohexane, we see that the dynamics are well correlated with the dynamics at 1990 cm^{-1}, and the growth of the final product at 2032 cm^{-1}.

This gives us a new picture of the reaction scheme, which is slightly different from the mechanism as originally published [70]. It is shown in figure 4.5 on page 66. We have the same initial photodynamics, with the prompt dissociation of the CO, and formation of the solvent complex, followed by vibrational cooling and partial de-chelation. As in the case of the ground state $Tp^*Rh(CO)_2$, there is an equilibrium between the η^3 and η^2 forms, though in the monocarbonyl solvent complex the equilibrium favors the η^2 form of the intermediate. The η^2 intermediate, then, provides most of the IR signal but it doesn't actually participate in the reaction, but takes population away from $\eta^3Tp^*Rh(CO)(RH)$, the reactive intermediate . From the initial de-chelation time, we know that the equilibrium is fast enough that it does not change the dynamics of the reaction. Comparison of the η^2 Tp^* complex with the η^2 Bp^* complex, which does not activate C–H bonds, suggests that the η^2 complex is not the reactive complex.

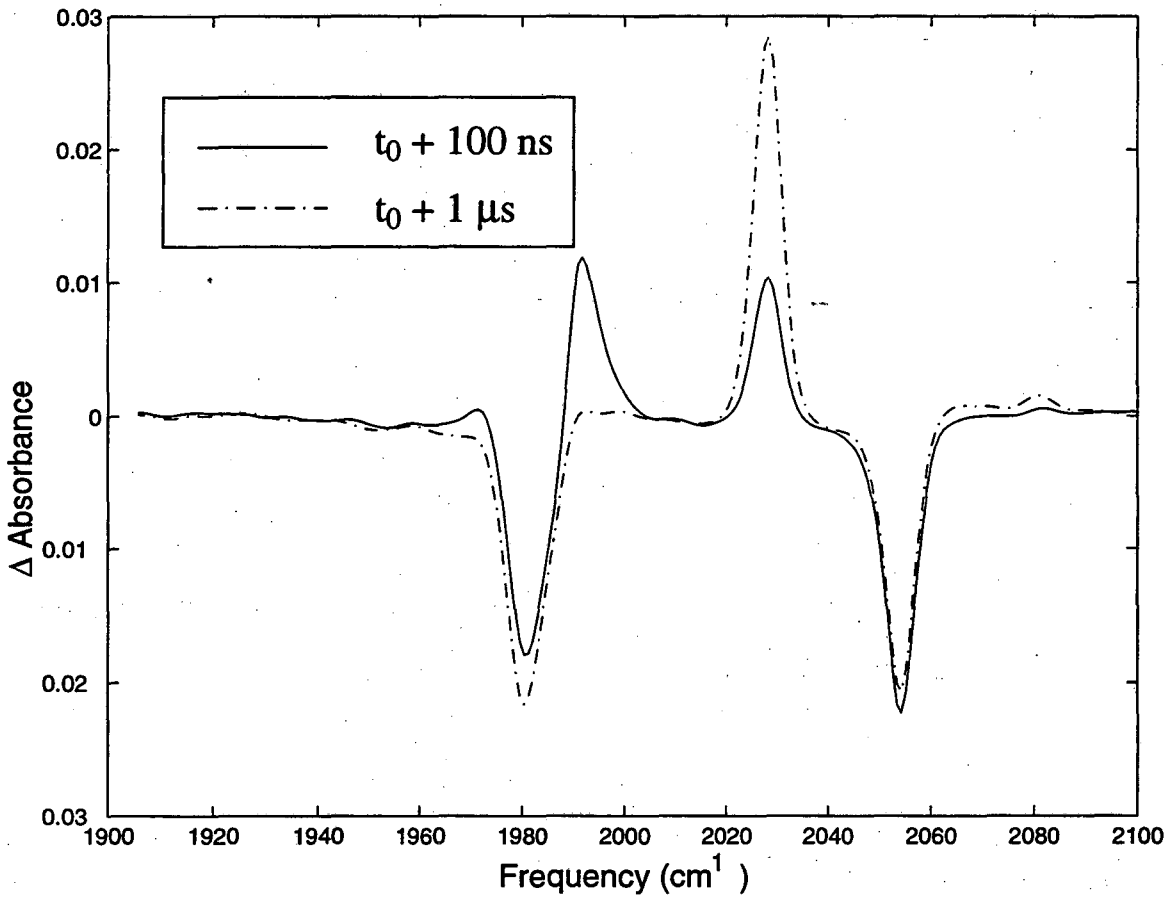

Figure 4.3: Time resolved spectra of C–H activation by Tp*Rh(CO)$_2$in cyclopentane. Note the peak at 1972 cm^{-1}which represents an η^2 intermediate

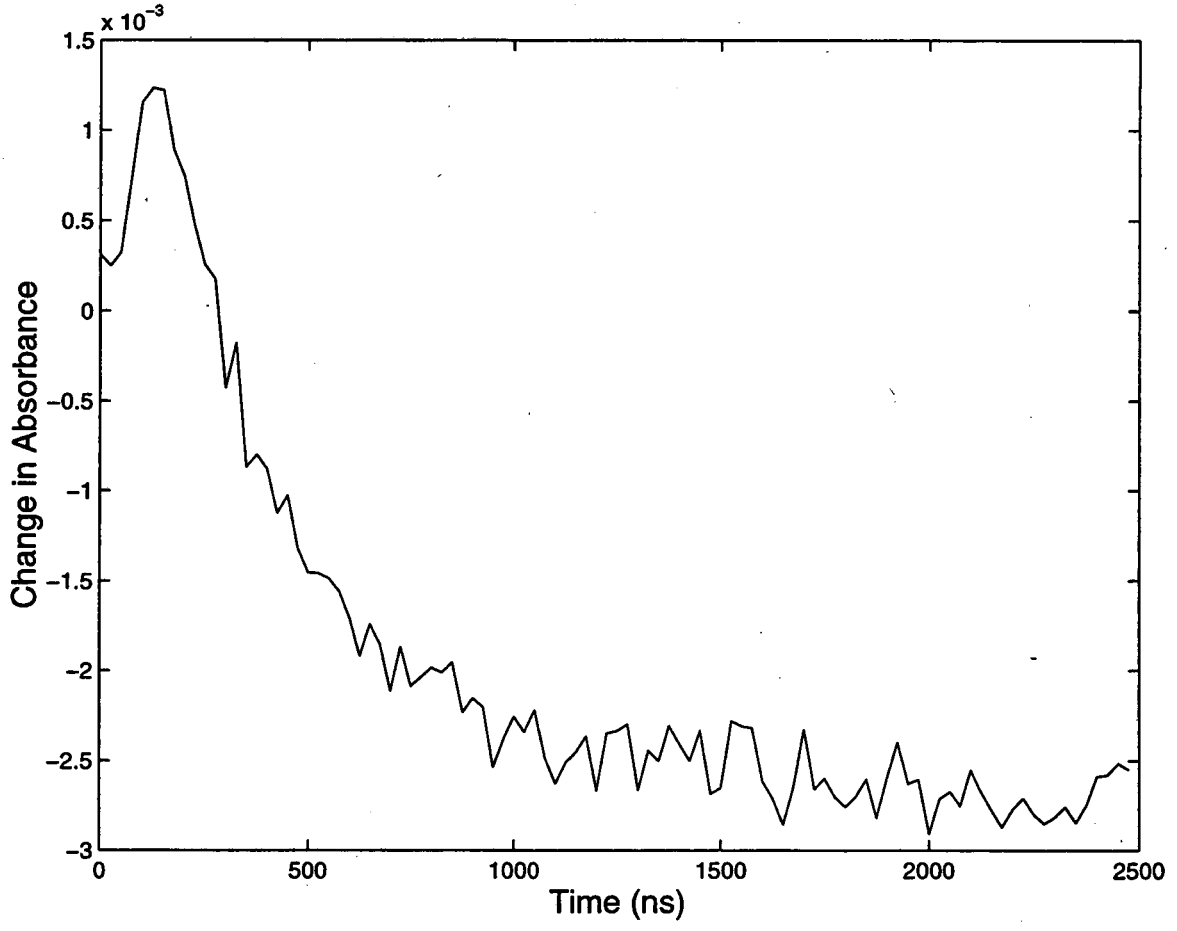

Figure 4.4: Kinetics of 1972 cm^{-1}peak in cyclopentane. The time constant is $\sim$ 200 ns, which is the same as the C–H activation time.

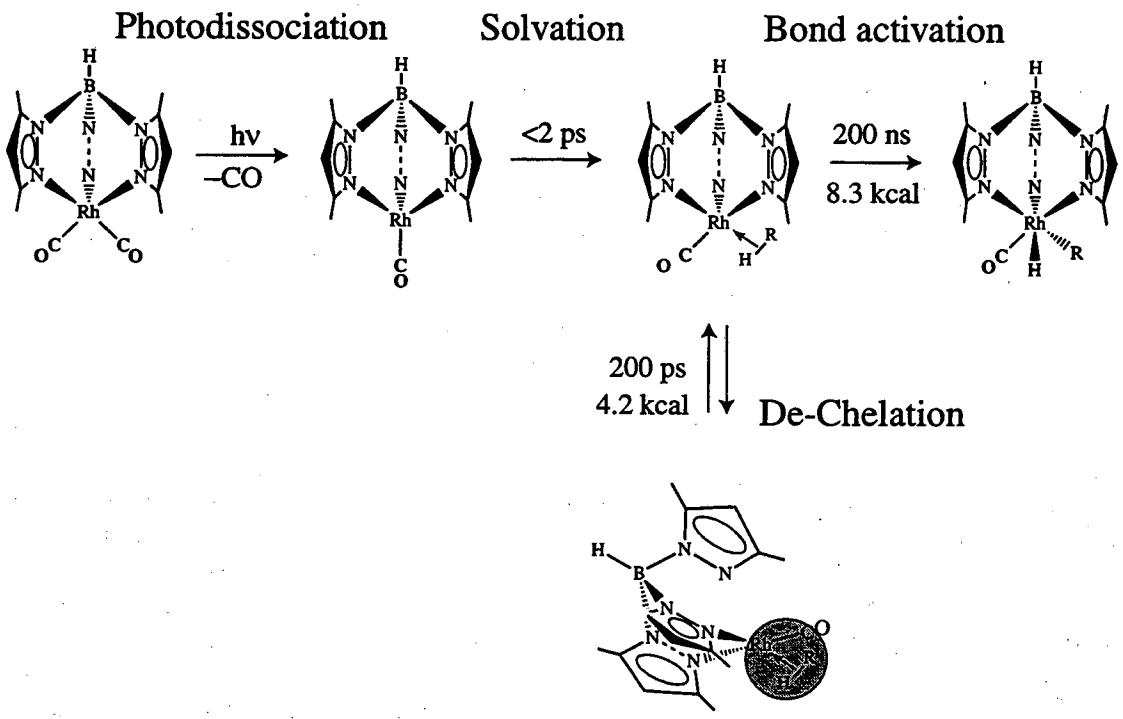

Figure 4.5: Proposed mechanism for the C–H reaction of $Tp^*Rh(CO)_2$.

This then suggests an important conclusion: That the de-chelation and re-chelation dynamics do not participate in the chemistry at all, and only effect the spectroscopy. This is important because this makes this system much more comparable to the $CpRh(CO)_2$ system, a system which has received considerably more study.

Recent studies on the C–H activation of alkanes by $CpRh(CO)_2$ have been carried out using nanosecond step-scan FTIR spectroscopy. Even though the quantum yield is only 1%, compared to 30% for $Tp^*Rh(CO)_2$, it is much more soluble than $Tp^*Rh(CO)_2$in alkane solutions, making detection of product formation possible. Figure 4.6 on the next page shows the nanosecond spectra and kinetics for the formation of the final C–H activated product for the photoreaction of $CpRh(CO)_2$ in cyclohexane. Fitting of the data to a standard instrument response function shows that the growth of the product peak is faster than 30 ns. making it much more similar to the reaction of linear alkanes in $Tp^*Rh(CO)_2$than cyclic alkanes in $Tp^*Rh(CO)_2$. This may be because of decreased steric hindrance from the Cp ligand compared to the Tp^* ligand. This is a system which warrants further study, especially since it can bridge the gap between the current time resolved infrared work and the work by the Moore and Bergman group here at U. C. Berkeley.

A recent comparison for the $Tp^*Rh(CO)_2$ C–H activation system is the recent work reported by Wick and Goldberg [87]. They have studied a similar system, Tp^*PtMe_3. This system starts out as η^2 in Tp^*, with the four ligand connections in a square planar geometry around the Pt(II) metal center. Their reaction proceeds by extracting one

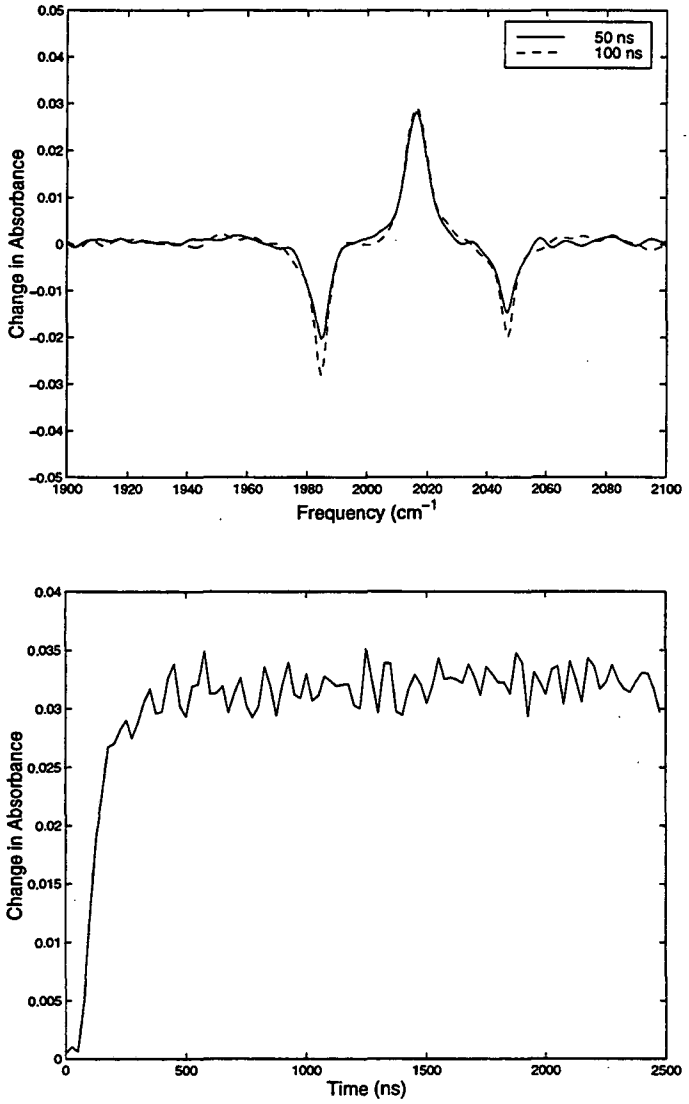

Figure 4.6: Nanosecond spectra and kinetics for the C–H activation reaction of $CpRh(CO)_2$ in cyclohexane

of the methyl groups with the strongly electrophilic $B(C_6H_{12})_3$, and this intermediate then undergoes C–H activation of a solvent molecule, and the Tp* ligand forms an η^3 alkyl hydride. This makes this very similar to the $Tp^*Rh(CO)_2$system in that there is both an oxidative addition step as well as the formation of a metal/ligand bond.

4.3 Effect of alkane structure on C–H bond activation

A matter of considerable interest is the differences in C–H bond activation dynamics between different types of carbon centers in organic molecules. It is well established in the literature that one of the most interesting features of C–H bond activation by unsaturated group 9 organometallic complexes is the selectivity of the reaction. A particularly good review has been written by Jones; [88] for saturated hydrocarbons the order is CH_4 > 1° C > 2° C > 3° C. For Iridium complexes, the kinetic produce is stable at room temperature, and a distribution of primary and secondary C–H bonds are broken in an alkane. [89] When the solution is heated above 100°C, the product converts to the primary C–H activated form. For Rhodium complexes, the secondary and higher products are much less stable, and are never isolated. This suggests that the conversion from secondary to primary C–H activated product must take place on a very short time scale for Rh complexes. While this reactivity is well established, there are still many questions about the reasons for this reactivity. It is,

therefore, interesting to compare the reaction dynamics of linear and cyclic alkanes in order to better understand these effects.

Ultrafast dynamics for the C–H activation reaction of $Tp^*Rh(CO)_2$in cyclohexane is shown in figure 4.1 on page 59, and data for $Tp^*Rh(CO)_2$in *n*-pentane is shown in figure 4.7 on page 72. This system has recently been studied using ultrafast infrared probing by Harris and co-workers [69,70]. During the first steps of the C–H activation reaction, a UV photon photodissociates a CO ligand from the parent compound, and the monocarbonyl forms a solvent complex. This happens on a time scale of < 2 ps, and is independent of the type of solvent. This monocarbonyl solvent complex is initially formed with excess energy, and this energy needs to be transferred from the complex to the surrounding solvent. For this system, this occurs with a time constant of $\sim$ 23 ps for cyclohexane. [69, 70] In the cyclohexane system we see evidence of vibrational hot bands associated with the 1972 cm^{-1}peak in the first intermediate. In the pentane data, however, the low energy tail of the 1972 cm^{-1}peak is broad and does not have definite structure. It may be that the vibrational cooling occurs on a shorter time scale in *n*-pentane, or that there is a solvent induced change in the coupling of the CO stretch with other modes in the molecule.

After vibrational cooling, there is formation of a new intermediate which has a CO stretch at 1990 cm^{-1}. This shows up in both *n*-pentane and cyclohexane, on approximately the same time scale. A fit to the kinetic scan in *n*-pentane, shown in figure 4.2 on page 60 that this peak has a formation time of 230 ps. This peak has

been identified as a partially de-chelated η^2-Tp*Rh(CO)(S) complex, where one of the Rh–N bonds has been broken. This assignment is based on several factors. First, measurements made by Purwoko *et al.* [64] show that in Tp*Rh(CO)$_2$there is an equilibrium between the η^2 and η^3 forms, with the η^3 as the favored form (K_eq=100). They found peaks at 2078 and 2009 cm^{-1}, a shift of 29 cm^{-1}from the η^3 stretching frequencies. This blue shift is similar to the shift seen in the femtosecond infrared data. Zaric and Hall [86] have recently performed density functional calculations on the Tp*Rh(CO)$_2$system, and they have shown that the energy of the η^2 monocarbonyl solvent complex is 9 kcal/mol stabilized with respect to the η^3 form. Finally, studies of the analogous Bp*Rh(CO)$_2$system [70] find that it forms a monocarbonyl, which also has a CO absorption at 1990 cm^{-1}, confirming the identity of the intermediate.

While on an ultrafast time scale the linear and cyclic solvents have similar behavior, on the nanosecond time scale we see significant differences. Figure 4.3 on page 74 shows a 3-dimensional representation of the reaction in cyclopentane during the nanosecond time scale, and figure 4.3 on page 75 shows the dynamics in cyclohexane. Figure 4.11 on page 77 shows the dynamics of the decay of the peak at 1990 cm^{-1}and the final product peak at 2032 cmcm^{-1}in cyclopentane. Figure 4.12 shows the dynamics of the intermediate and product in cyclohexane. These cyclic alkanes show similar behavior, with decay of the η^2 intermediate and growth of the final product on a time scale of $\sim$ 200 ns.

C–H activation by Tp*Rh(CO)$_2$in linear alkanes shows very different behavior.

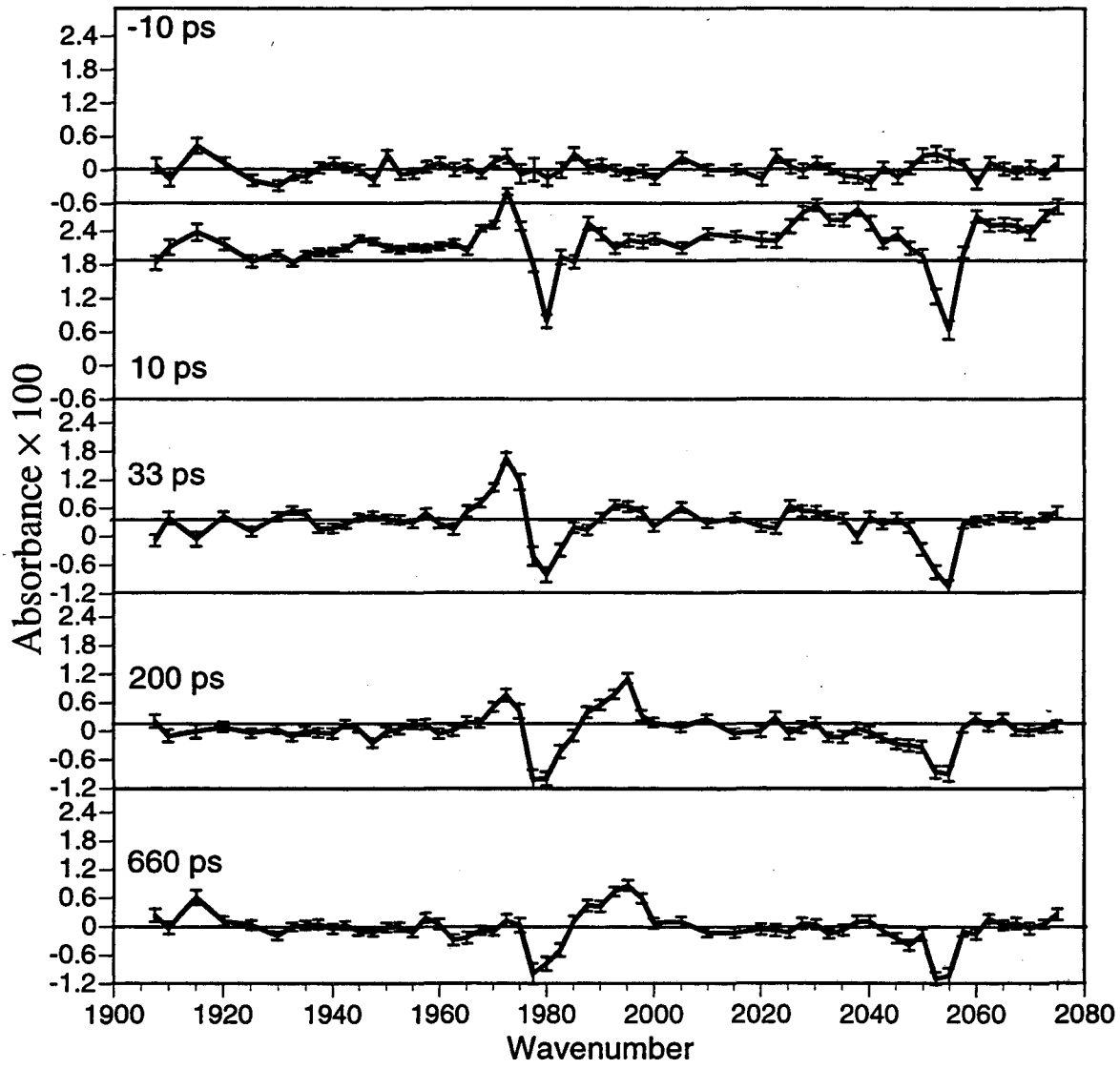

Figure 4.7: Femtosecond spectra of C–H activation by $Tp^*Rh(CO)_2$in *n*-pentane

Figure 4.10 shows spectra at 50 and 100 ns after photoexcitation in *n*-pentane and *n*-hexane. These show that the C–H activation reaction is completed in a time much shorter than the instrument response function of our detection system. The difference in the kinetic behaviors of linear and cyclic alkanes is shown in figure 4.13 on page 79. From the ultrafast IR measurements (see figure 4.7 on the preceding page) we know that there is no absorption due to product at 660 ps after photoexcitation. Measurements made with a faster detection system suggest that the C–H activation time is much shorter than 20 ns, and so we can assume that is between 1 and 10 ns. This is a factor of 20 - 200 times faster than for cyclic alkanes, supporting the observation that C–H activation by Rh complexes strongly favors activation of primary carbons.

An important question to ask is then, what is the difference between the cyclic alkanes and the linear alkanes. This is an important question and should give us insight into the underlying mechanism of the reactions and will also help in the development of more selective C–H activation systems. We consider two possible causes of the difference. The first is that steric hindrance, caused by the locked configuration of the neighboring CH_2 groups makes the barrier for the C–H bond breakage higher, and therefore slows the time scale of the reaction. The other possibility is that there are electronic differences between the CH_3 and the CH_2 groups which change the barrier. In order to investigate the differences we have investigated the reactivity with methyl-cyclohexane. This has an identical structure to cyclohexane, but with one methyl group. We would assume that, based on the previous observation in the

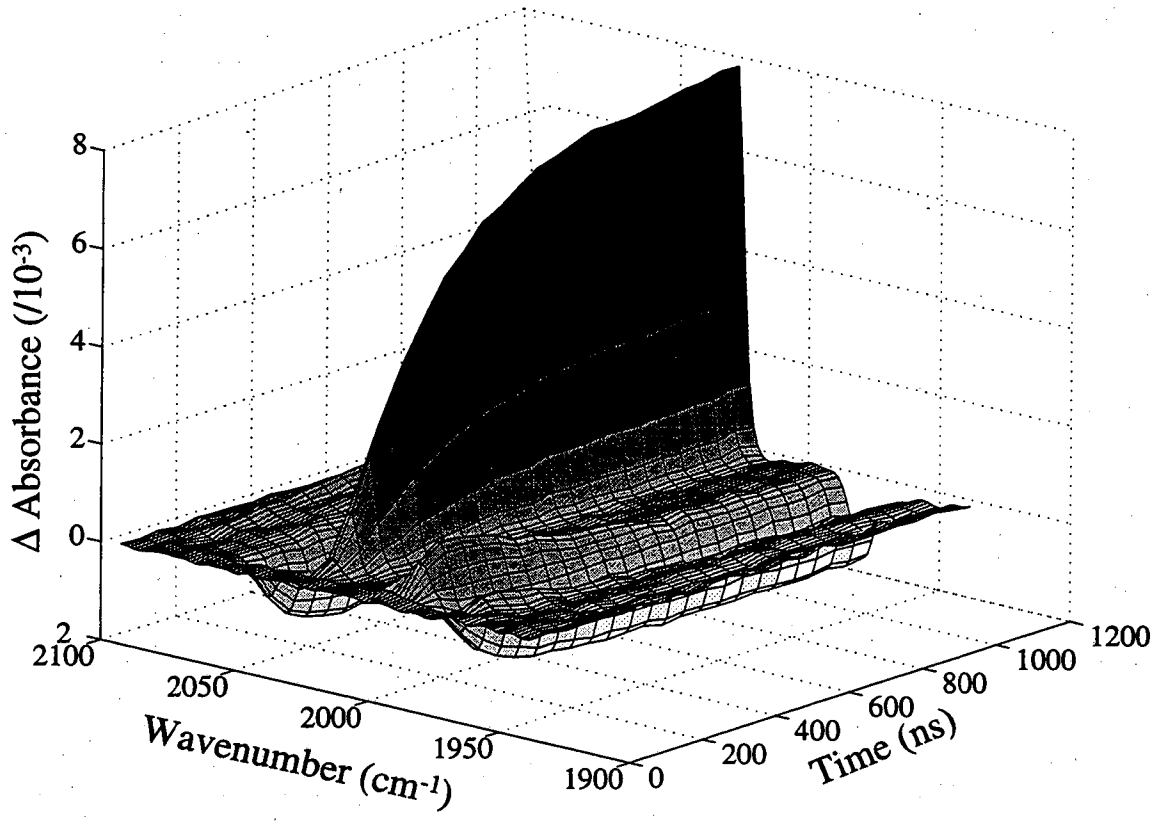

Figure 4.8: Spectral evolution of $Tp^*Rh(CO)_2$ in cyclopentane from 1 to 2500 ns

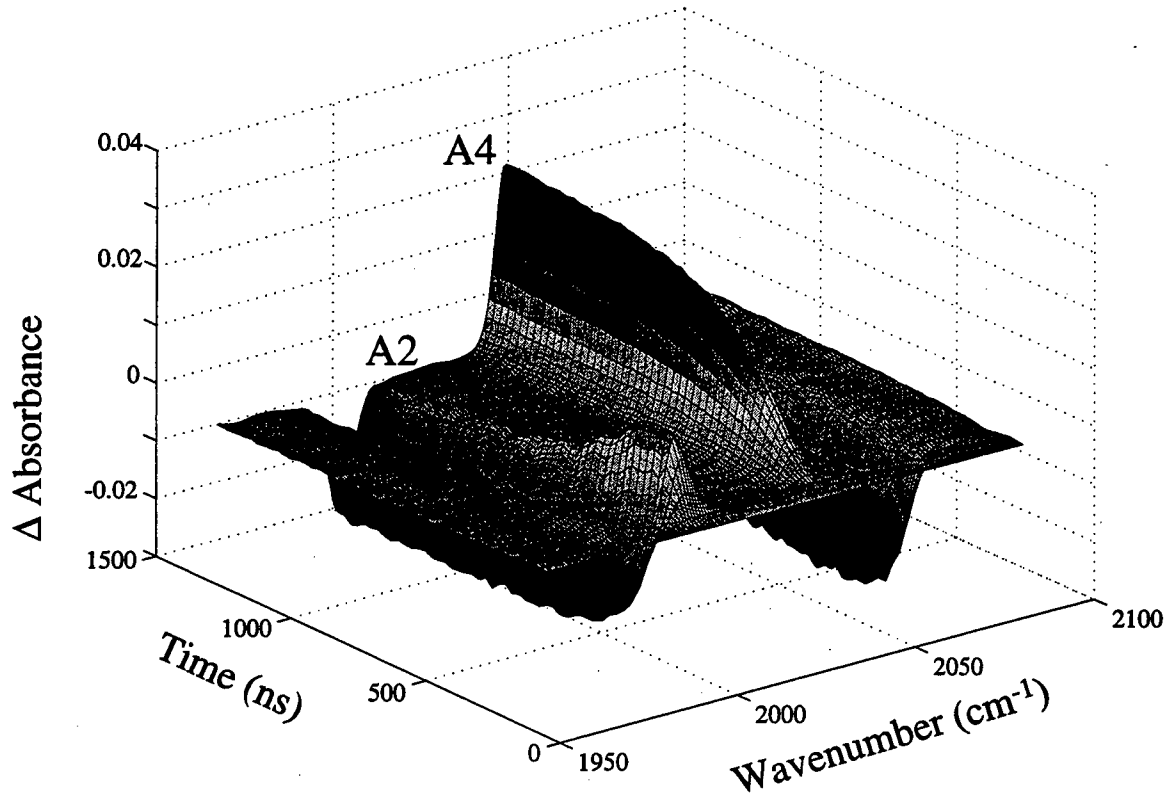

Figure 4.9: Spectral evolution of $Tp^*Rh(CO)_2$ in cyclohexane from 1 to 2500 ns

Figure 4.10: Nanosecond spectra of $Tp^*Rh(CO)_2$in linear solvents.

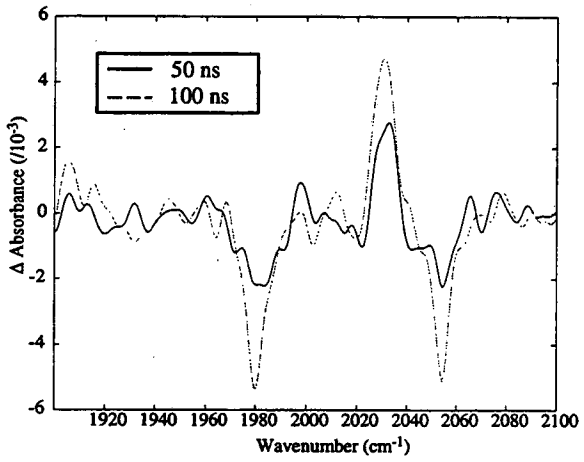

(a) *n*-hexane

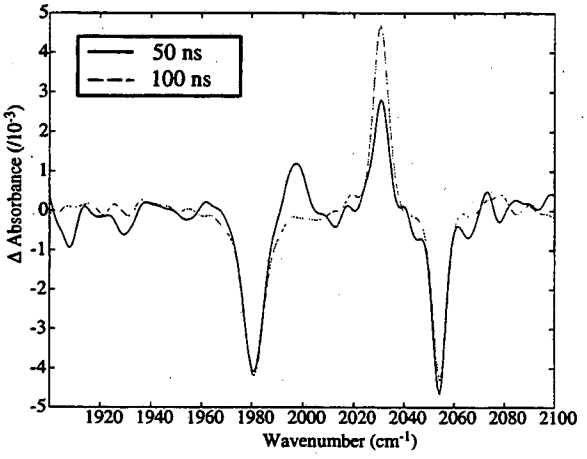

(b) *n*-pentane

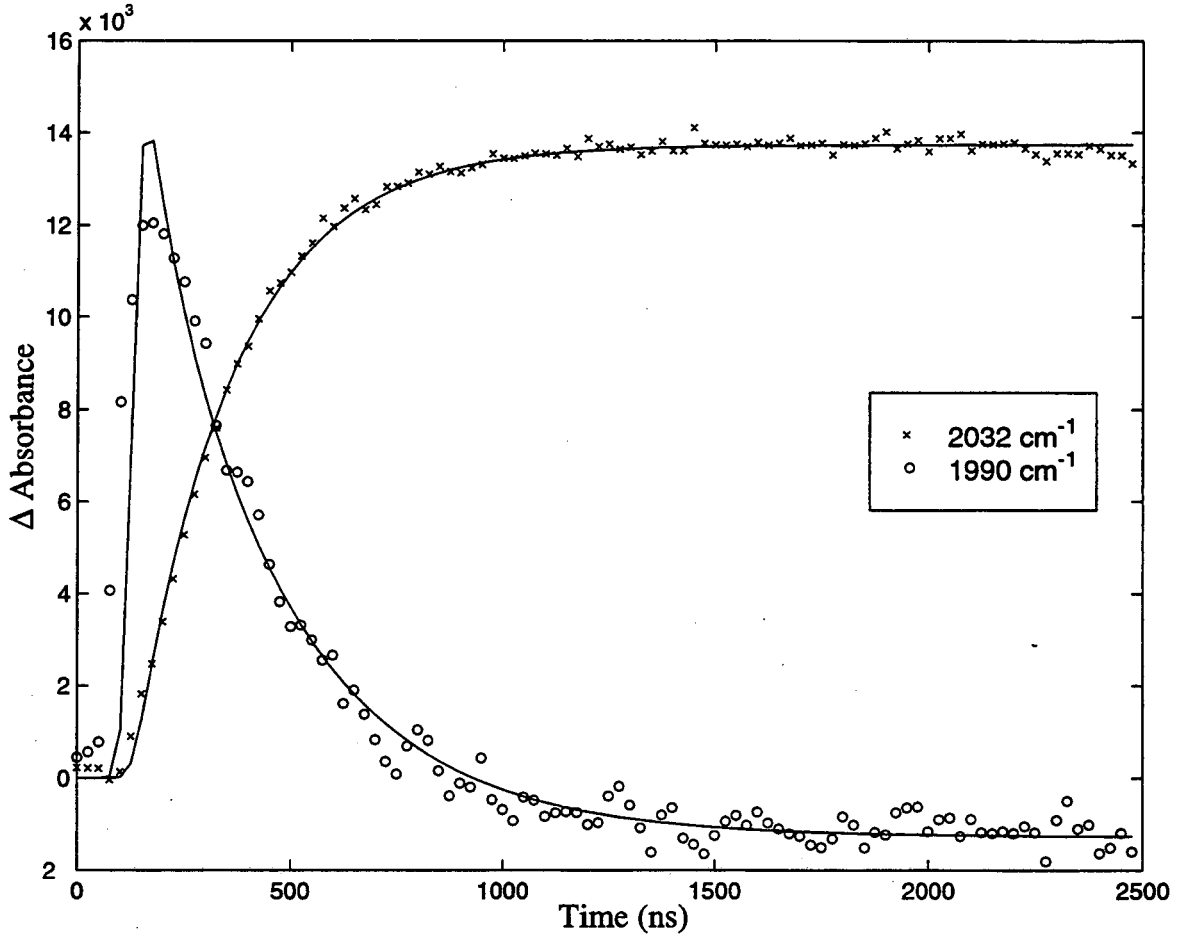

Figure 4.11: Kinetics of product and intermediate in cyclopentane

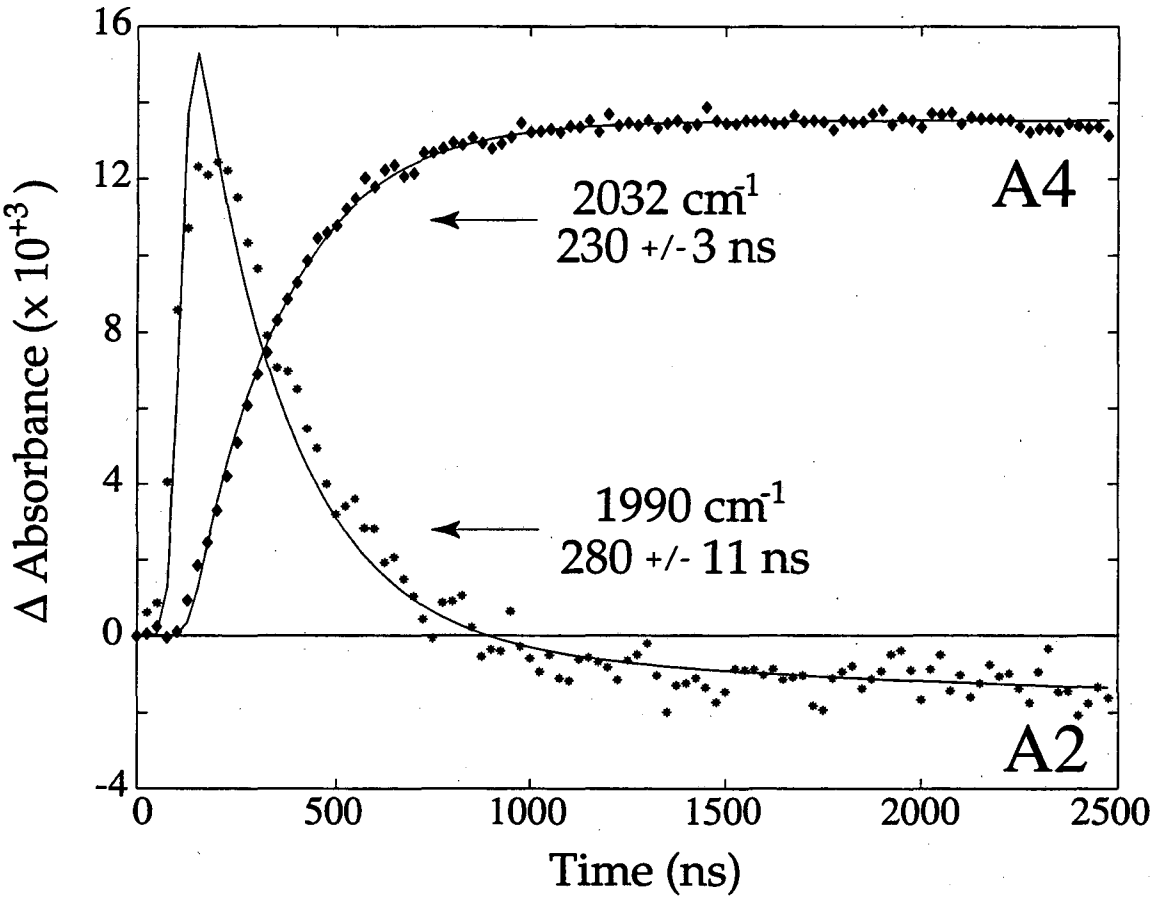

Figure 4.12: Kinetics of product and intermediate in cyclohexane

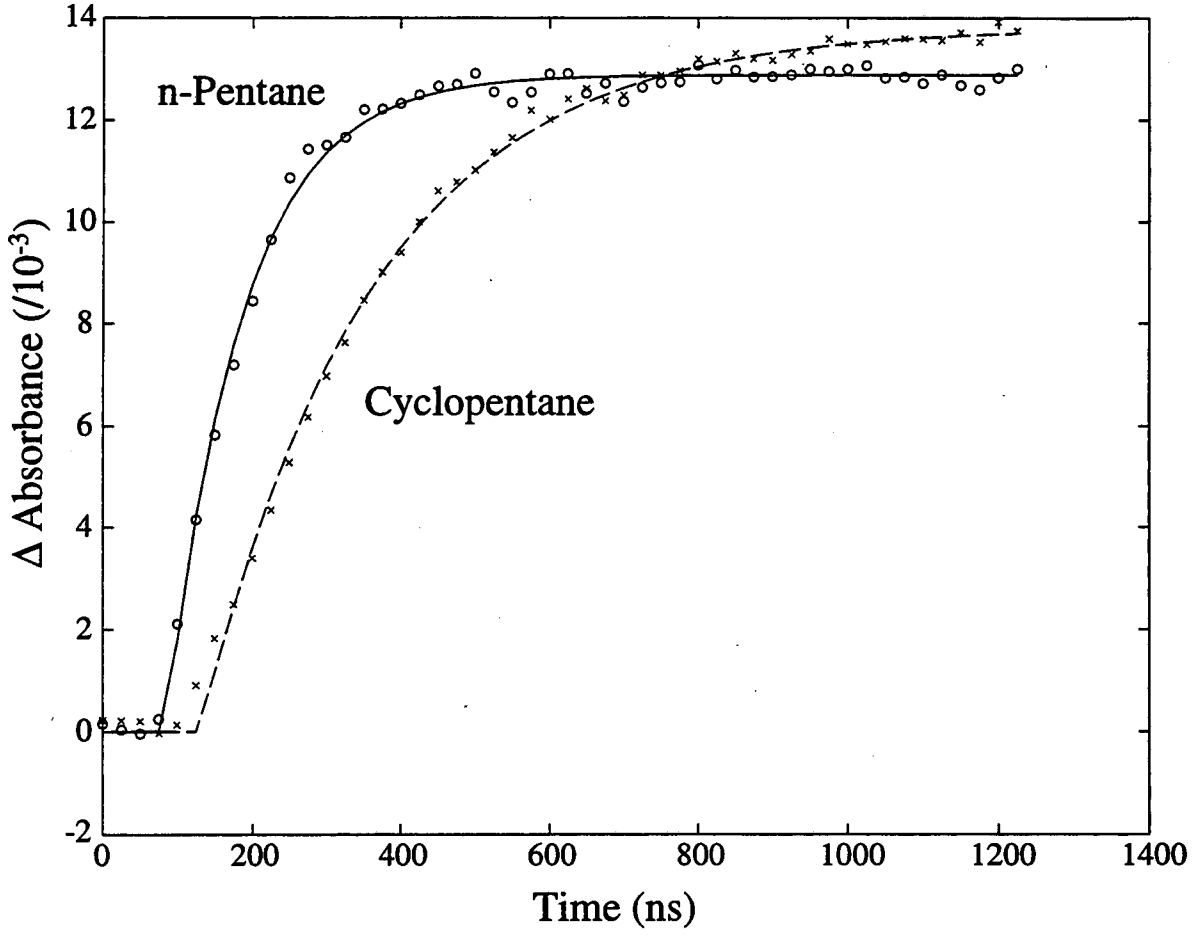

Figure 4.13: Kinetics of C–H activation of *n*-pentane and cyclopentane by $Tp^*Rh(CO)_2$.

rates, the reaction would favor the methyl group over the ring methylene groups. This assumes that the alkane complex is labile, allowing the alkane to reorient itself from a CH_2 group oriented toward the Rh metal center, to the CH_3 oriented toward the metal.

Spectra for $Tp^*Rh(CO)_2$in methyl-cyclohexane taken at two different times are shown in figure 4.14 on the facing page, showing the growth of the product at 2032 $cm^{-1}$and the intermediate at 1990 cm^{-1}. Note that the intermediate is partially covered by the bleach at 1980 cm^{-1}. Kinetics for the product and intermediate CO stretches are shown in figure 4.15 on page 82. Only nanosecond data is available, but it clearly shows that the reaction in methyl-cyclohexane proceeds with dynamics similar to an *n*-alkane. This suggests that the reaction does in fact proceed more favorably with the methyl group rather than with the methylene group, even when there are more methylene groups in the structure.

Another important data set involves the mixing of linear and cyclic alkanes. In these experiments, we have mixed known concentrations of *n*-pentane and cyclopentane, and measured the time scale of bond activation over a range of concentrations. Figure 4.16 on page 84 shows the dynamics at two concentrations. The first curve shows the dynamics in pure *n*-pentane, the second pure cyclopentane, and the third, a mixture of 20 % *n*-pentane in cyclopentane. Figure 4.17 on page 85 shows a plot of the fitted rise times versus the mole fraction concentration of *n*-pentane in cyclopentane. We can see two important things in this data. The first is that even

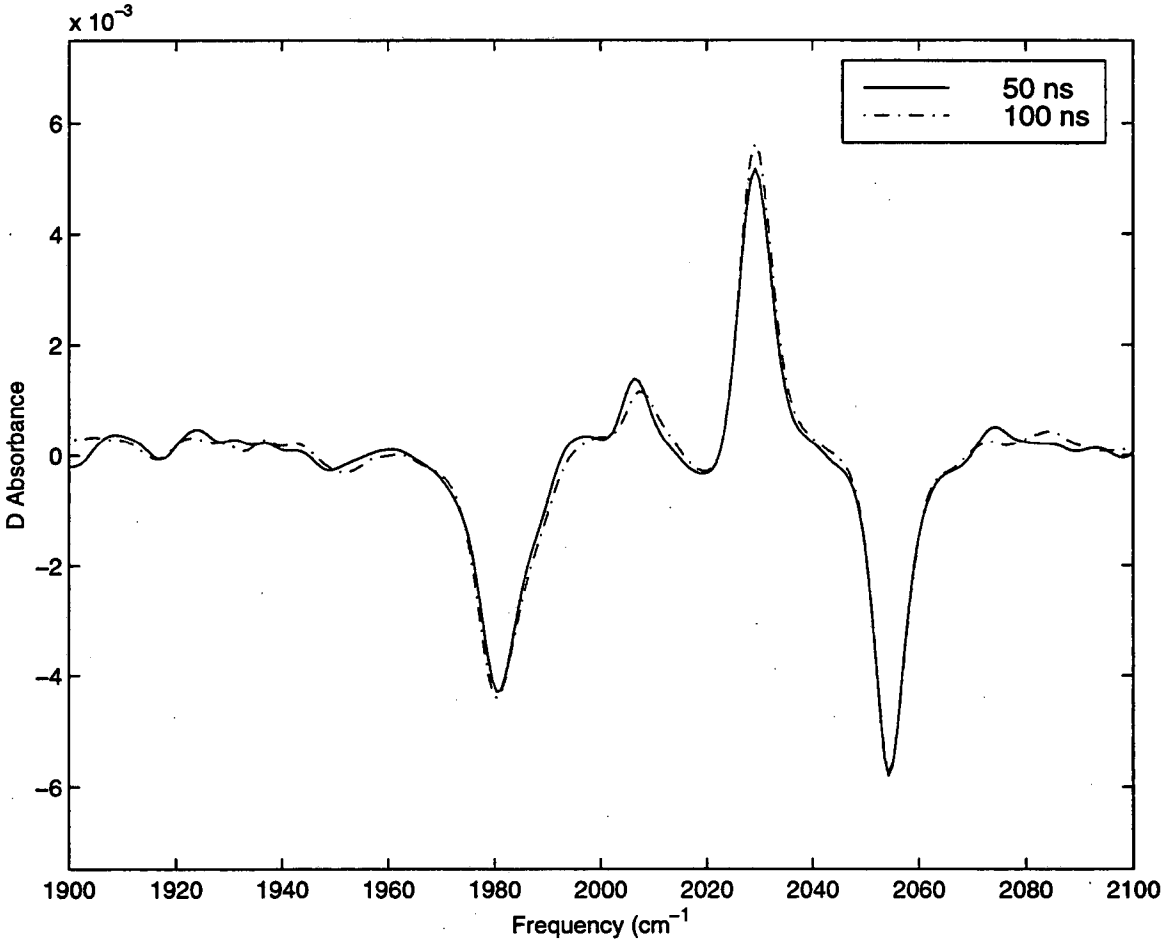

Figure 4.14: Spectra for C–H activation of methyl-cyclohexane by $Tp^*Rh(CO)_2$

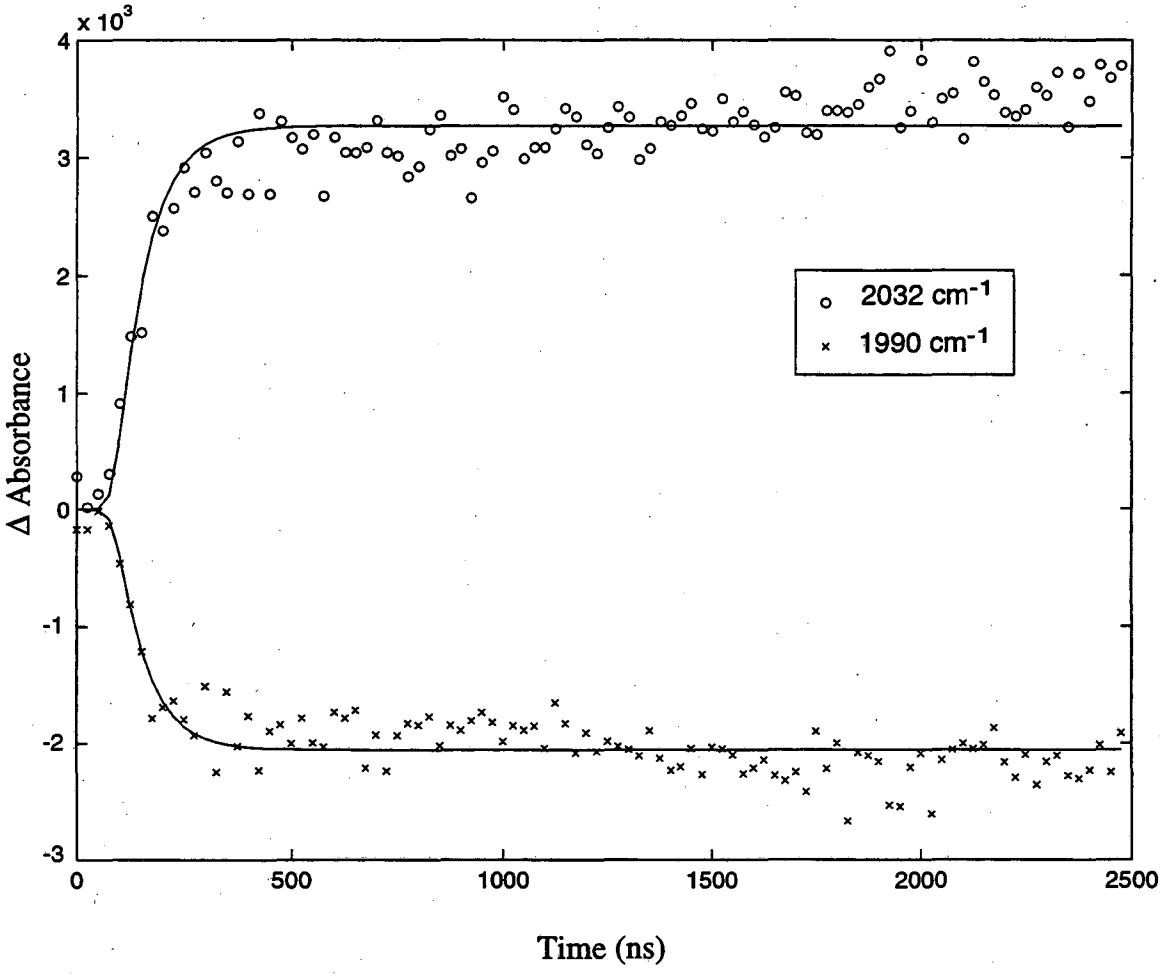

Figure 4.15: Kinetics for product and intermediate for C–H activation by $Tp^*Rh(CO)_2$of methyl-cyclohexane. Note that the absorption at 1990 $cm^{-1}$is negative at long times due to the parent bleach at 1980 cm^{-1}.

at low concentrations, the dynamics of the reaction are significantly altered by the *n*-pentane. The second, and possibly more important, is that the dynamics for the reaction seem to saturate at some concentration and not change as more *n*-pentane is added. This suggests that the reaction becomes a competition between the 180 ns C–H bond activation time and the 80 ns substitution of the initial cyclopentane solvent molecule for a *n*-pentane solvent molecule.

4.4 C–H activation in aromatic systems

So far in this work, we have focused primarily on C–H bonds in alkane systems. While the C–H activation process is particularly important for alkanes, there are many other chemical systems in which C–H bonds can be activated. One of the most interesting classes of compounds to study C–H bond activation on are aromatic systems. These molecules have significantly different C–H bonds because of their aromatic ring structure. Previously studies, by Purwoko *et al.* [67], examined the photochemical C–H activation reaction by $Tp^*Rh(CO)_2$in a series of aromatic and alkane solvents, and found that the C–O stretching frequency in the aryl hydride product is shifted 20 cm^{-1}higher in energy than the alkyl hydride product (2050 cm^{-1}vs. 2030 cm^{-1}). They also found that the photochemical quantum yield for aromatic solvents is significantly lower than for alkanes. These studies show much about the overall reaction, and show that there are differences between alkanes and arenes in these C–H activation reactions. Their work did not, however, shed light on

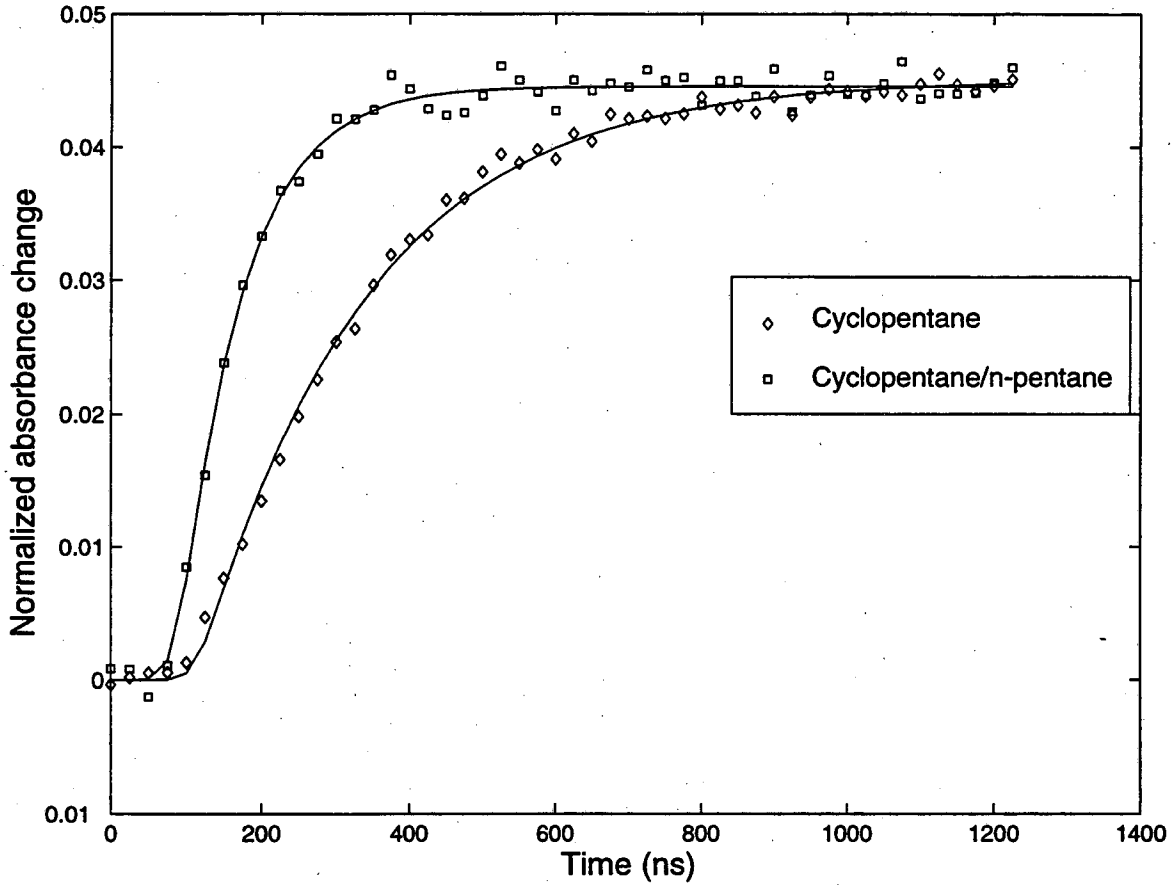

Figure 4.16: Growth of alkyl hydride in pure cyclopentane, and in a mixture of cyclopentane and n-pentane.

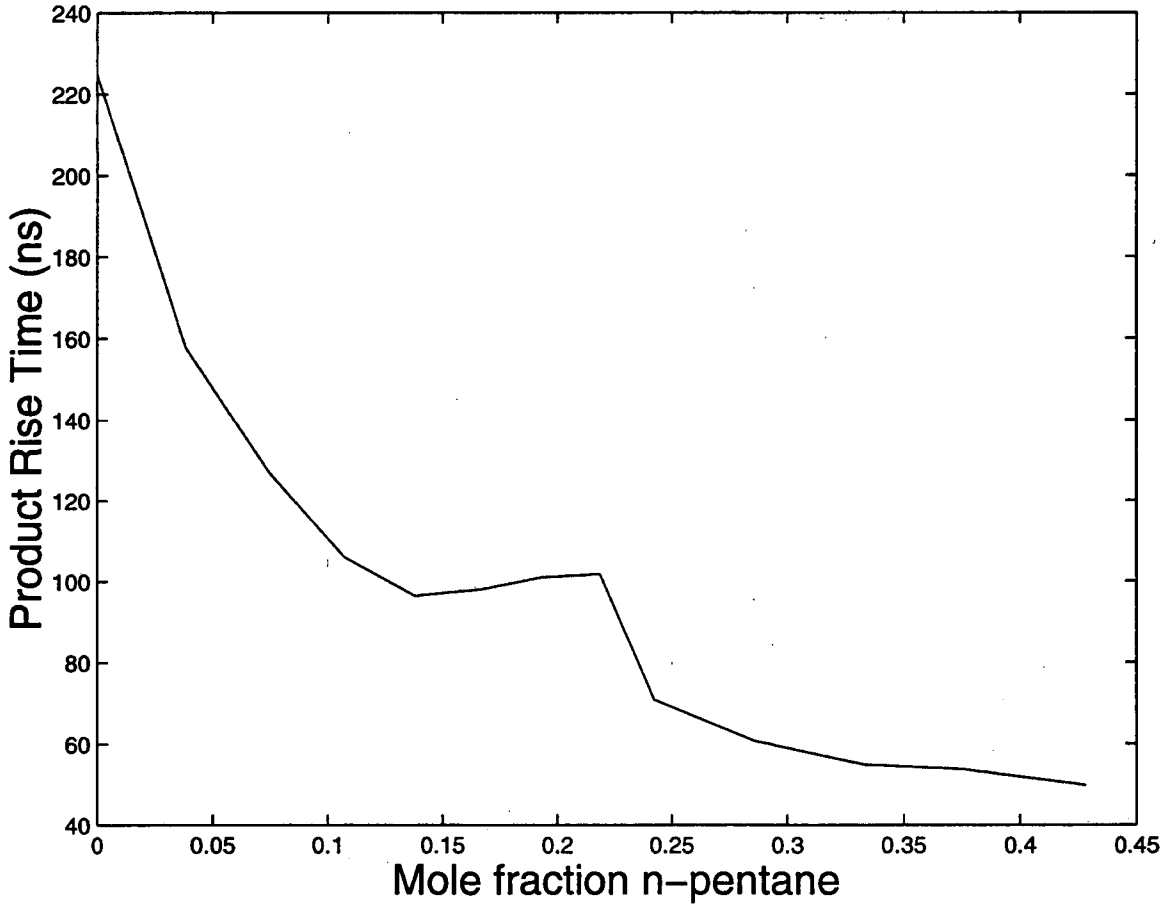

Figure 4.17: Formation time of final product as a concentration of n-pentane in cyclopentane

differences in the mechanism for reaction in this system.

Looking first at benzene, the simplest aromatic molecule, we see very interesting behavior. If we look at the transient absorption of the $Bp^*Rh(CO)_2$system in d-benzene, shown in figure 4.4 on the facing page, we see that in the nanosecond region there are bleaches at 2010 and 2080 $cm^{-1}$and a product absorption at 1990 cm^{-1}. If we compare this to the spectrum of $Bp^*Rh(CO)_2$in cyclohexane, the position of the product complex is less than 2 cm^{-1}shifted. Studies by Yeston [90] of $Bp^*Rh(CO)_2$in liquid Kr and Xe also show a solvent complex at 1990 cm^{-1}. The lack of dependence of the frequency of the C–O stretch on the nature of the solvent (rare gas vs alkane vs aromatic) suggests that the Rh–Solvent interaction is very weak. Like the alkane systems, we also saw no sign of C–H activated product in the reaction of $Bp^*Rh(CO)_2$with benzene.

Spectra of $Tp^*Rh(CO)_2$in benzene show behavior which is significantly different than the behavior of $Tp^*Rh(CO)_2$in cyclohexane. In cyclohexane [69, 70] (see figure 4.20) we see an instantaneous bleach at 1980 and 2050 cm^{-1}which represents the dissociation of one CO group to form the monocarbonyl. The monocarbonyl quickly complexes with a solvent molecule to form a complex which absorbs at 1972 cm^{-1}. At the earliest times in benzene, we see in the femtosecond scans a small peak at 1965 cm^{-1}which should also correspond to a solvent complex. At later times (200 ps in cyclohexane) the cyclohexane undergoes a transition from the η^3-$Tp^*Rh(CO)(S)$ to an η^2-$Tp^*Rh(CO)(S)$ complex which then lasts for hundreds of nanoseconds in cyclic

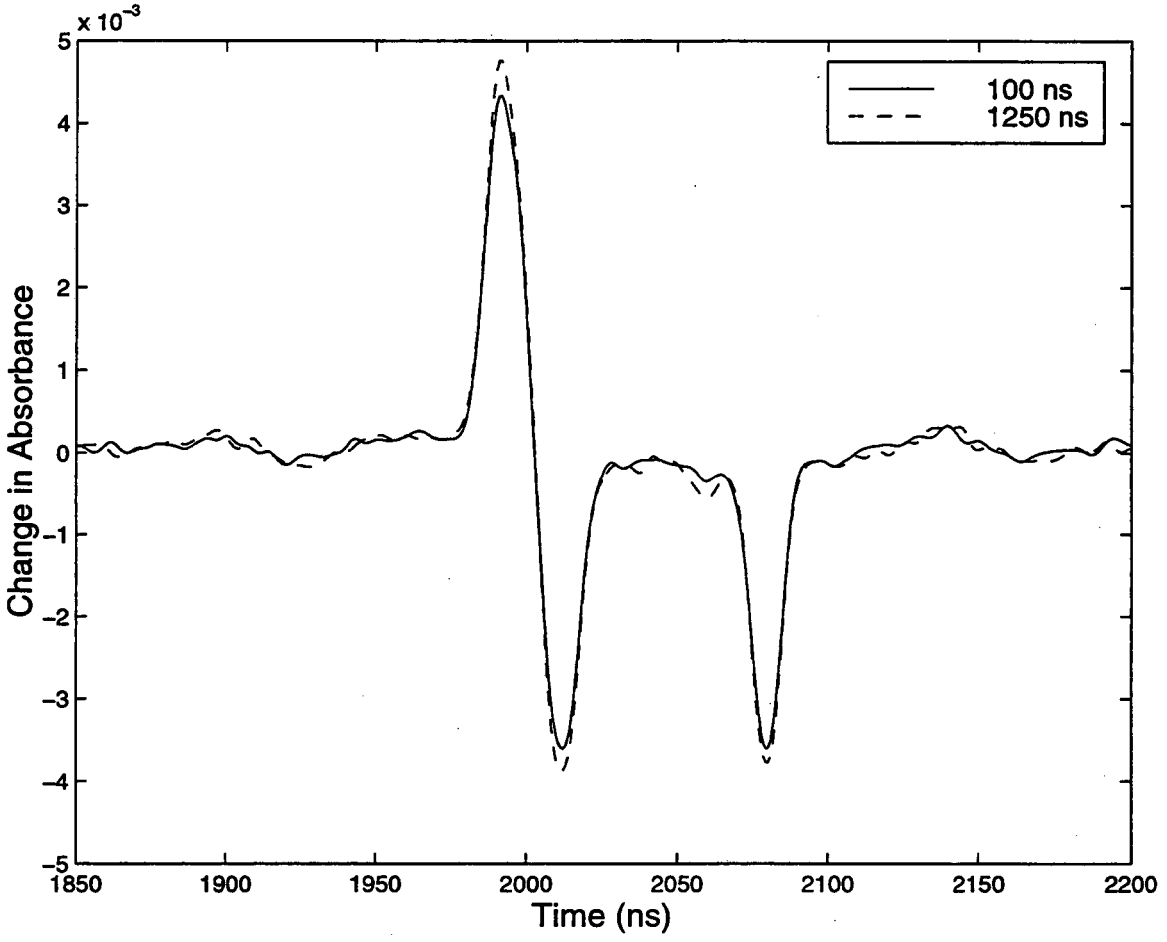

Figure 4.18: Transient nanosecond spectra of Bp*Rh(CO)(H)(phenyl) complex in benzene

solvents. This change is evident in the spectrum by the change of the monocarbonyl absorption from 1972 $cm^{-1}$to 1990 cm^{-1}.

In d_6-benzene the situation is somewhat different. We can see in the nanosecond spectrum, shown in figure 4.22 on page 94, that there are two peaks. The first is at 2005 $cm^{-1}$and is present within 10 ns after excitation, but decays away on a time scale of 1.8 μs. The second is at 2043 cm^{-1}, and shows a two part rise, one a rise which is faster than the instrument rise, and the other with a time constant of 2.0 μs. These kinetics are shown in figure 4.23 on page 95. From comparison with static measurements of the spectrum, we know that the peak at 2043 $cm^{-1}$is the final C–H activated product. We also know from the $Bp^*Rh(CO)_2$in d_6-benzene measurements that the η^2-$Tp^*Rh(CO)$(benzene) complex absorbs at 1990 cm^{-1}. Thus the peak at 2005 $cm^{-1}$is neither final fully activated nor a partially de-chelated intermediate, as we saw in alkane solution. This suggests that there is a new complex which forms in aromatic systems which is different than alkane activation. This is comparable to the case of Si–H bond activation [91, 92] where there are also multiple pathways. In the case of Si–H bond activation we see that the electronic excited state partitions some complexes into a long lived intermediate, while others react in <100 ps. Since we did not see multiple pathways in alkane solutions due to multiple electronic states, it seems unlikely that this is an explanation for this system. It seems more probable that some portion of the molecules initially form a weak sigma complex between the Rh and a C–H bond, and then changes into a more strongly bound sigma complex

between the Rh and a C–C bond, and that this then goes on to form a C–H activated complex.

We can also look at the effect of adding a CH_3 group to an aromatic ring. Nanosecond spectra and kinetics for $Tp^*Rh(CO)_2$reacting with toluene are shown in figures 4.24 on page 96 and 4.25 on page 97. It was shown previously, that upon addition of a methyl group to a cyclohexane ring, the C–H activation took place almost exclusively at the methyl group. This makes sense because the primary carbon of the methyl group shows faster activation kinetics than the secondary carbon on the cyclohexane ring. In the case of toluene, we see that the peaks are identical in position to the peaks in benzene, and that there is no product peak at 2032 cm^{-1}, corresponding to an activated methyl group. We also note that the time scale for C–H bond activation is the same for toluene as it is for benzene, further showing that the methyl group is not participating in the chemistry. This is especially interesting since the C–H activation time for the aromatic rings is so much longer than the time for primary carbons in methyl groups.

This gives us a proposed mechanism for C–H activation by $Tp^*Rh(CO)_2$in aromatic solutions. A diagram of this mechanism is shown in figure 4.19 on page 91. Initially, a CO is photodissociated, and a weak solvent complex forms. This is a weak η^3 complex, which absorbs at 1960 cm^{-1}. The reaction then splits to give two pathways. The first pathway goes from the η^3 Rh–H–C sigma complex to an η^2 R–H–C complex, and then to a final aryl hydride product in less than 50 ns. The second

pathway goes from the η^3 Rh–H–C sigma complex to an Rh–C–C complex. This complex is stable with respect to the sigma complex, and thus the activation time for the reaction from this complex is 1.8 μs. The reaction for $Tp^*Rh(CO)_2$in aromatic shows similarities to the analogous reaction in alkane solvent, but we also see new reaction pathways, including a Rh–C–C complex which are different from the alkane solvent. Further study, including study of C–H activation in non-aromatic solvents, such as 1-hexene, will help further elucidate this very interesting reaction.

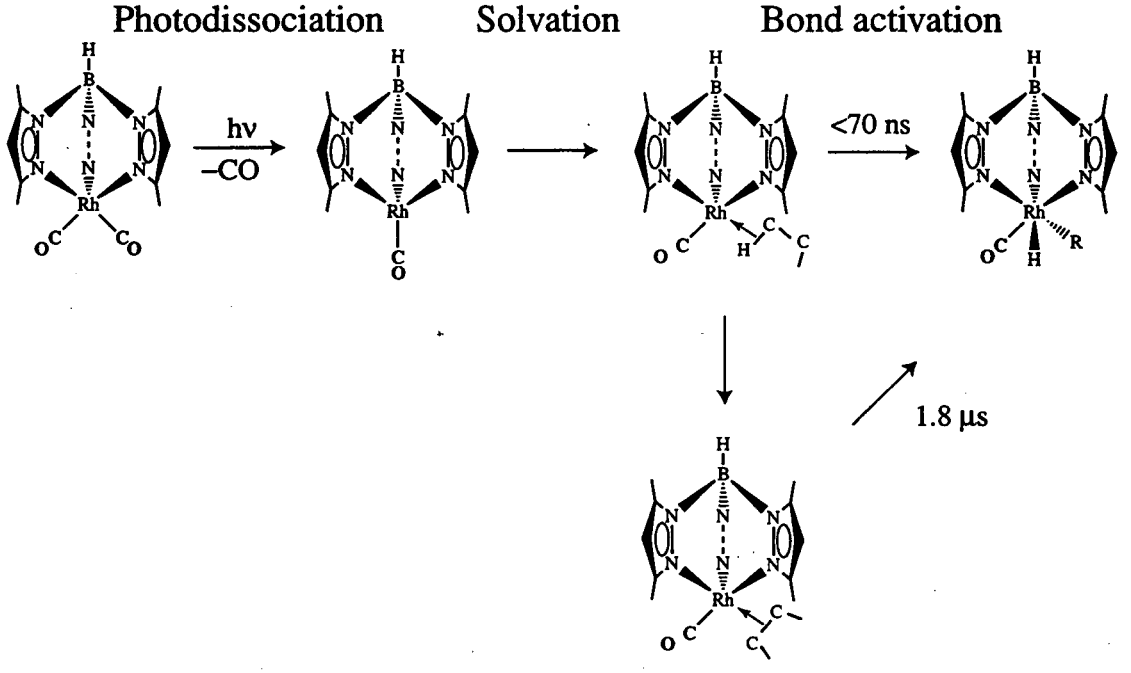

Figure 4.19: Proposed mechanism for C–H activation of benzene by $Tp^*Rh(CO)_2$

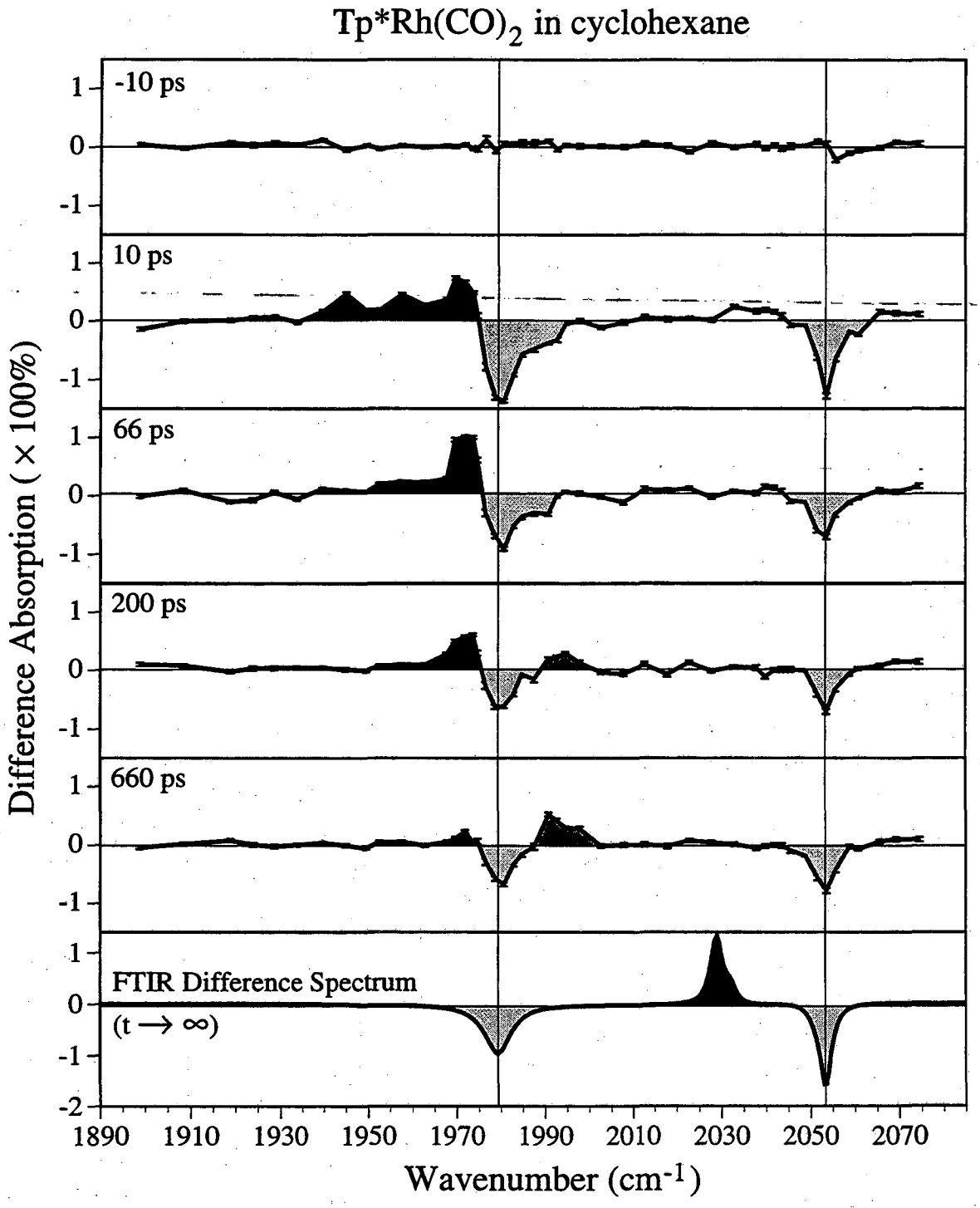

Figure 4.20: Femtosecond spectra of $Tp^*Rh(CO)_2$in cyclohexane.

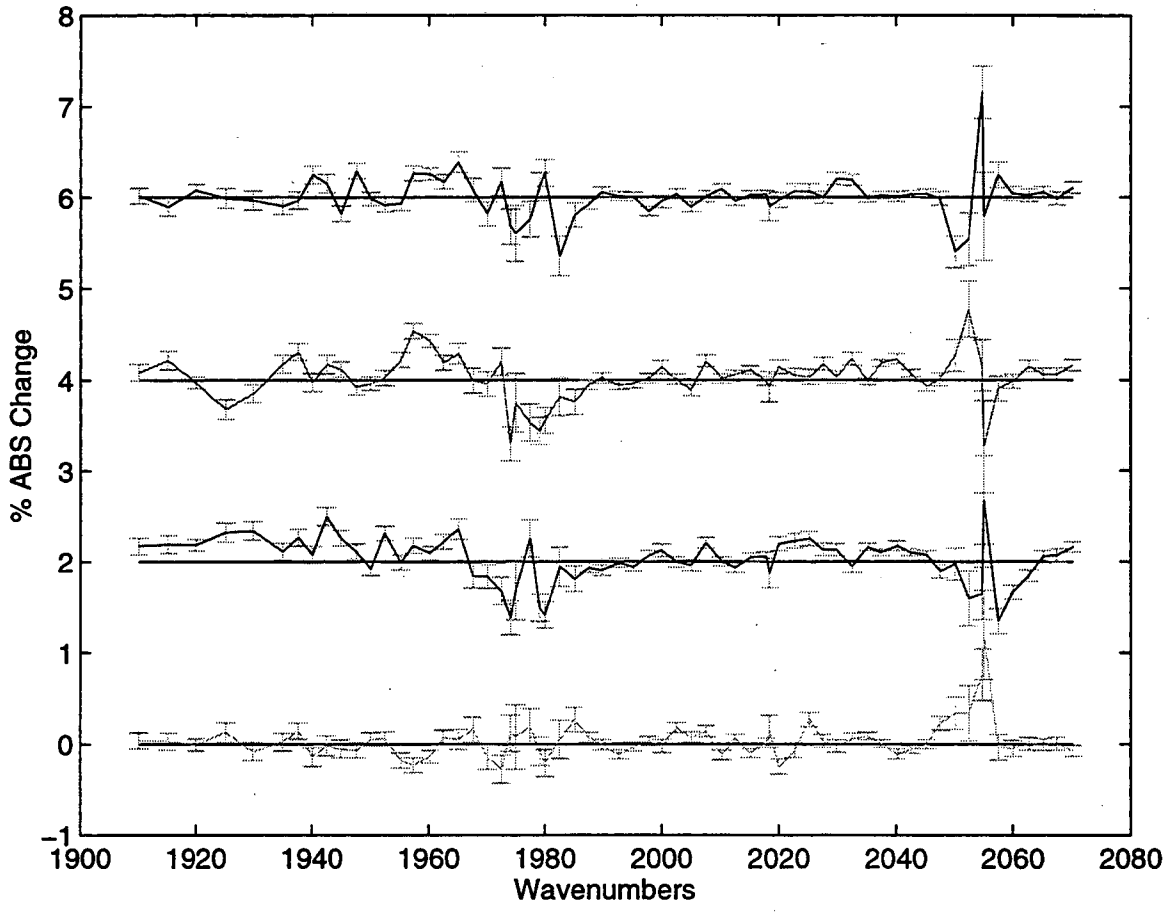

Figure 4.21: Femtosecond spectra of $Tp^*Rh(CO)_2$in d_6-benzene. Note the small peak at 1960 cm^{-1}

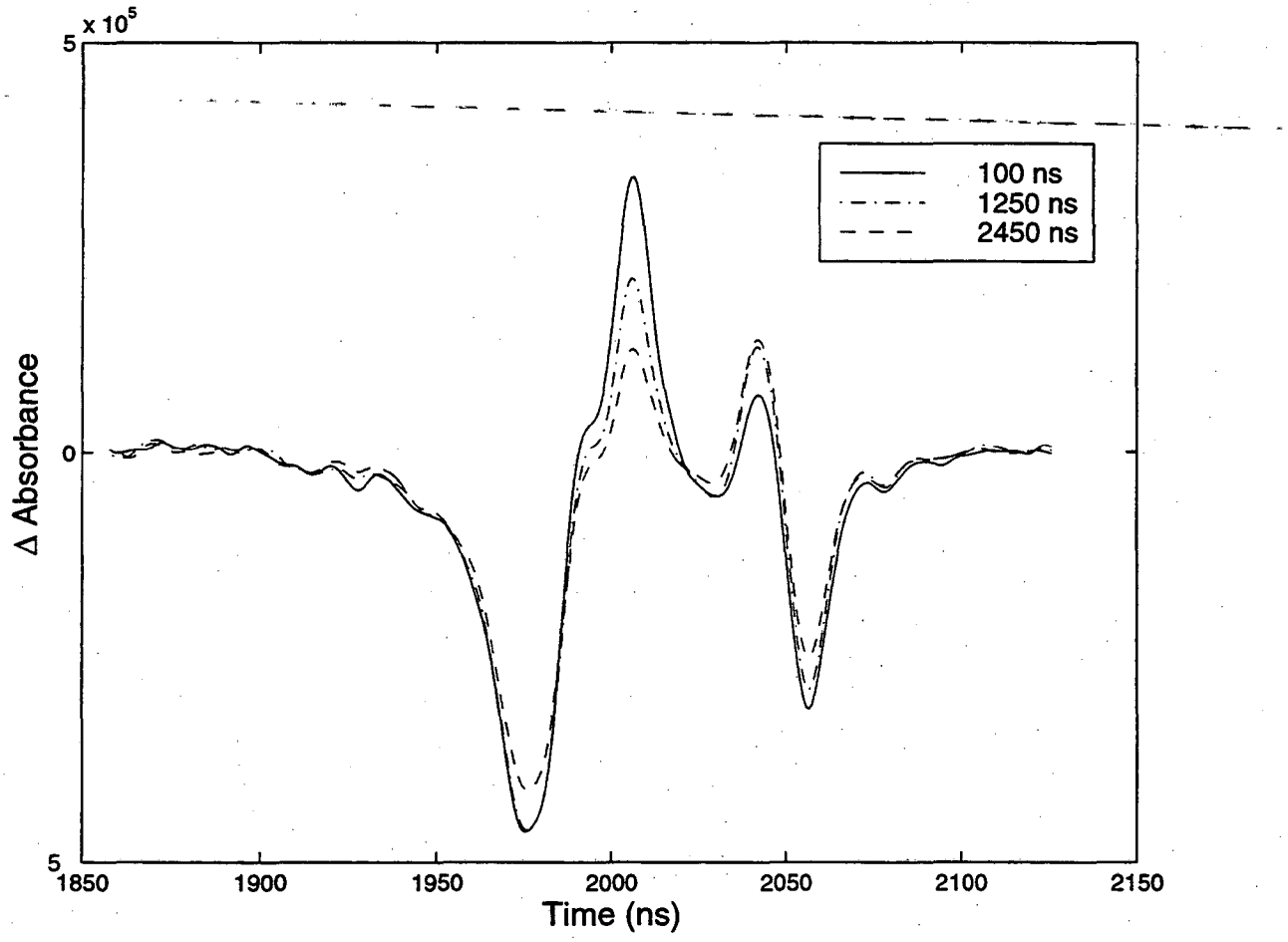

Figure 4.22: Nanosecond spectra of $Tp^*Rh(CO)_2$in d_6-benzene at several times

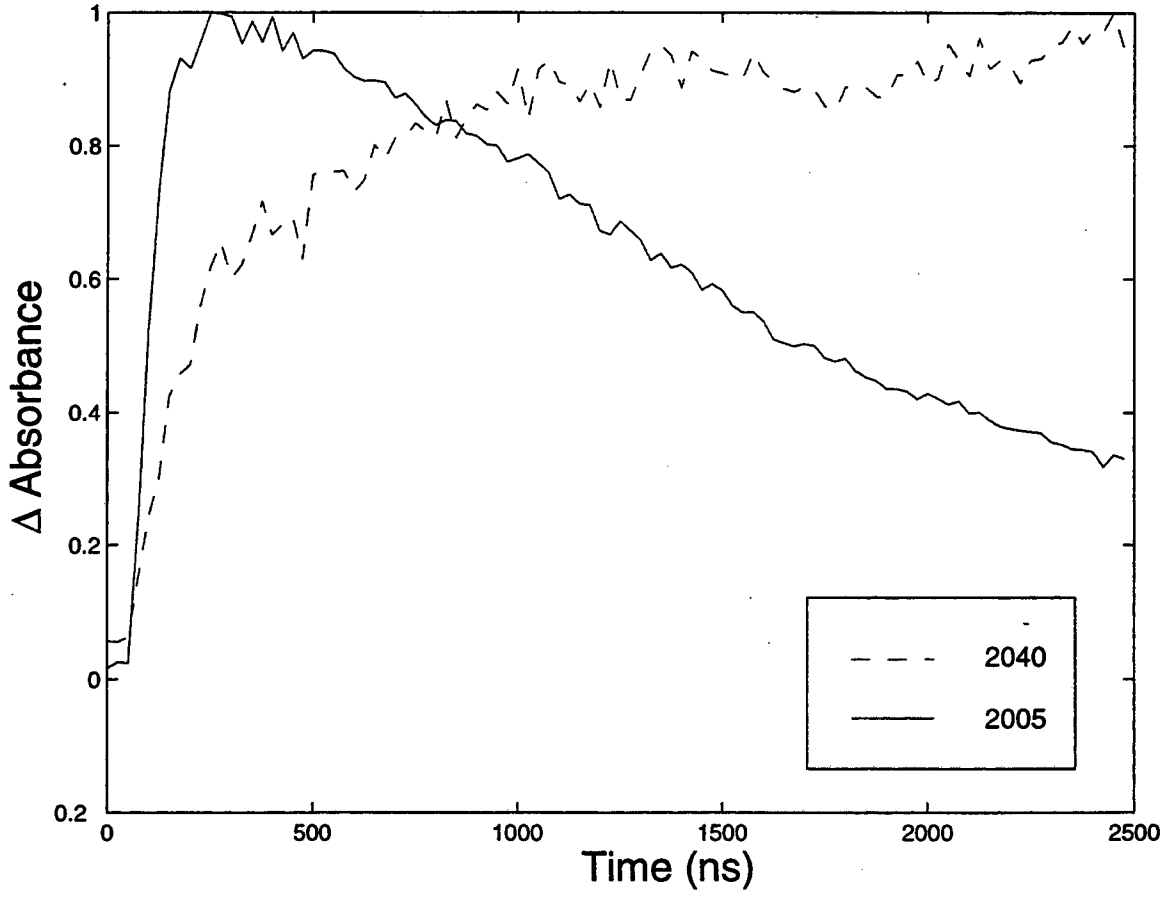

Figure 4.23: Kinetics of $Tp^*Rh(CO)_2$in d_6-benzene

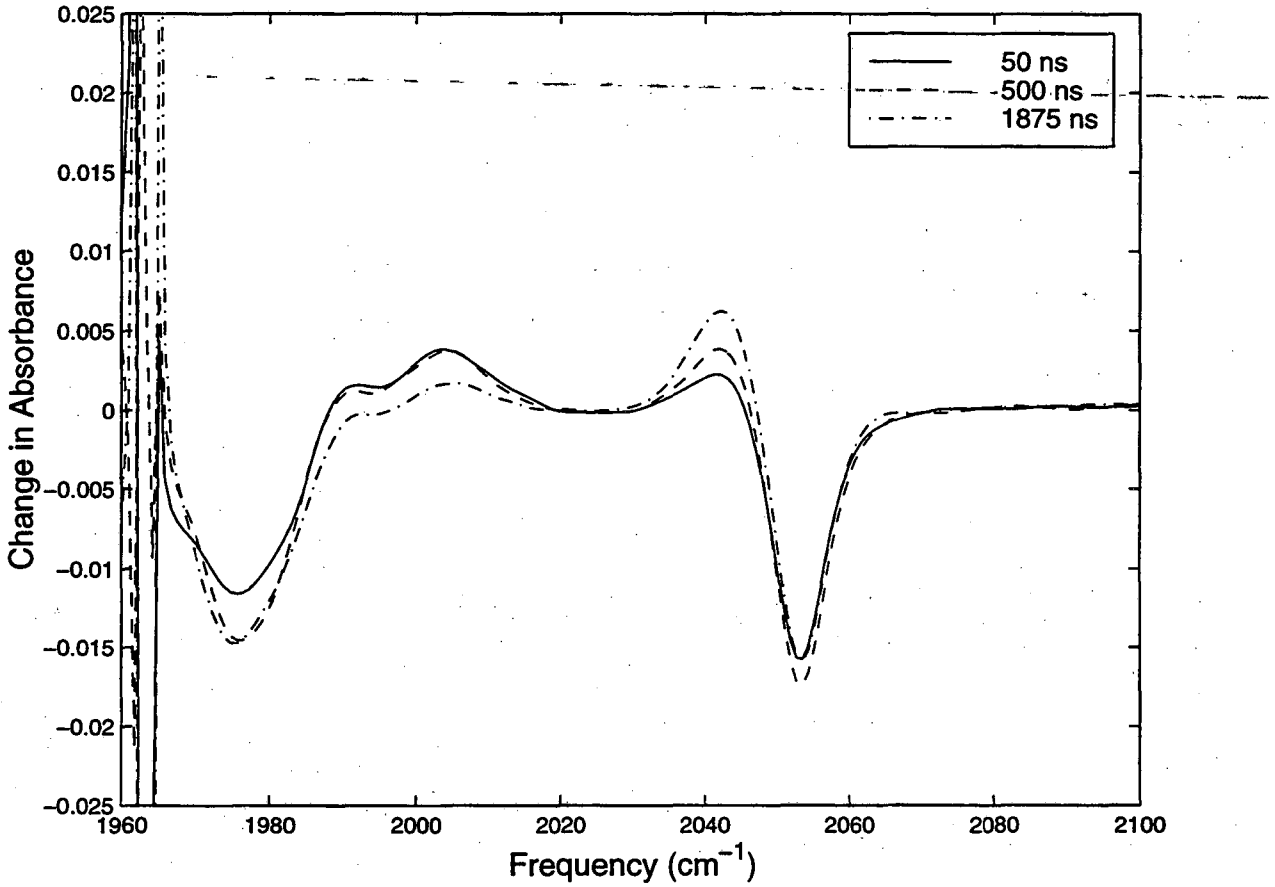

Figure 4.24: Nanosecond Spectra for C–H activation by Tp*Rh(CO)$_2$in toluene

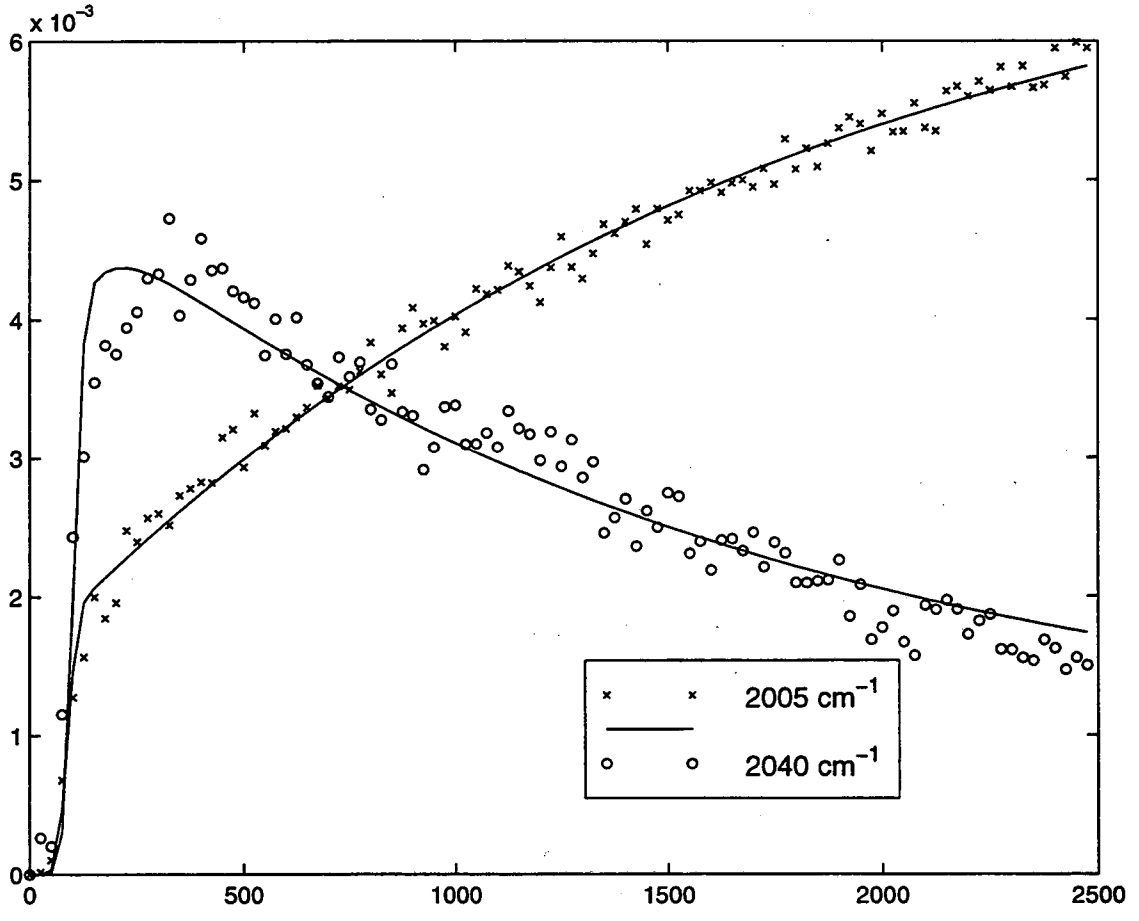

Figure 4.25: Nanosecond Kinetics for C–H activation by $Tp^*Rh(CO)_2$in toluene

Chapter 5

Non-CO probing

5.1 Transient Fingerprint spectroscopy

An important issue in examining the spectroscopy of organometallic photochemistry, is the source of the signal. Most of the studies which have been performed on these chemical systems depend on CO, CN, or N_3 groups which act as reporter groups, but are not actually part of the reaction. Our work looking at $Tp^*Rh(CO)_2$ [69, 70] involved probing the CO group which was not dissociated from the Rhodium center.

Looking in the fingerprint region is especially difficult for reactions in which the solvent participates, because the solvent will always have strong absorbances in the region which is of greatest spectroscopic interest in the product molecule. It is thus impossible to observe the shifts in C-H absorbances of the alkane molecules as they undergo bond activation. It is possible, however, by using a deuterated solvent to

observe the changes in the vibrational modes of the Tp* ligand during the reaction. This will then give us detailed information on structural changes in the ligand.

In order to examine the spectra of the Tp* ligand, we have performed studies of $Tp^*Rh(CO)_2$in C_6D_{12}. Because it has no C-H bonds, C_6D_{12} is transparent in the 1100 - 2000 cm^{-1}region of the IR spectrum, and so it is possible to monitor the modes of the Tp* ligand in that spectral region. In order to perform the experiments, the $Tp^*Rh(CO)_2$is dissolved in dry C_6D_{12} and the sample kept under a dry N_2 atmosphere. The concentration of $Tp^*Rh(CO)_2$is fixed by its solubility to 1 mM. This concentration gives an absorbance of 0.6 OD in a 1 mm path length at the pump wavelength of 355 nm. Because of the cost of the perdeutero solvent, the sample size had to kept to a minimum, and the solvent distilled and re-used after each run. With 20 ml of sample, and a pump power of 4 mJ at 355 nm, the samples showed degradation after 5 or 6 scans, and had to be changed. This degradation is largely because of the small volume, as we have run 50 - 100 ml for 20 or 30 scans with no sample degradation.

In order to probe in the fingerprint region, we also need to change the spectrometer. For these measurements, we used a 40 ns MCT detector with a band gap at 8 μm. With the addition of a narrow pass filter, we could scan from 1250 - 2000 cm^{-1}allowing us to see both the fingerprint region of the spectrum, and the parent absorption at 1980 $cm^{-1}$for sample monitoring.

If we look at the fingerprint region spectrum of the $Tp^*Rh(CO)_2$molecule in a

KBr pellet 5.5(a) on page 111 we can see that there are strong CO absorbances at 1980 and 2050 cm^{-1}, and a broad absorption from 1450 $cm^{-1}$and to 1250 cm^{-1}. We can also see that there is a sharp peak at 1545 cm^{-1}, which can also be seen in the IR spectrum of the analogous $Bp^*Rh(CO)_2$ molecules shown in figure 5.5(b) on page 111.

The peak at 1545 $cm^{-1}$is in an interesting part of the spectra. It is too high in frequency to be a methyl bending mode, and too low to be a C–H stretching mode. It is present in the IR spectrum of the Tp^* ligand, and so must be a mode associated with the pyrazole ring. This mode has been assigned as on of the fundamental ring stretches of the pyrazole, which occur from 1340 $cm^{-1}$to 1540 cm^{-1}depending on substitution. [93] We have assigned the identity of the second intermediate, with a C–O stretch at 1990 $cm^{-1}$to be a partially de-chelated $\eta^2Tp^*Rh(CO)(S)$ complex, and we would expect changes in the pyrazole ring connectivity to cause changes in the pyrazole ring stretches.

If we look at the 1500 cm^{-1}section of the spectrum in the transient data, as in figure 5.2 on page 108 we see that in fact there are changes centered around this peak. We can see at early times there is a shift to higher frequency, from 1540 $cm^{-1}$to 1550 cm^{-1}, and at later times, a shift back to lower frequency. This derivative like structure is indicative of a shifting of a peak to a slightly higher energy. The kinetics at several energies are shown in figure 5.6 on page 112, along with the kinetics of the growth of the final product. Parameters for these fits are shown in table 5.2. Note that the recovery of the bleach signal at 1551 $cm^{-1}$is very similar to growth of the CO stretch

at 2032 cm^{-1}.

A concern in looking at signals of the shape is that they can also be caused by thermal effects due to heating of the sample [94]. The pump pulse has deposited significant thermal energy into the sample, and this thermal energy causes local changes in the index of refraction. These optical changes in the sample can cause transient signals near strong absorptions, even when no chemistry is occurring. Thus it is important to confirm that the changes which we see are chemical and not thermal in nature. We can do this by looking at the kinetics of the spectral changes. We know that the thermal changes should decay on the microsecond time scale, and should be uncorrelated with the chemistry. Changes which are representative of the chemistry should take place on a time scale which is correlated with the chemistry. Results of these fits to these transients are shown in table 5.2. From this data we can see two important facts. First, we can see that the timescales for the 1541 and 1550 cm^{-1}peaks are in very good agreement with the transients in the CO region, showing that the spectral shift is almost certainly associated with chemical changes, and no thermal artifacts. Second, we see that the timescale for C–D activation is 1.8 times longer than the C–H activation. This is in good agreement with other measurements [59] which show a change in kinetics due to the change in the zero point energy of the C–H and C–D bonds.

This provides confirmation from non C–O stretches that intermediate **B** is really an η^2 species. We can see changes in the pyrazole stretch which are correlated to this

change in chelation state. We have also shown, for the first time, non-CO transient spectroscopy of an irreversible chemical system. This is important because it will allow for the direct probing of ligand dynamics in chemical reactions. It will also allow for the study of organometallic compounds which do not have a CO ligand, such as the compound $CpIrP(R_3)H_2$ (R = Ph or Me) which was originally studied by Janowicz and Bergman [53].

5.2 Metal Hydride Stretch

In the C—H activation work, the mode which is of most interest is the metal-hydride stretch which is formed in the product. In the case of $Tp^*Rh(CO)_2$, this is a Rh—H stretch. This is an important mode to observe because it provides confirmation of the exact point in the reaction scheme where the C—H bond is broken. This stretch has not been observed before in the time domain.

Previous measurements of a similar C—H bond activation system, $CpIr(CO)_2$ showed an Ir—H stretch at 2150 cm^{-1} [54, 95] in the final alkyl hydride product. Taking into account only the reduced mass change for Rh vs. Ir, the stretch should be 2130 cm^{-1}. Of course differences in metal-hydrogen interactions will probably shift this, but we still expect the stretch to be in the 2100 cm^{-1}region. Static FTIR spectra, however, do not show any peaks in the final product in this region of the spectra.

Ab initio calculations have been performed on various C–H activated complexes.

It has been recently shown by Jonas *et al.* [19] that density functional theory can calculate vibrational modes for metal carbonyls with predictive accuracies. Results from our calculations are shown in table 5.1. The Tp*Rh(CO)[H][CH_3] complex show a frequency for the Rh–H stretch at 2110 cm^{-1}. This is in a clear region of the CO region of the spectra, and the CO stretch shows *very* good agreement with experiment, though it is somewhat red shifted. This is for a large basis set, but with no polarization or diffuse functions. Since there is a Rh metal, it would be good to include both of these basis set expansions, however the calculations were too difficult to do for such a large system. The results for CpIr(CO)(H)(Me) are also hopeful, since they agree well with experiment.

Rather than performing the calculations on the full basis set with the Tp ligand, I varied the basis set with a smaller system, CpRh(CO)(H)(Me). Note the difference between the CpRh results with and without diffuse functions. Without the diffuse functions, there is a 137 cm^{-1}difference between the C–O and Rh–H stretches. When we add diffuse functions, this decreases to only 2 wavenumbers. Analysis of the displacements of the atoms in the normal modes confirms that while the C–O and Rh–H modes are weakly coupled with no diffuse functions, they are more strongly coupled when diffuse functions are added. This suggests that for the Tp*Rh(CO)(H)(CH_3) results the Rh–H may be lower in frequency than 2109.6 rather than higher in frequency as the C–O stretch would suggest. Unfortunately, I was unable to compute IR intensities in order to get further comparison with the observed CO spectra.

Molecule/ basis set	C–O stretch (cm^{-1})	experiment	Rh–H stretch(cm^{-1})	experiment
Tp*Rh LACVP	1991.2	2032	2110	?
CpIr LACVP	1982	1982[a]	2270	2150[a]
CpIr LACVP*	2091	1982	2252	2150
CpRh LACVP	1986	2037[b]	2123	?
CpRh LACVP*	2106	2037	2108	?

Table 5.1: *Ab initio results for C–H activated complexes*

[a]From reference [54,95]
[b]From reference [59]

Figure 5.2 on the facing page shows a series of transient spectra during the course of the C—H bond activation reaction. The negative peaks at 1980 and 2050 cm^{-1} represent bleaching of the parent CO peaks from the parent species. The peak at 1990 cm^{-1} has been assigned to be an η^2- Tp*Rh$(CO)_2$ complex, which then forms the final Tp*Rh(CO)(R)H alkyl hydride product. If we expand the region on the high energy side of the product, we see a small peak at 2080 cm^{-1} (see figure 5.2 on page 106 inset). Plotting the intensity of this peak against time shows that it has temporal behavior similar to the CO stretch in the final product at 2032 cm^{-1}. This supports the possibility that the peak at 2080 cm^{-1} is the Rh—H stretch which we would like to observe.

In order to confirm the assignment of this peak, it is necessary to look at the effect of isotopic substitution on the position of this peak. If this is really the Rh—H

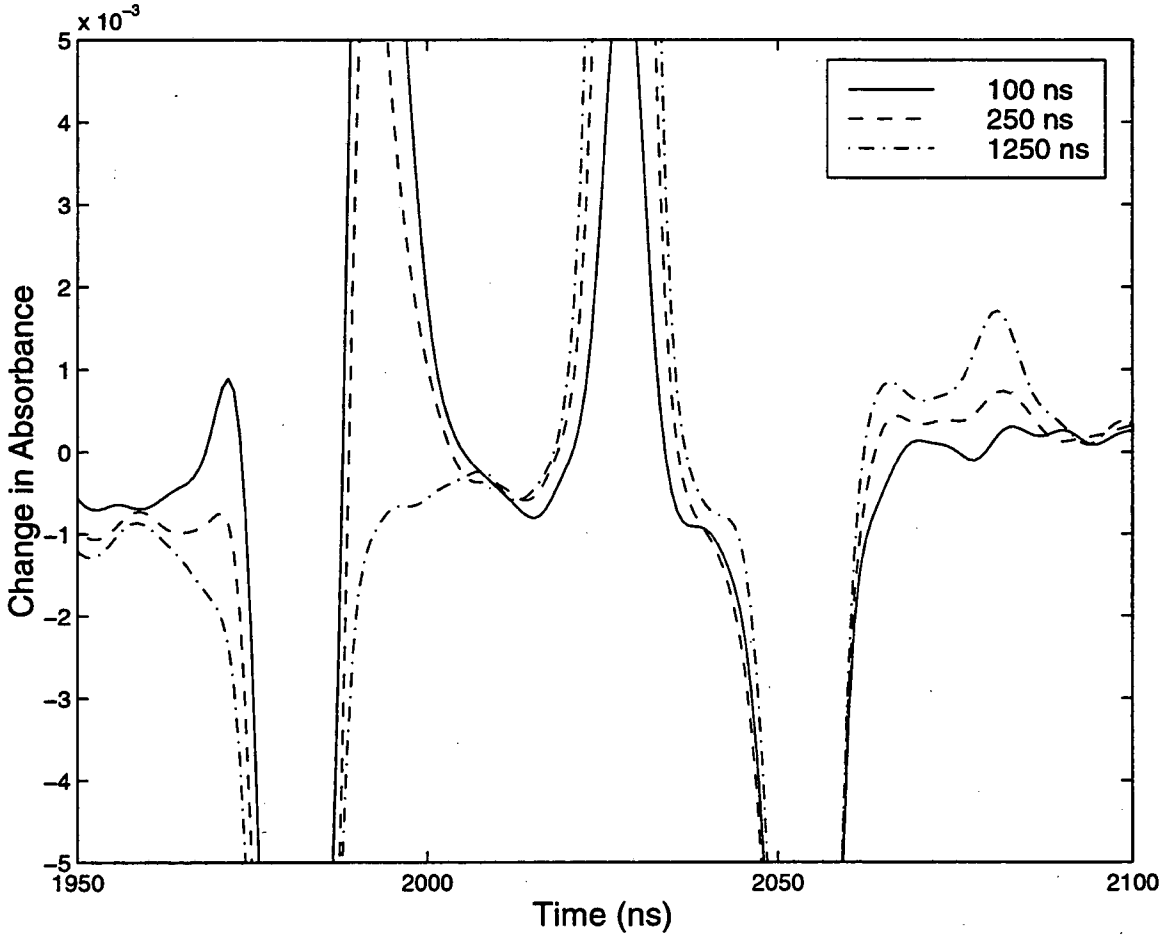

Figure 5.1: Spectrum of the Rh–H stretch in Tp*Rh(CO)(H)(R)

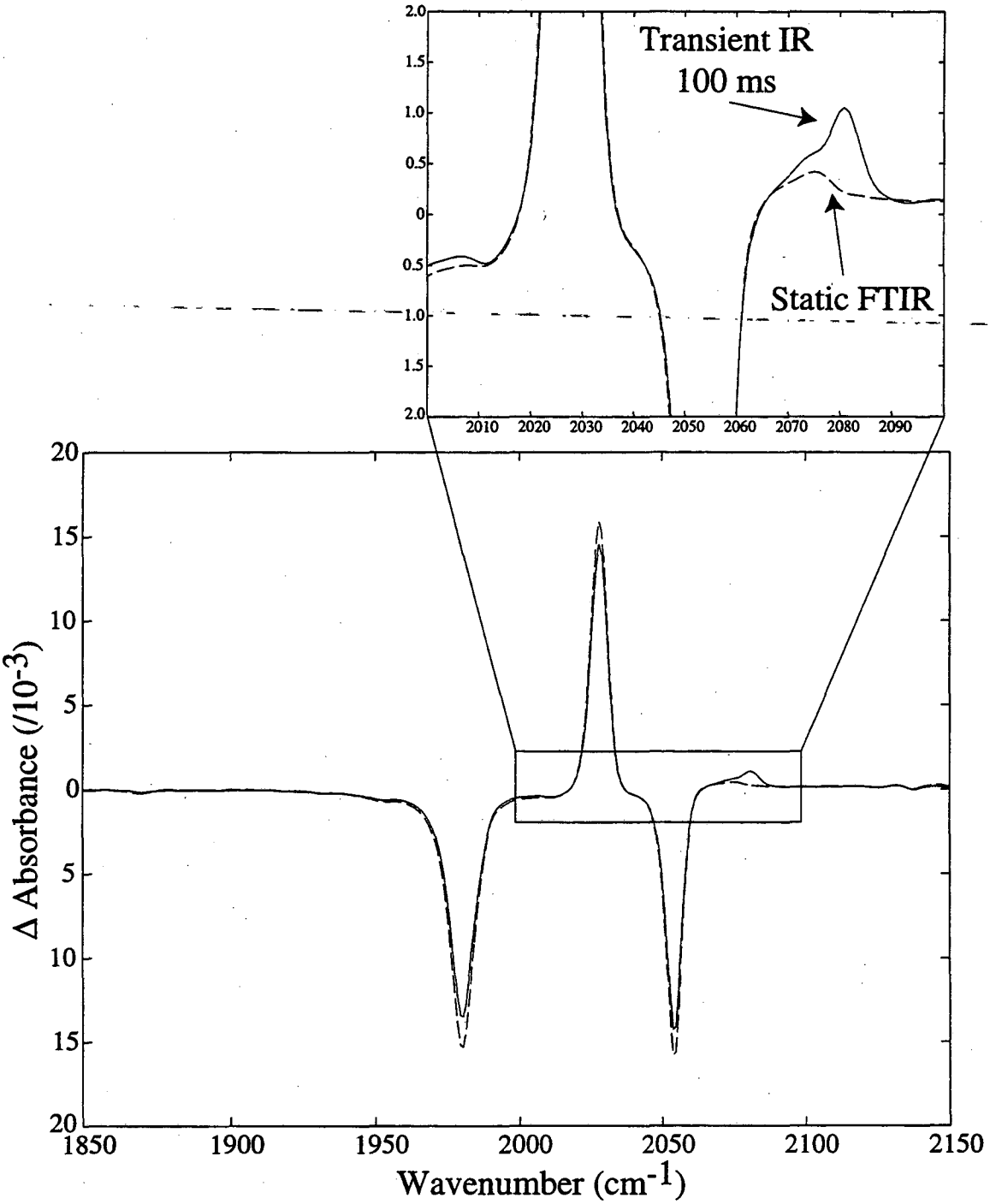

Figure 5.2: Millisecond FTIR of Rh–H stretch at 2080 cm^{-1}

stretch, performing the reaction in a perdeutero alkane solvent should shift the peak from 2080 cm^{-1} to $\frac{1}{\sqrt{2}}$ 2080 cm^{-1}, or 1470 cm^{-1}. Spectra of the 1300 to 1600 cm^{-1} region of the spectra for $Tp^*Rh(CO)_2$ in perdeutero-cyclohexane (C_6D_6) are shown in figure 5.2 on the following page. The spectra look noisy, but actually contain significant information. The spectrum shows a peak at 1483 cm^{-1} at late times which is not there at early times. Plotting the signal at 1483 cm^{-1} against time (figure 5.2 on page 109), we see that this peak also grows in with a time constant of 500 ns, similar to the time constant of the CO stretch in the final product. This peak is therefore assigned to be the Rh—D stretch in the final alkyl deuteride product. Calculating the integrated absorption intensity, we can say that the absorption cross section of the 2032 $cm^{-1}$is approximately $\frac{1}{50}$ that of the CO stretch of the product. The signal to noise thus represents a tremendous step forward in sensitivity for time resolved infrared measurements.

It is interesting that the peak at 2080 cm^{-1} is not seen in the static difference spectra taken at long times. This is surprising since it has been assumed that the alkyl hydride is stable at least for hours in the dark. FTIR scans taken in rapid scan mode, show that the peak at 2080 cm^{-1}decays with a time constant of 100 ms. Observing the peak at 2032 cm^{-1}, we observe *no* change in the peak position or intensity on that time scale. This is especially interesting since the alkyl hydride product for this reaction has never been isolated. In their experiments, Gosh and Graham only isolated the product as a chloride which they formed by reaction with

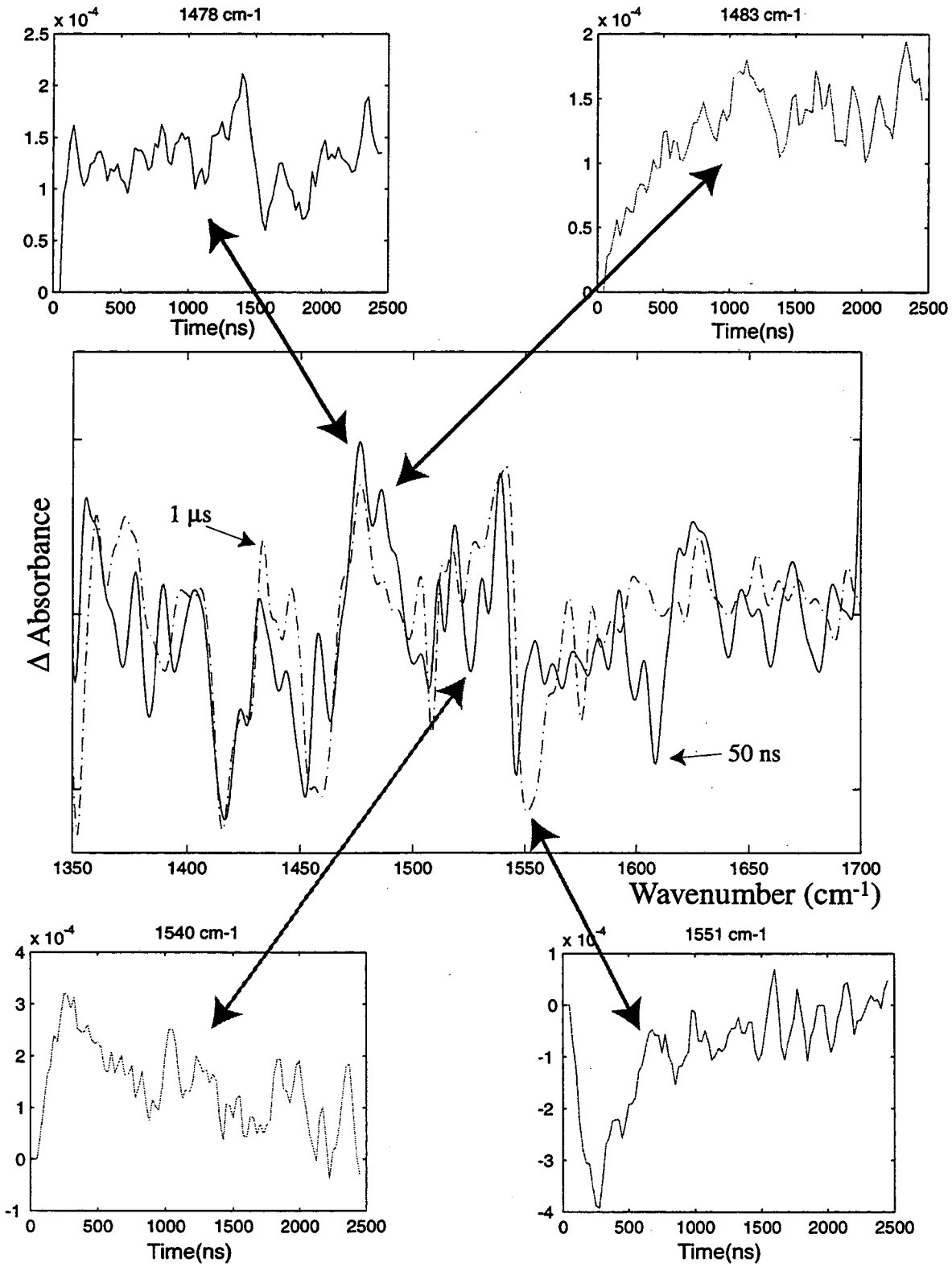

Figure 5.3: Rh–D stretch region nanosecond time resolved spectra and kinetic traces of $Tp^*Rh(CO)_2$in perdeuterocyclohexane.

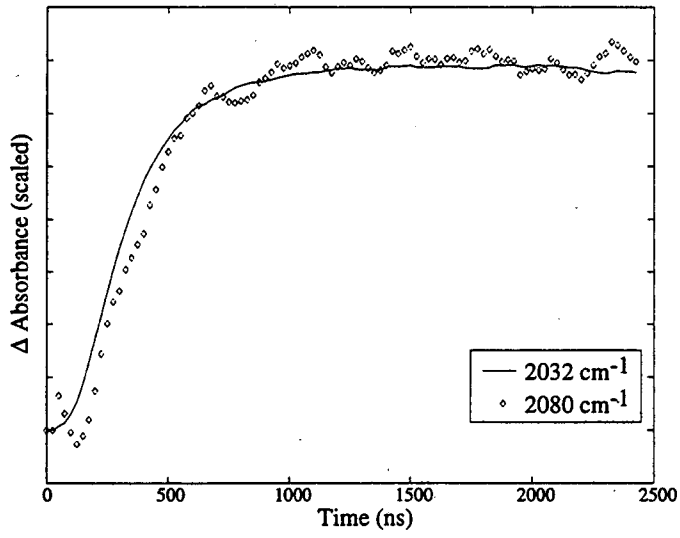

(a) Cyclopentane

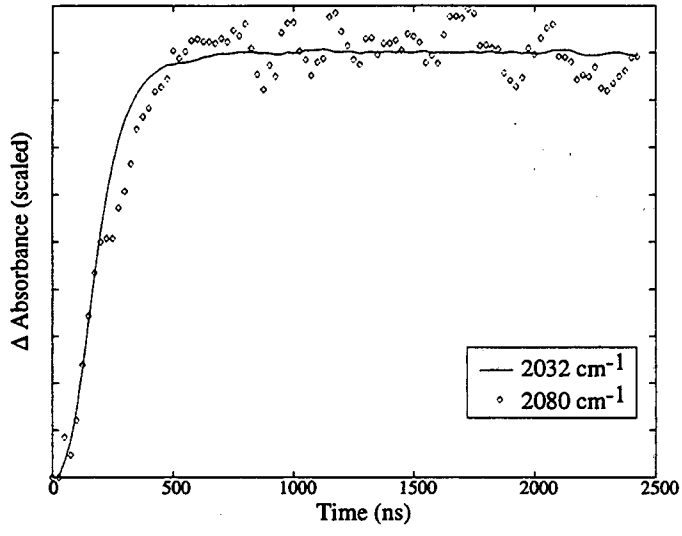

(b) *n*-Pentane

Figure 5.4: $Tp^*Rh(CO)_2$nanosecond kinetics are 2032 and 2080 cm^{-1}.

Frequency (cm^{-1})	Amplitude	Time Constant (ns)
2032	1	516 ns
1540	1	383 ns
1551	1	495 ns

Table 5.2: Fitting parameters for pyrazole stretches

CCl_4. It is possible that the product which has always been assumed to be the product has been a side product. This shows the importance of directly measuring the modes associated with the product of interest rather than looking at spectator modes. In this case, the CO stretch at 2032 cm^{-1}does not show that chemistry on the millisecond time scale, and so we miss important information which only comes from measuring the Rh—H stretch.

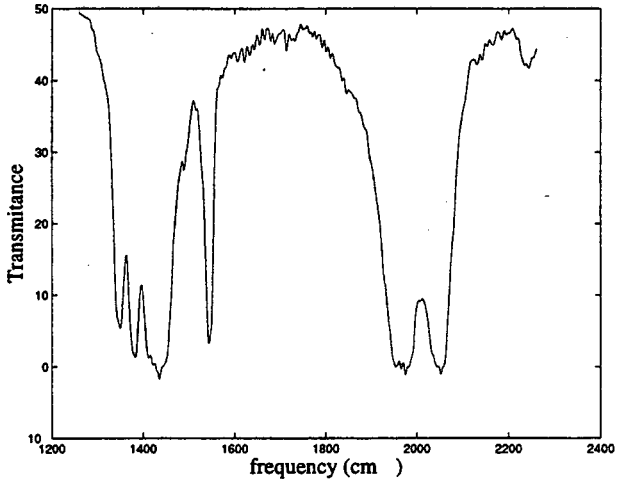

(a) $Tp^*Rh(CO)_2$

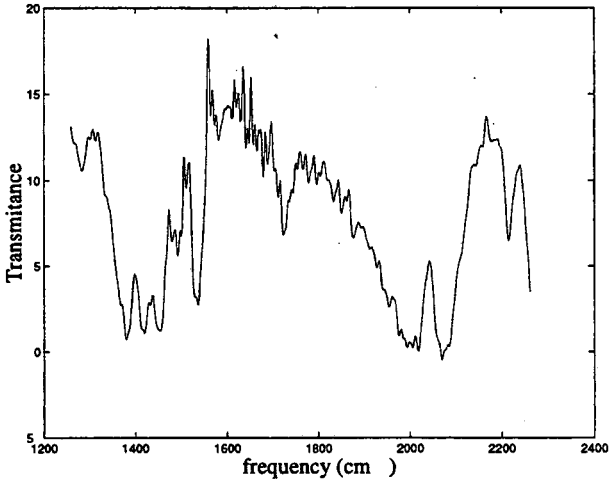

(b) $Bp^*Rh(CO)_2$

Figure 5.5: Static transmission spectra of $Tp^*Rh(CO)_2$and $Bp^*Rh(CO)_2$in KBr pellet

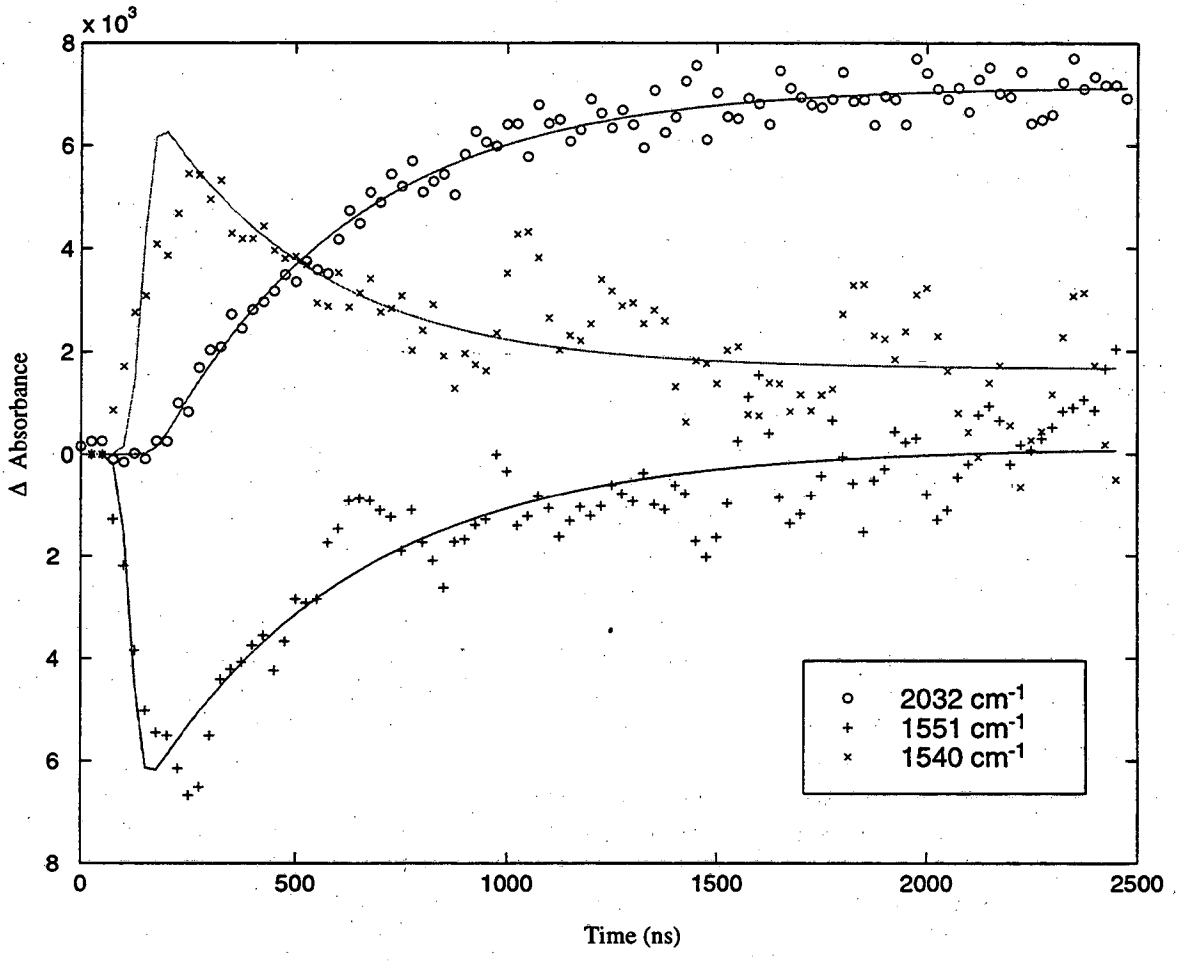

Figure 5.6: Fitting of the fingerprint spectral features. Parameters for the fit are given in table 5.2 on page 110. Signals at 1551 and 1540 $cm^{-1}$are scaled by a factor of 25.

Chapter 6

Conclusion

The development of femtosecond and nanosecond time resolved infrared instruments has allowed us unprecedented insight into complex chemical systems. The development of C–H activation chemistry through homogeneous organometallic compounds has opened a new field of synthetic chemistry. The combination of these two fields of science has opened up new possibilities of understanding chemical reactivity. The work presented here, and work by other members of the the Harris research group [3,70,71,91,92], has shown that it is possible to follow the course of a complex reaction from the earliest bond breaking and energy transfer dynamics, through the structural and electronic intermediates, to the bond breaking steps, and finally to products. Studies of ligand dynamics in the $Tp^*Rh(CO)_2$system show a richness in chemistry which has implications in many other chemical systems. Studies of reaction time scales based on alkane structure show that rearrangement of solvent complex in

the $Tp^*Rh(CO)_2$system happens on a time scale much less than 1 ns. This provides important insight into the observed reaction selectivity of C–H activation reactions.

This work has also shown considerable new spectroscopy. Measurements have been carried out across all relevant time scales, allowing assignment of all intermediates. We have performed the first nanosecond stepscan FTIR measurements on an irreversible chemical system, and have shown that we can observe changes in the CO stretch bands. We have also shown important new time resolved spectroscopy of non-CO stretches, measuring both Rh–H stretches and changes in the pyrazole ring modes during C–H activation reactions. This opens up new possibilities in studying organometallic photochemistry by allowing for the study of chemical systems which have other ligands, such as $P(Me)_3$ or $P(Ph)_3$.

This work has also shown how much chemistry which still needs to be studied. A question of considerable interest is the comparison of the reactivity of $CpRh(CO)_2$ and $Tp^*Rh(CO)_2$, and the nanosecond measurements on the $CpRh(CO)_2$ system shown here can be extended with studies in the femtosecond and picosecond domain. Recent work on C–H activation carried out in our research group [91,92] have started to examine the analogous Si–H bond activation reactions of $CpMn(CO)_3$ which have important parallels. A study of the Si–H activation reactions of $CpRh(CO)_2$ and $Tp^*Rh(CO)_2$would help draw important parallels to the present work. Finally, a study of the pump wavelength dependance of the mechanism of this reaction would help us to better understand the initial reaction steps.

Bibliography

[1] King, J. C.; Asplund, M. C.; Harris, C. B., in *Ultrafast Phenomena IX*, Springer Verlag, 1994 .

[2] Lian, T. Q.; Bromberg, S. E.; Asplund, M. C.; Yang, H.; Harris, C. B., *Journal of Physical Chemistry* **1996**, *100*, 11994–12001.

[3] Yang, H., Ph.D. thesis, U. C. Berkeley, **2000**.

[4] Murnane, M. M.; Kapteyn, H. C.; Huang, C.-P.; Asaki, M. T.; Garvey, D., personal communication.

[5] Huang, C.-P.; Asaki, M. T.; Backus, S.; Murnane, M. M.; Kapteyn, H. C.; Nathel, H., *Optics Letters* **1992**, *17*, 1289–1291.

[6] Murnane, M. M., *Sub-picosecond laser produced plasmas*, Ph.D. thesis, U. C. Berkeley, **1989**.

[7] Russell, D. J., *Vibrational Relaxation in Liquids: Comparisons between Gas Phase and Liquid Phase Theories*, Ph.D. thesis, U. C. Berkeley, **1990**.

[8] George, M. W.; Poliakoff, M.; Turner, J. J., *analyst* **1994**, *119*, 551–560.

[9] Poliakoff, M.; Weitz, E., *Advances in Organometallic Chemistry* **1986**, *25*, 277–316.

[10] Uhmann, W.; Becker, A.; Taran, C.; Siebert, F., *Applied Spectroscopy* **1991**, *45*, 390–397.

[11] Gregoriou, V. G.; Daun, M.; Schauer, M. W.; Chao, J. L.; Palmer, R. A., *Applied Spectroscopy* **1993**, *47*, 1311 – 1316.

[12] Palmer, R. A.; Chao, J. L.; Dittmar, R. M.; Gregoriou, V. G.; Plunkett, S. E., *Applied Spectroscopy* **1993**, *47*, 1297 – 1310.

[13] Sun, H.; Frei, H., *J. Phys. Chem. B.* **1997**, *101*, 205–209.

[14] Hu, X. H.; Frei, H.; Spiro, T. G., *Biochemistry-usa.* **1996**, *35*, 13001–13005.

[15] Hage, W.; Kim, M.; Frei, H.; Mathies, R. A., *J. Phys. Chem.* **1996**, *100*, 16026–16033.

[16] Kauffmann, E.; Frei, H.; Mathies, R. A., *Chem. Phys. Lett.* **1997**, *266*, 554–559.

[17] Tro, N. J.; King, J. C.; Harris, C. B., *Inorganica Chimica Acta* **1995**, *229*, 469–471.

[18] Zhang, J. Z.; Harris, C. B., *Journal of Chemical Physics* **1991**, *95*, 4024–4032.

[19] Jonas, V.; Thiel, W., *Journal of Chemical Physics* **1996**, *105*, 3636–3648.

[20] Harris, A. L.; Berg, M.; Harris, C. B., *Journal of Chemical Physics* **1986**, *84*, 788.

[21] Berg, M.; Harris, A. L.; Brown, J. K.; Harris, C. B., *Optics Letters* **1984**, *9*, 50–52.

[22] King, J. C., *Ultrafast Studies of Photodissociation in Solution: Dissociation, Recombination and Relaxation*, Ph.D. thesis, U. C. Berkeley, **1995**.

[23] Lewis, J. W.; Yee, G. G.; Kliger, D. S., *Reviews of Scientific Instruments* **1987**, *58*, 939–944.

[24] Lewis, J. W.; Yee, G. G.; Kliger, D. S., *Reviews of Scientific Instruments* **1987**, *58*, 945–949.

[25] Trofimenko, S., *Journal of the American Chemical Society* **1967**, *89*, 6288–6294.

[26] May, S.; Reinsalu, P.; Powell, J., *Inorganic Chemistry* **1980**, *19*, 1582–1589.

[27] Harris, A. L.; Brown, J. K.; Harris, C. B., *Annual Review of Physical Chemistry* **1988**, *39*, 341.

[28] Chuang, T. J.; Hoffman, G. W.; Eisenthal, K. B., *Chemical Physics Letters* **1974**, *25*, 201.

[29] Nesbitt, D. J.; Hynes, J. T., *Journal of Chemical Physics* **1982**, *77*, 2130.

[30] Xu, X. B.; Lingle, R.; Yu, S. C.; Chang, Y. J.; Hopkins, J. B., *Journal of Chemical Physics* **1990**, *92*, 2106 – 2107.

[31] Johnson, A. E.; Levinger, N. E.; Barbara, P. F., *Journal of Physical Chemistry* **1992**, *96*, 7841.

[32] Alfano, J. C.; Kimura, Y.; Walhout, P. K.; Barbara, P. F., *Chemical Physics* **1993**, *175*, 147.

[33] Kliner, D. A. V.; Alfano, J. C.; Barbara, P. F., *Journal of Chemical Physics* **1993**, *98*, 5375.

[34] Banin, U.; Ruhman, S., *Journal of Chemical Physics* **1993**, *98*, 4391.

[35] Banin, U.; Ruhman, S., *Journal of Chemical Physics* **1993**, *99*, 9318.

[36] Banin, U.; Kosloff, R.; Ruhman, S., *Isr. J. Chem.* **1993**, *33*, 141.

[37] Banin, U.; Kosloff, R.; Ruhman, S., *Chemical Physics* **1994**, *183*, 289.

[38] Papanikolas, J. M.; Vorse, V.; Nedal, M. E.; Campagnola, J. R.; Lineberger, W. C., *Journal of Chemical Physics* **1992**, *97*, 7002–7005.

[39] Papanikolas, J. M.; Vorsa, V.; Nedal, M. E.; Campagnola, P. J.; Buchenau, H. K.; Lineberger, W. C., *Journal of Chemical Physics* **1993**, *99*, 8733–8750.

[40] Benjamin, I.; Whitnell, R. M., *Chemical Physics Letters* **1993**, *204*, 45–52.

[41] Benjamin, I.; Banin, U.; Ruhman, S., *Journal of Chemical Physics* **1993**, *98*, 8337.

[42] Pugliano, N.; Szarka, A. Z.; Gnanakaran, S.; Triechel, M., *Journal of Chemical Physics* **1995**, *103*, 6498–6511.

[43] Barbara, P. F.; Jarzeba, W., *Advanced Photochemistry* **1990**, *15*, 1–68.

[44] Rosenthal, S. J.; Jimenez, R.; Fleming, G. R.; Kumar, P. V.; Maroncelli, M., *Journal of Molecular Liquids* **1994**, *60*, 25–56.

[45] Lian, T. Q.; Kholodenko, Y.; Hochstrasser, R. M., *Journal of Physical Chemistry* **1995**, *99*, 2546–2551.

[46] Daul, C.; Baerends, E. J.; Vernooijs, P., *Inorganic Chemistry* **1994**, *33*, 3538–3543.

[47] Lian, T.; Yang, H.; Asplund, M.; Harris, C. B., *Femtosecond IR Studies of Solvation by Probing the Solvent*, New York: Springer, 1996 pp. 300–301.

[48] Kelley, D. F.; Pogge, J. L., *Chemical Physics Letters* **1995**, *238*, 16–24.

[49] Cushing, J. P.; Butoi, C.; Kelley, D. F., *Journal of Physical Chemistry A* **1997**, *101*, 7222–7230.

[50] Garnett, J. L.; Hodges, R. J., *Journal of the American Chemical Society* **1967**, *89*, 4546.

[51] Hodges, R. J.; Garnett, J. L., *Journal of the American Chemical Society* **1968**, *72*, 1673.

[52] Jetz, W.; Graham, W. A. G., *Inorganic Chemistry* **1971**, *10*, 4–9.

[53] Janowicz, A. H.; Bergman, R. G., *Journal of the American Chemical Society* **1982**, *104*, 352–355.

[54] Hoyano, J. K.; Graham, W. A. G., *Journal of the American Chemical Society* **1982**, *102*.

[55] Weiller, B. H.; Wasserman, E. P.; Moore, C. B.; Bergman, R. G., *Journal of the American Chemical Society* **1992**, *115*, 4326–4330.

[56] Wasserman, E. P.; Moore, C. B.; Bergman, R. G., *Science* **1992**, *255*, 315–318.

[57] Bengali, A. A.; Schultz, R. H.; Moore, C. B.; Bergman, R. G., *Journal of the American Chemical Society* **1994**, *116*, 9585–9589.

[58] Bengali, A. A.; Bergman, R. G.; Moore, C. B., *Journal of the American Chemical Society* **1995**, *117*, 3879–3880.

[59] Schultz, R. H.; Bengali, A. A.; Tauber, M. J.; Weiller, B. H.; E. P. Wasserman, K. R. K.; Moore, C. B.; Bergman, R. G., *Journal of the American Chemical Society* **1994**, *116*, 7369–7377.

[60] Dougherty, T. P.; Heilweil, E. J., *Journal of Chemical Physics* **1994**, *100*, 4006–4009.

[61] Grubbs, W. T.; Dougherty, T. P.; Heilweil, E. J., *Chemical Physics Letters* **1994**, *227*, 480–484.

[62] Bromberg, S. E.; Lian, T. Q.; Bergman, R. G.; Harris, C. B., *Journal of the American Chemical Society* **1996**, *118*, 2069–2072.

[63] Lees, A. J.; Purwoko, A. A., *Coordination Chemistry Reviews* **1994**, *132*, 155–160.

[64] Purwoko, A. A.; Lees, A. J., *Inorganic Chemistry* **1995**, *34*, 424–425.

[65] Ghosh, C. K.; Graham, A. G., *Journal of the American Chemical Society* **1987**, *109*, 4726.

[66] Ghosh, C. K.; Graham, A. G., *Coordination Chrmistry Reviews* **1989**, *111*, 375.

[67] Purwoko, A. A.; Tibensky, S. D.; Lees, A. J., *Inorganic Chemistry* **1996**, *35*, 675.

[68] Lees, A. J., *Journal of Organometallic Chemistry* **1998**, *554*, 1 – 11.

[69] Lian, T.; Bromberg, S. E.; Yang, H.; Proulx, G.; Bergman, R. G.; Harris, C. B., *Journal of the American Chemical Society* **1996**, *118*, 3769–3770.

[70] Bromberg, S. E.; Yang, H.; Asplund, M. C.; Lian, T.; McNamara, B. K.; Kotz, K. T.; Yeston, J. S.; Wilkens, M.; Frei, H.; Bergman, R. G.; Harris, C. B., *Science* **1997**, *278*, 260–263.

[71] Bromberg, S. E., *Ultrafst Studies of Organometallic Photochemistry: The Mechanism of Carbon-Hydrogen Bond Activation in Solution*, Ph.D. thesis, U. C. Berkeley, **1998**.

[72] Heilweil, E. J.; Cavanagh, R. R.; Stephenson, J. C., *Chemical Physics Letters* **1987**, *134*, 181–188.

[73] Beckerle, J. D.; Casassa, M. P.; Cavanagh, R. R.; Heilweil, E. J.; Stephensen, J. C., *Chemical Physics* **1992**, *160*, 487 – 497.

[74] King, J. C.; Zhang, J. Z.; Schwartz, B. J.; Harris, C. B., *Journal of Chemical Physics* **1993**, *99*, 7595–7601.

[75] Lee, M.; Harris, C. B., *Journal of the American Chemical Society* **1989**, *111*, 8963–8965.

[76] Bucher, U. E.; Currao, A.; Nesper, R.; Ruegger, H.; Venanzi, L. M.; Younger, E., *Inorg. Chem.* **1995**, *34*, 66–74.

[77] Kuykendall, V.; Thomas, J. K., *Langmuir.* **1990**, *6*, 1346–1350.

[78] Perez, P. J.; Poveda, M. L.; Carmona, E., *Angew. Chem. Int. Ed.* **1995**, *34*, 231–233.

[79] Breheny, C. J.; Draper, S. M.; Grevels, F. W.; Klotzbucher, W. E.; Long, C.; Pryce, M. T.; Russell, G., *Organometallics.* **1996**, *15*, 3679–3687.

[80] Szajek, L. P.; Lawson, R. J.; Shapley, J. R., *Organometallics.* **1991**, *10*, 357–361.

[81] Szajek, L. P.; Shapley, J. R., *Organometallics.* **1994**, *13*, 744–744.

[82] Szajek, L. P.; Shapley, J. R., *Organometallics.* **1993**, *12*, 3772–3775.

[83] Basolo, F., *New Journal of Chemistry* **1994**, *18*, 19–24.

[84] O'Conner, J. M.; Casey, C. P., *Chemical Reviews* **1987**, *87*, 307–318.

[85] Purwoko, A. A.; Tibensky, S. D.; Lees, A. J., *Inorganic Chemistry* **1996**, *35*, 7049–7055.

[86] Hall, M., Personal Communication, **1996**.

[87] Wick, D. D.; Goldberg, K. I., *Journal of the American Chemical Society* **1997**, *119*, 10235–10236.

[88] Jones, W. D., *Actuvation and Functionalization of Alkanes*, New York: Wiley, 1989 pp. 111–150.

[89] Buchanan, J. M.; Struker, J. M.; Bergman, R. B., *Journal of the American Chemical Society* **1986**, *108*, 1537 - 1550.

[90] Yeston, J., Personal Communication, **1998**.

[91] Yang, H.; Kotz, K. T.; Asplund, M. C.; Harris, C. B., *Journal of the American Chemical Society* **1997**, *119*, 9564–9565.

[92] Yang, H.; Asplund, M. C.; Kotz, K. T.; Wilkens, M. J.; Harris, C. B.; Frei, H., *Journal of the American Chemical Society* **1998**, *In press*.

[93] Bellamy, L. J., *The Infrared Spectra of Complex Molecules*, New York: Chapman and Hall, 1975 pp. 311–320.

[94] Yuzawa, T.; Kato, C.; George, M. W.; Hamaguchi, H., *Applied Spectroscopy* **1994**, *48*, 684–690.

[95] Banister, J. A.; Cooper, A. I.; Howdle, S. M.; Jobling, M.; Poliakoff, M., *Organometallics* **1996**, *15*, 1804–1812.

Appendix A

FTIR Analysis Procedure

The Brueker FTIR instrument which we used for Stepscan FTIR measurements uses a custom computer program, `Opus` which controls the spectrometer, and performs many data analysis functions. From a given experiment, it gathers a 3-D data file, containing one spectrum at each time slice. Tools are provided in the program to extract individual time slices, or averages of series of consecutive time slices. While this is useful for looking at individual spectra, for kinetics measurements a method is needed to extract information about a single frequency over a range of times. Unfortunately, the `Opus` program proved incapable of doing this form of analysis. It thus became necessary to change from the `Opus` form of data into a form which can be manipulated by a program such as `Matlab` which will then allow more flexible analysis.

This data conversion is performed in two stages. The first stage takes place

within the Opus program. A set of macro files, MasterAC and MasterDC were written to change from the Opus internal data representation to a generic tab separated, ASCII file with x, y data sets for each frequency. These macro files are scripts which automatically execute Opus commands on a set of data files. The first, MasterAC takes as an input a series of AC, or time resolved scans, and outputs a series of ASCII files, named 1.001 through 1.100 (assuming 100 time slices), 2.001 through 2.100 and so on. Each file contains a spectrum for one time delay. MasterDC accepts as input a series of DC or static files, which we use to convert from single beam spectra to absorbance spectra. It outputs a series of files, 1.000, 2.000, and so on.

One important variable which must be checked for each run is number of 25-blocks variable. This is used in MasterAC and describes the number of time slices in the AC data file. For most runs this is 4, meaning 100 time slices. If longer or shorter runs are taken, this must be changed. The text of these macros follows.

```
Macro: MasterDC.MAC
=================================================
1              (1) Set Value of: lopcount = 1

2  /  \          (2) Start Loop, Loop Index = 0
                    For Each: 400
3  |  |          (3) Set Value of: outputfilename = <[,3]loopcount>
|  |
4  |  |          (4) Extract
|  |               Input File(s): [400:ScSm/Multiple]    No Output File
5  |  |          (5) Wait Time:0
|  |
6  |  |          (6) Load File: <inputpath>/backgrnd.0
|  |               On Error: Warning and Abort Macro
7  |  |          (7) Wait Time: 0
|  |
8  |  |          (8) Data Point Table
|  |               Input File(s): [401:ScSm]   No Output File
9  |  |          (9) Wait Time: 0
|  |
10 |  |          (10) Delete Data Blocks
|  |               Input File(s): [401]  No Output File
11 |  |          (11) Wait Time:0
|  |
12 |  |          (12) Calculate: (<loopcount>)+1=(<loopcount>)
|  |  |
13 \  /          (13) End Loop, Loop Index=0

--------------------

List of Variables
=================

*FILE NAME:          400 = DC File
*NUMERIC:            loopcount = 10
*STRING FOR EDIT:    outputfilename = 9.000
*STRING FOR EDIT:    inputpath = c:\matt\tmp\rawdata
*STRING FOR EDIT:    outputpath = c:\matt\tmp\asciidat
FILE VARIABLE        401 = backgrnd.0
```

```
Macro: MasterAC.MAC
===================================

1                (1)  Set Value of: outputnumber = 1.001

2                (2)  Set Value of: Loopcount = 1

3  /  \          (3)  Start Loop, Loop Index = 0
                   For Each: 401
4  |   |         (4)  Extract
|  |               Input File(s): [401:ScSm/Multiple]   No Output File
5  |   |         (5)  Wait Time: 0
|  |
6  |   |         (6)  Set Value of: masterfilenumber = 1.001
|  |
7  |   |         (7)  Wait Time: 0
|  |
8  |  /  \       (8)  Start Loop, Loop Index = 1
|  | |             Loop Count: number of 25-blocks
9  | |    |      (9)  Submacro: c:\matt\macro\newsub.mac
|  | |             7 Variable(s) passed, 0 Variable(s) returned
10 | |    |      (10) Calculate: (<masterfilenumber>)+.025 = (<masterfilenumber>)
|  | |
11 | |    |      (11) Calculate: (<outputnumber>)+.025 = (<outputnumber>)
|  | |
12 | \    /      (12) End Loop, Loop Index = 1
|  |
13 |   |         (13) Calculate: (<Loopcount>)+1=(<Loopcount>)
|  |
14 |   |         (14) Calculate: (<Loopcount>)+0.001=(<outputnumber>)
|  |
15 |   |         (15) End Loop, Loop Index = 0


List of Variables
=================

*FILE VARIABLE:        401 = signal
*NUMERIC:              masterfilenumber = 1.101
*STRING FOR EDIT:      inputpath = c:\matt\tmp\rawdata
*STRING FOR EDIT:      backfile = 1.000
*STRING FOR EDIT:      outputpath = c:\matt\tmp\asciidat
```

```
NUMERIC:              outputnumber = 1.001
*STRING FOR EDIT:     lowfreq =
*STRING FOR EDIT:     highfreq =
*NUMERIC:             number of 25-blocks
*NUMERIC              Loopcount = 10
```

```
Macro: newsub.mac
==================

1               (1)  Dialog: No. 4, untitled

2               (2)  Wait Time: 0

3  /   \        (3)  Start Loop, Loop Index = 0
                  Loop Count: 25*
4  |   |        (4)  Set Value of: filename = <[,3]filenumber>
|  |
5  |   |        (5)  Set Value of: outputfile = <[,3]filenumber>
|  |
6  |   |        (6)  Wait Time = 0
|  |
7  |   |        (7)  Load File: <inputpath>\<filename>
|  |              On Error: Warning and Abort Macro
8  |   |        (8) Wait Time:0
|  |
9  |   |        (9)  Data Point Table
|  |              Input File(s): [401:ScSm]    No Output File
10 |   |        (10) Wait Time: 0
|  |
11 |   |        (11) Delete Data Blocks
|  |              Input File(s): [401]   No Output File
12 |   |        (12) Calculate: (<filenumber>)+0.001=(<filenumber>)
|  |
13 |   |        (13) Calculate:(<outputfilenumber>)+0.001=(<outputfilenumber>)
|  |
14 |   |        (14) Wait Time: 0
|  |
```

```
15 |   |        (15) Set Value of: filename = <[,3]filenumber>
|  |
16 |   |        (16) Set Value of: outputfile = <[,3]outputfilenumber>
|  |
17 |   |        (17) Wait Time: 0
|  |
18 \   /        (18) End Loop, Loop Index = 0


List of Variables
=================

*STRING FOR EDIT:      background = 1.000
*NUMERIC:              filenumber = 1.101
*STRING FOR EDIT:      filename = 1.101
*STRING FOR EDIT:      outputfile = 9.101
*STRING FOR EDIT:      inputpath = c:\matt\tmp\rawdata
*STRING FOR EDIT:      outputpath = c:\matt\tmp\asciidat
 FILE VARIABLE:        401 = <filename>
*STRING FOR EDIT:      lowfreq =
*STRING FOR EDIT:      highfreq =
*NUMERIC:              outputfilenumber = 9.101
```

After processing by these macros, the data is compressed into a file using the program `pkzip.exe`, and the data is transferred to a computer in our lab. This data is uncompressed, and imported into the program `MATLAB` by one of two scripts. These scripts perform three basic functions.

1. Reading in n files with m frequencies, and forming a $n \times m$ matrix from these values.

2. Averaging p repetitions of an experiment

3. Converting the single beam scans into Absorbance units.

These functions are performed by two different `MATLAB` scripts. The choice of scripts is dictated by the desired information. The first script, `STEP2ABS` accepts as input a series of files from the `OPUS` macros, and produces a series of matrices, `single, single2, trans, trans2, absorb and absorb2`. These are pairs of matrices containing mean and sum of squares for single beam, transmission and absorption data. From this data, it is possible to calculate the deviations for each data set. The second macro,

STEP2ABS3D is similar, but produces as an output a 3-dimensional matrix $m \times n \times p$ containing each experiment individually. This allow averaging over subsets of experiments in a group, or isolation of a single experiment in a group. These scripts are `MATLAB` m-files, and so are easily portable and readable.

STEP2ABS.m

```
%Load stepscan data into a matlab,
%find the mean and sum of squares of
%each of single beam, transmission and absorbance data.

ampfac=input('Amplification Factor');
timeslice=input('Number of Time Slices');
fid=fopen('1.000','r');
bdata=fscanf(fid,'%f  %f',[2,inf]);
fclose(fid);
freqs=length(bdata)
dmatrix=zeros(timeslice,freqs);
single=zeros(timeslice,freqs);
trans=zeros(timeslice,freqs);
absorb=zeros(timeslice,freqs);
single2=zeros(timeslice,freqs);
trans2=zeros(timeslice,freqs);
absorb2=zeros(timeslice,freqs);
data2=zeros(freqs);



filenumber=1;
filename=sprintf('%0.3f',filenumber);
while exist(filename) == 2,
    for i=1:timeslice+1,
        filename=sprintf('%0.3f',filenumber+(i-1)/1000);
        fid=fopen(filename,'r');
        if i==1,
            data=fscanf(fid,'%f  %f',[2,inf]);
        else
            bbb=fscanf(fid,'%f');
            data(2,:)=bbb';

        end

        dmatrix(i,:)=data(2,:);
        fclose(fid);
    end
```

```
    for i=2:timeslice+1,
        single(i-1,:)=single(i-1,:)+dmatrix(i,:);
        single2(i-1,:)=single2(i-1,:)+dmatrix(i,:).*dmatrix(i,:);
        tt=1+dmatrix(i,:)./(ampfac*dmatrix(1,:));
        trans(i-1,:)=trans(i-1,:)+tt;
        trans2(i-1,:)=trans2(i-1,:)+tt.*tt;
        absorb(i-1,:)=absorb(i-1,:)+real(-log10(tt));
        absorb2(i-1,:)=absorb2(i-1,:)+real(-log10(tt)).^2;

    end
    filenumber=filenumber+1
freq=data(1,;);
end
```

STEP2ABS3D.m

```
% Load stepscan data into a 3-D matrix.
% You must be in the directory with the data files.
% This assumes the data is in the files 1.000 - 1.n, 2.000 - 2.n
% and so on.
ampfac=input('Amplification Factor');
timeslice=input('Number of Time Slices');
fid=fopen('1.000','r');
bdata=fscanf(fid,'%f  %f',[2,inf]);
fclose(fid);
freqs=length(bdata)


filenumber=1;
filename=sprintf('%0.3f',filenumber);
while exist(filename) == 2,
    for i=1:timeslice+1,
        filename=sprintf('%0.3f',filenumber+(i-1)/1000);
        fid=fopen(filename,'r');
        if i==1,
            data=fscanf(fid,'%f  %f',[2,inf]);
        else
            bbb=fscanf(fid,'%f');
            data(2,:)=bbb';
```

```
        end

        dmatrix(i,:)=data(2,:);
        fclose(fid);
    end
    for i=2:timeslice+1,
        single(i-1,:,filenumber)=dmatrix(i,:);
        tt=1+dmatrix(i,:)./(ampfac*dmatrix(1,:));
        trans(i-1,:,filenumber)=tt;
        absorb(i-1,:,filenumber)=real(-log10(tt));

    end
    filenumber=filenumber+1
freq=data(1,:)';
end
```

Appendix B

Technical Specifications

Table B.1: Technical specifications of the femtosecond IR spectrophotometer.

Component	Attribute	Value	Units
Ti:Sapph. Oscillator			
	Input power[1]	5.0	W
	Output power	400	mW
	Repetition rate	80	MHz
	Output wavelength[2]	817	nm
	Pulse width	40	fs
Nd:YAG Laser			
	Output power	15.0	W
	Repetition rate	30	Hz
	Pulse energy	500	mJ
	Output wavelength[3]	532	nm
	Pulse width	6	ns
820 nm Pulse Chain			
	Pulse energy	20	μJ
	Pulse width	70	fs

continued...

[1]Coherent Innova 300 CW Ar^+ laser, all lines green.
[2]Peak wavelength; output is uncertainty broadened by $\tilde{2}0$ nm FWHM
[3]Frequency doubled using second harmonic generation(SHG).

Component	Attribute	Value	Units
700 nm Pulse Chain			
	Pulse energy	100	μJ
	Pulse width	70	fs
590 nm Pulse Chain			
	Pulse energy	400	μJ
	Pulse width	200	fs
IR Pulses			
	Pulse energy	2	μJ
	Pulse width	80	fs
UV Pulses			
	Pulse energy	16	μJ
	Pulse width	200	fs
Overall Time Resolution		240	fs

Appendix C

FTIR parameters

The step-scan FTIR measurements were made on a standard Bruker IFS-88 spectrometer. Following are standard settings used in making the measurements shown in this work.

Table C.1: FTIR parameters for Step Scan measurements.

Component	Attribute	Value	Units
Acquisition			
	Folding limits (InSb)	1316, 2633	cm^{-1}
	Folding limits (MCT)	1220, 1820	cm^{-1}
	Collection Mode	*Single Sided*	
	Resolution	4	cm^{-1}
	Stabilization delay	0	ms
	Delay before measurement	0	ms
	Results Spectrum	*Transmission*	
	Time Resolution	25	ns
	Number of Time Slices	100	
	Repeat Count	30	
	Trigger Delay	0	ms
	Positioning Delay	40	ms
	Triggering Polarity	0(*rising edge*)	

continued...

Component	Attribute	Value	Units
	Sampling Source	0	
Fourier Transform			
	Apodization	$Blackman - Harris\ 3 - term$	
	Frequency Limits	1600, 2600	cm^{-1}
	Phase Correction	*Mertz*	
	Phase Resolution	32	
	Zero Filling Factor	4	
Optics			
	Aperature	6	mm
	Beam splitter	*KBr*	
	Detector	*MCT*	
	Source	*Globar*	

Ernest Orlando Lawrence Berkeley National Laboratory
One Cyclotron Road | Berkeley, California 94720

Prepared for the U.S. Department of Energy under Contract No. DE-AC03-76SF00098